General Disclaimer

One or more of the Following Statements may affect this Document

- This document has been reproduced from the best copy furnished by the organizational source. It is being released in the interest of making available as much information as possible.

- This document may contain data, which exceeds the sheet parameters. It was furnished in this condition by the organizational source and is the best copy available.

- This document may contain tone-on-tone or color graphs, charts and/or pictures, which have been reproduced in black and white.

- This document is paginated as submitted by the original source.

- Portions of this document are not fully legible due to the historical nature of some of the material. However, it is the best reproduction available from the original submission.

The Investigation of Tethered

Satellite System Dynamics

Contract NAS8-36160

Quarterly Report #2

For the period 1 December 1984 through 14 February 1985

Principal Investigator

Dr. Enrico Lorenzini

March 1985

CONTENTS

CONTENTS (Cont.)

CONTENTS (Cont.)

The Investigation of Tethered

Satellite System Dynamics

Contract NAS8-36160

Quarterly Report #2

For the period 1 December 1984 through 14 February 1985

Principal Investigator
Dr. Enrico Lorenzini

Co-Investigators
Mr. David A. Arnold
Dr. Mario D. Grossi
Dr. Gordon E. Gullahorn
Mr. William Harrold
Prof. Robert G. Hohlfeld

March 1985

Prepared for
National Aeronautics and Space Administration
Marshall Space Flight Center, Alabama 35812

Smithsonian Institution
Astrophysical Observatory
Cambridge, Massachusetts 02138

The Smithsonian Astrophysical Observatory
is a member of the
Harvard-Smithsonian Center for Astrophysics

PRECEDING PAGE BLANK NOT FILMED

Abstract

This reports deals with three major topics related to TSS dynamics:

a) The update of the SAO rotational dynamics computer code. The program is now suitable to deal with inclined orbits. The output has been also modified in order to show the satellite Euler angles referred to the rotating orbital frame.

b) The development of the three-dimensional high resolution computer program SLACK3. The code simulates the three-dimensional dynamics of a tether going slack taking into account the effect produced by boom rotations. Preliminary simulations on the three-dimensional dynamics of a recoiling slack tether are shown in this report.

c) The development of a program to evaluate the electric potential around a severed tether immersed in a plasma. The potential is computed on a three-dimensional grid axially symmetric with respect to the tether longitudinal axis. The electric potential variations due to the plasma are presently under investigation.

1.0 INTRODUCTION

This is the second quarterly report submitted by SAO under contract NAS8-36160, "The Investigation of Tethered Satellite System Dynamics," Dr. Enrico Lorenzini, PI, and covers the period from 15 November 1984 through 16 February 1985.

2.0 TECHNICAL ACTIVITY DURING REPORTING PERIOD AND PROGRAM STATUS

2.1 Tss Rotational Dynamics Analysis

2.1.1 Introductory Remarks -

The SKYHOOK computer code was updated with a preliminary rotational dynamics package in 1982. This study is documented in the report "Study of Tethered Satellite Active Attitude Control," October 1982, NASA Contract NAS8-33691. The satellite was modeled as a rigid body and the tension transmitted by the tether was the only external perturbation acting upon the satellite. The three Euler rigid body equations were added to SKYHOOK along with the nine equations relating the body-axis angular velocities to the derivatives of the direction cosines. Once the direction cosines are obtained, the Euler angles are computed. This method has the major drawback of integrating nine additional equations that can be reduced to three.

The body-axis angular velocities, ω_1, ω_2, ω_3 of the Euler rigid body equations can be converted to Euler angular velocities and then integrated a second time to get the Euler angles. The direct integration of the Euler angular velocities will therefore increase the computer code efficiency and

reduce the CPU time. The only drawback related to this approach is that the equations become singular when the roll angle approach 0°, that is to say (with the SKYHOOK reference frame conventions) when the vertical body axis of the satellite is perpendicular to the equatorial plane. This condition however is a limit condition that can be encountered only in special situations. Both integration options will be kept available in the SKYHOOK computer code to have the greatest flexibility.

The other major modification is the implementation of a new force package and of a new torque package that models the effect of thruster activation. In-plane, out-of-plane and in-line thrusters provide, in an ideal situation, forces applied to the satellite center-of-mass (c.m.). In the actual situation they also produce spurious torques because of misalignments. These torques must appear on the right hand side of the rigid body Euler equations. However, this doesn't mean that a thruster activation produces a satellite rotation only through misalignment. Even if a lateral force acting upon the satellite is directed exactly toward the satellite c.m., rotations are still produced by the different moments of inertia of the satellite and the tether. This effect is modeled in SKYHOOK so that the tether bends differently depending upon the point of application of the external force and the mass distribution of the system.

The update of the output is also necessary in SKYHOOK. Presently the computer code plots the satellite attitude with respect to the inertial reference frame. Plots cannot be interpreted immediately especially if the orbit is not equatorial. Reference frame transformations are necessary to convert the inertial Euler angles to the rotating reference frame Euler angles. In this way the satellite attitude is referred to the local vertical and the local horizon and the output has an immediate interpretation.

This way of dealing with inertial Euler angle has made it difficult to set up the initial conditions for SKYHOOK. For this reason, the rotational dynamics SKYHOOK has been used, in the past, for equatorial orbit only (in this case the problem is greatly simplified). The matrix transformation implemented to modify the output can also be used for setting up initial conditions in order to generalize the program to any type of orbit. All these modifications are in progress. Some of them will be fully operative in our computer code in the near future.

2.1.2 Matrix Transformation From Inertial Reference Frame To Orbiting Reference Frame -

The attitude dynamic equations integrated by SKYHOOK make use of the direction cosine matrix. From that matrix we derive the Euler angles with respect to the inertial reference frame (x,y,z) (see Figure 2.1.1). If we want to refer the satellite attitude to the orbiting reference frame $(x',$ $y',$ $z')$ we must derive the rotation matrix that relates the orbiting reference frame to the inertial reference frame. If we call $[R_{OI}]$ the rotation matrix that transform orbiting axis into inertial axis and $|R_{BI}|$ the rotation matrix that transform satellite body axis into inertial axis we have:

$$\begin{bmatrix} x_I \\ y_I \\ z_I \end{bmatrix} = [R_{BI}] \begin{bmatrix} x_B \\ y_B \\ z_B \end{bmatrix} \qquad (2.1.1)$$

and

$$
\begin{bmatrix} x_I \\ y_I \\ z_I \end{bmatrix} = [R_{OI}] \begin{bmatrix} x' \\ y' \\ z' \end{bmatrix}
\qquad (2.1.2)
$$

so that

$$
\begin{bmatrix} x' \\ y' \\ z' \end{bmatrix} = [R_{OI}]^T [R_{BI}] \begin{bmatrix} x_B \\ y_B \\ z_B \end{bmatrix}
\qquad (2.1.3)
$$

where

$$
[R_{OI}]^T = [R_{IO}]
\qquad (2.1.4)
$$

is the transposed of the matrix $[R_{OI}]$ while (x_B, y_B, z_B) is the satellite body-axis reference frame as shown in Figure 2.1.1. The matrix $[R_{OI}]$ is derived through three sequential rotations of the inertial reference frame (x_I, y_I, z_I) in order to transform it into the orbiting reference frame (x', y', z'). The first rotation is around the axis z_I and defines the line of nodes of the orbit so that the angle β is the argument of nodes, the second one is around the transformed axis y_I' and defines the orbit inclination i and the third one is around the transformed axis z_I' and defines the argument of latitude γ. Because of the orientation of the orbiting reference frame adopted in SKYHOOK and depicted in Figure 2.1.1 the inertial reference frame needs to be further rotated 180° around the

axis x'. This extra rotation implies a change in sign of the second and third row of the rotation matrix so that:

$$[R_{IO}] = \begin{bmatrix} 1 & 0 & 0 \\ 0 & -1 & 0 \\ 0 & 0 & -1 \end{bmatrix} \begin{bmatrix} \cos\gamma & \sin\gamma & 0 \\ -\sin\gamma & \cos\gamma & 0 \\ 0 & 0 & 1 \end{bmatrix} \begin{bmatrix} 1 & 0 & 0 \\ 0 & \cos i & \sin i \\ 0 & -\sin i & \cos i \end{bmatrix} \begin{bmatrix} \cos\beta & \sin\beta & 0 \\ -\sin\beta & \cos\beta & 0 \\ 0 & 0 & 1 \end{bmatrix} \quad (2.1.5)$$

and finally:

$$[R_{IO}] = \begin{bmatrix} \cos\gamma\cos\beta - \sin\gamma\sin\beta\cos i & \cos\gamma\sin\beta + \sin\gamma\cos\beta\cos i & \sin\gamma\sin i \\ \sin\gamma\cos\beta + \cos\gamma\cos i\sin\beta & \sin\beta\sin\gamma - \cos\gamma\cos\beta\cos i & -\cos\gamma\sin i \\ -\sin i\sin\beta & \sin i\cos\beta & -\cos i \end{bmatrix} \quad (2.1.6)$$

The rotation matrix between the satellite body reference frame and the inertial reference frame was derived in the Interim Report "Study of Tethered Satellite Active Attitude Control," G. Colombo, October 1982, Contract NAS8-33691. The reverse transformation matrix, from body-axis to inertial axis is as follows:

$$[R_{BI}] = \begin{bmatrix} \cos\psi\cos\phi- & -\sin\psi\cos\phi- & \sin\theta\sin\phi \\ \cos\theta\sin\phi\sin\psi & \cos\theta\sin\phi\cos\psi & \\ \cos\psi\sin\phi+ & -\sin\psi\sin\phi+ & -\sin\theta\cos\phi \\ \cos\theta\cos\phi\sin\psi & \cos\theta\cos\phi\cos\psi & \\ \sin\psi\sin\theta & \cos\psi\sin\theta & \cos\theta \end{bmatrix} \qquad (2.1.7)$$

In equation (2.1.7) ψ is the pitch angle, θ is the roll and ϕ is the yaw angle of the satellite. All of them are referred to the inertial reference frame so that they give the inertial attitude of the satellite.

The matrix to transform the body reference frame into the rotating reference frame is therefore given by:

$$[R_{BO}] = [R_{IO}] \ [R_{BI}] \qquad (2.1.8)$$

where the matrix $[R_{IO}]$ and $[R_{BI}]$ are given by expression (2.1.6) and (2.1.7) respectively. The matrix multiplication is not performed analytically since it is more convenient to implement it on the computer. Once the matrix $[R_{BO}]$ is obtained we can derive the Euler angles with respect to the orbiting reference frame as follows:

$$[R_{BO} = \begin{bmatrix} a_1 & a_2 & a_3 \\ \beta_1 & \beta_2 & \beta_3 \\ \gamma_1 & \gamma_2 & \gamma_3 \end{bmatrix} \qquad (2.1.9)$$

and

$$\tan \phi\prime = - \frac{a_3}{\beta_3}$$

$$\tan \psi\prime = \frac{\gamma_1}{\gamma_2}$$

$$\tan \theta\prime = \sqrt{\gamma_1{}^2 + \gamma_2{}^2 / }\ \gamma_3 \qquad (2.1.10)$$

The last relation has an unavoidable sign ambiguity. The sign is chosen positive for convenience.

The matrix $[R_{BO}]$ can also be written starting from the Euler angles relative to the orbiting reference frame ($\psi\prime$, $\theta\prime$, $\phi\prime$). Referring to equation (2.1.9) the elements of the matrix can be written as follows:

$$a_1 = \cos\psi\prime\cos\phi\prime - \cos\theta\prime\sin\phi\prime\sin\psi\prime$$

$$a_2 = -\sin\psi\prime\cos\phi\prime - \cos\theta\prime\sin\phi\prime\cos\psi\prime$$

$$a_3 = \sin\theta\prime\sin\phi\prime$$

$$\beta_1 = \cos\psi\prime\sin\phi\prime + \cos\theta\prime\cos\phi\prime\sin\psi\prime$$

$$\beta_2 = -\sin\psi\prime\sin\phi\prime + \cos\theta\prime\cos\phi\prime\cos\psi\prime$$

$$\beta_3 = -\sin\theta\prime\cos\phi\prime$$

$$\gamma_1 = \sin\psi\prime\sin\theta\prime$$

$$\gamma_2 = \cos\psi\prime\sin\theta\prime$$

$$\gamma_3 = \cos\theta\prime \qquad (2.1.11)$$

Because of equation (2.1.8) the matrix of the body-axis direction cosines in inertial axis is given by:

$$[R_{BI}] = [R_{IO}]^T\ [R_{BO}] \qquad (2.1.12)$$

The matrix [R_{IO}] can be built in a similar way as shown in equation (2.1.11) by just substituting (γ, i, β) to (ψ', θ', ϕ') in the same order. Once the matrix [R_{BI}] is obtained, the inertial Euler angles can be derived with expression formally similar to equations (2.1.10). This reverse process is necessary in setting up inertial initial conditions in the SKYHOOK preprocessor DUMBEL, in the case of a generic orbit, starting from rotating reference frame initial conditions. Before this time, the conversion had been done in the simplified case of circular and equatorial orbit.

The satellite angular velocities can also be derived fairly easily by using the velocity composition and the matrix transformation, as follows:

$$
\begin{bmatrix} \omega_1 ' \\ \omega_2 ' \\ \omega_3 ' \end{bmatrix} = \begin{bmatrix} \omega_1 \\ \omega_2 \\ \omega_3 \end{bmatrix} - [R_{BI}]^T \begin{bmatrix} \Omega_x \\ \Omega_y \\ \Omega_z \end{bmatrix}
\qquad (2.1.13)
$$

In equation (2.1.13) (ω_1', ω_2', ω_3') are the body-axis angular velocity components as measured from an observer moving with the rotating reference frame; (ω_1, ω_2, ω_3) are the inertial angular velocity components in body-axis; (Ω_x, Ω_y, Ω_z) are the inertial angular rates of the rotating reference frame in inertial axis while the matrix [R_{BI}]^T = [R_{IB}] transforms the components from inertial axis to body-axis. The vector (ω_1, ω_2, ω_3) has a special significance because its components are the quantities measured by a gyro package strapped down to the satellite. (ω_1', ω_2', ω_3') are similar components but they are obtained from the inertial vector (ω_1, ω_2, ω_3) after filtering out the orbital motion of the system.

All these matrix transformations allows the simulation program to switch from the inertial reference frame representation to the orbiting

reference frame representation and vice versa. The outcome is to present the output in a physically meaningful form and to have the possibility of setting up initial conditions in SKYHOOK for a generic orbit.
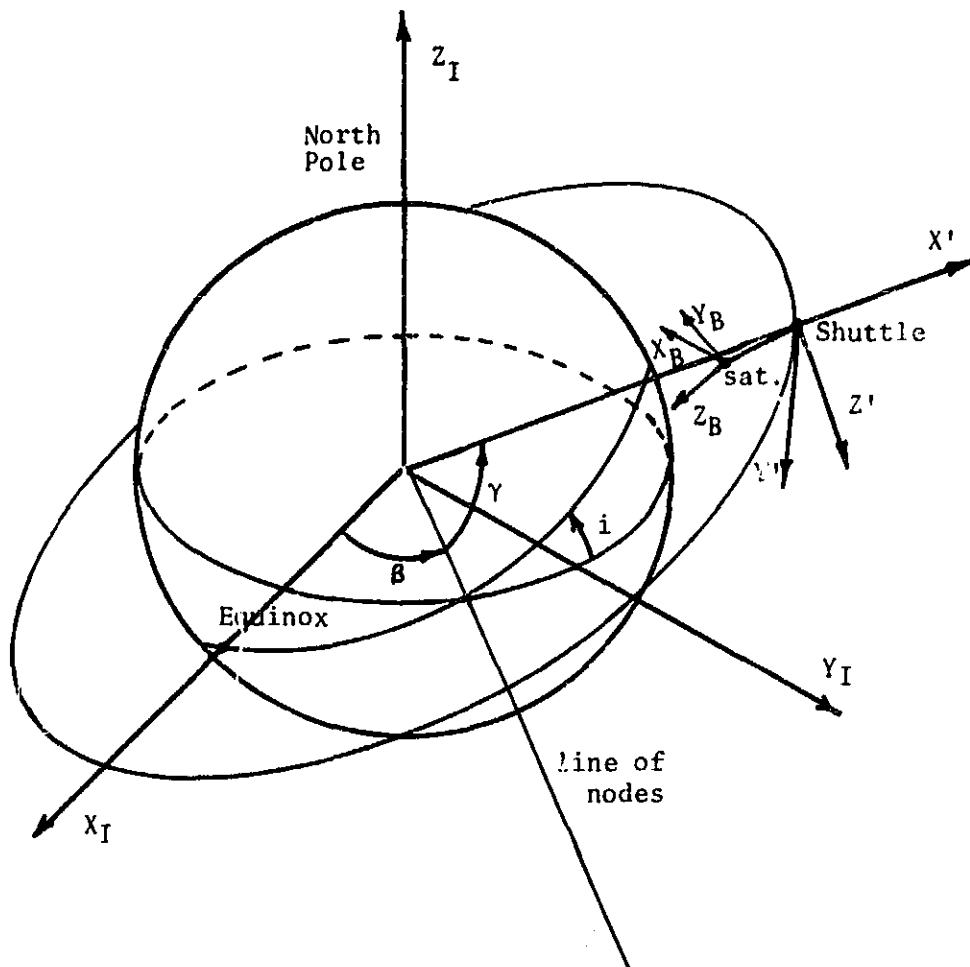
Figure 2.1.1   Satellite Rotational Dynamics.
System Reference Frames.

2.1.3 Relations Between The Euler Angular Velocities And The Body-Axis
Angular Velocities -

   In the present version of SKYHOOK the body-axis angular velocities are
derived from the integration of Euler equations of the satellite.   The
body-axis angular velocities are then related to the derivatives of the
direction cosines. After a second integration the direction cosine matrix
is obtained and the inertial Euler angles are derived by means of equations
like (2.1.10).   This process can be strongly simplified as follows: a)
after the first integration of the Euler equations, the body-axis angular
velocities can be analytically transformed to Euler angular velocities, b)
inertial Euler angles can then be directly obtained with a second integra-
tion.

   The body-axis angular velocities are related to Euler angular veloci-
ties as follows:

$$
\begin{bmatrix} \omega_1 \\ \omega_2 \\ \omega_3 \end{bmatrix} = \begin{bmatrix} \sin\theta\sin\psi & \cos\psi & 0 \\ \sin\theta\cos\psi & -\sin\psi & 0 \\ \cos\theta & 0 & 1 \end{bmatrix} \begin{bmatrix} \dot{\phi} \\ \dot{\theta} \\ \dot{\psi} \end{bmatrix}
\qquad (2.1.14)
$$

If the transformation matrix is reversed (note that this is not an orthogo-
nal matrix) we get:

$$\begin{bmatrix} \dot{\phi} \\ \dot{\theta} \\ \dot{\psi} \end{bmatrix} = \begin{bmatrix} \sin\psi/\sin\theta & \cos\psi/\sin\theta & 0 \\ \cos\psi & -\sin\psi & 0 \\ -\sin\psi\cot g\theta & -\cos\psi\cot g\theta & 1 \end{bmatrix} \begin{bmatrix} \omega_1 \\ \omega_2 \\ \omega_3 \end{bmatrix} \qquad (2.1.15)$$

The problem associated with equation (2.1.15) is that it becomes singular when the inertial roll angle $\theta = 0°$ that is to say when the satellite longitudinal axis is perpendicular to the equatorial plane. This means, for example, that in the case of an equatorial orbit, equation (2.1.15) becomes singular when the satellite is at 90 degree with respect to the tether (because of the reference frame conventions in SKYHOOK $\theta = 0°$ in this case). As the orbital inclination increases the margin on the inertial roll angle that makes equation (2.1.15) singular is reduced. Far from the polar orbit, however, there are no problems in running SKYHOOK with this more efficient procedure.

The line that we are following is to have both options available in the computer code in order to use the novel and more efficient approach when possible. The standard option will be used for the special cases when the satellite attitude is near a singularity.

2.1.4 Torque And Force Package Update -

The external torques acting upon the satellite are as follows:

a. The yaw torque provided by the yaw control thrusters

b. The spurious torques due to misalignments of the out-of-plane,
    in-plane and in-line thrusters

c. The torques due to the passive dampers of the satellite

d. The torque due to the tether tension

Since, in our computer code, the satellite attitude dynamics is modeled, by
Euler equations, all the external torques must be expressed in satellite
body-axis. The Euler equations of the satellite are given by:

$$\begin{bmatrix} I_1\dot{\omega}_1 - \omega_2\omega_3 \ (I_2-I_3) \\ I_2\dot{\omega}_2 - \omega_3\omega_1 \ (I_3-I_1) \\ I_3\dot{\omega}_3 - \omega_1\omega_2 \ (I_1-I_2) \end{bmatrix} = \vec{N}_{Ten} + \vec{N}_{YT} + \vec{N}_{MIS} + \vec{N}_{Dam} \qquad (2.1.16)$$

In (2.1.15), the vector $\vec{N}_{Ten}$ is the torque due to the tether tension (it is
already modeled in the computer code), the vector $\vec{N}_{YT}$ is the torque due to
the yaw thrusters, the vector $\vec{N}_{MIS}$ is the torque due to thruster misalign-
ments and $\vec{N}_{Dam}$ is the one due to the dampers on board the satellite.

I_1, I_2, I_3 are the satellite moments of inertia and ω_1, ω_2, ω_3 are the
components of the satellite rotational velocity in body-axis. The torque
$\vec{N}_{YT}$ has one component only, along the vertical axis of the satellite, so
that:

$$\vec{N}_{YT} = \begin{bmatrix} 0 \\ 0 \\ N_{3YT} \end{bmatrix}$$

(2.1.17)

N_{3YT} must be modeled according to the latest version of the AERITALIA control logic. In general it is a pulse modulated signal, presently with an amplitude of 1 Nm. Pulses are modulated according to the yaw angle ϕ and the yaw angular rate $\dot{\phi}$ in order to stabilize the yaw attitude of the satellite or to maintain a constant spin rate.

The torque $\vec{N}_{MIS}$ can be itemized in terms of in-plane, out-of-plane and in-line thrusters as follows:

$$\vec{N}_{MIS} = \begin{bmatrix} F_{IP} \\ 0 \\ 0 \end{bmatrix} X \left\{ b_1 \right\} + \begin{bmatrix} 0 \\ F_{OP} \\ 0 \end{bmatrix} X \left\{ b_2 \right\} + \begin{bmatrix} 0 \\ 0 \\ F_{IL} \end{bmatrix} X \left\{ b_3 \right\}$$

(2.1.18)

In equation (2.1.18) F_{IP}, F_{OP} and F_{IL} are the thrust level of the in-plane, out-of-plane and in-line thruster respectively. The vectors b_1, b_2 and b_3 are the arms of the thrust vectors with respect to the satellite c.m. Since the satellite is spherical and the thrusters are located on the outer shell, the arm vector can be expressed in terms of angular misalignments as follows:

$$b_k = R \begin{bmatrix} \sin\alpha_{k,1} \\ \sin\alpha_{k,2} \\ \sin\alpha_{k,3} \end{bmatrix}$$

(2.1.19)

where:

$$k = (1,2,3) \quad \text{and} \quad \alpha_{k,j} = 0 \quad \text{if} \quad k = j \quad\quad (2.1.20)$$

$$\alpha_{k,j} \neq 0 \quad \text{if} \quad k \neq j$$

$\alpha_{k,j}$ are the cartesian components of the angular misalignment between the actual thruster longitudinal axis and its theoretical position. In the case of an in-plane thruster, for example, the overall angular misalignment is given by:

$$|\alpha_1| = \sin^{-1} [\sin^2(\alpha_{1,2}) + \sin^2(\alpha_{1,3})]^{1/2} \quad\quad (2.1.21)$$

where $x_B = 1$, $y_B = 2$ and $z_B = 3$; x_B, y_B and z_B, being the satellite body axis.

The thrust levels F_{IP}, F_{OP} and F_{IL} must be modeled according to the selected control logic. In particular the in-line thruster has a two-staged thrust level and it is switched on, in a continuous operation mode, every time that the tension falls below 2N as follows:

$$F_{IL} = 1N \quad \text{if} \quad 1N < T \leq 2N$$

$$F_{IL} = 2N \quad \text{if} \quad T \leq 1N \quad\quad (2.1.22)$$

where T is the tether tension.

The most efficient way to activate the out-of-plane thrusters is when the satellite crosses the local vertical so that its velocity is maximum. To further improve the efficiency it is convenient to let the out-of-plane

oscillation build up to 20° or 30° and then fire the thruster at the next crossing. The firing time is given by:

$$\Delta t_{OP} = (m_{ss} + \frac{1}{3} m_t)\ V_{OPmax}/E_{OP} = (m_{ss} + \frac{1}{3} m_t)\ (2\Omega\ B_{max}\ \ell)/E_{OP} \quad (2.1.23)$$

In equation (2.1.23) m_{ss} is the satellite mass, m_t is the tether mass (that is negligible for short tether length), V_{OPmax} is the out-of-plane velocity of the satellite at the crossing of the local vertical, B_{max} is the amplitude of the out-of-plane angle of the tether before thruster activation. All the other terms are self explanatory. It is interesting to notice that the satellite velocity V_{OPmax} is fairly constant with the tether length. In fact from the out-of-plane rotational energy conservation (it holds true in first approximation because the damping is very low) we get:

$$V_{OPmax} = 2\Omega B_o \ell_c / [\,(m_{ss} + \frac{1}{3}\ \mu\ell)/(m_{ss} + \frac{1}{3}\ \mu\ell_o)\,]^{1/2} \quad (2.1.24)$$

In equation (2.1.24) the index "o" stands for values computed at the beginning of retrieval and μ is the linear density of the tether. For tethers few kilometers long, equation (2.1.24) is essentially independent from the tether length ℓ.

The in-plane thruster control logic is theoretically similar to the out-of-plane one. However, the in-plane control is more complicate because the tether oscillation has a variable bias dependent upon the Coriolis force and the air drag. The firing time will have an expression similar to equation (2.1.23), as follows:

$$\Delta t_{IP} = (m_{ss} + \frac{1}{3} m_t) V_{IPmax}/E_{IP} = (m_{ss} + \frac{1}{3} m_t)\ (\sqrt{3}\ \Omega\ A_{max}\ \ell)/E_{IP} \quad (2.1.25)$$

This time, however, all the angular quantities must be computed from the in-plane bias and the in-plane thrusters must be activated when the satellite crosses it. The evaluation of the in-plane oscillation bias could be performed by software processing of the radar observations (if this is at all feasible). A simplified analytical expression for it, valid for an exponential retrieval control law, is as follows:

$$A_b = \frac{1}{3} \sin^{-1} \left[\frac{2}{t_c \Omega \cos(A_b)} - \frac{1}{2} \frac{S}{m_{ss}} C_D \rho_A \frac{(R_o+H)^2}{\ell} \right] \qquad (2.1.26)$$

Equation (2.1.26) can be further simplified, for small angle, by assuming $\cos(A_b) \simeq 1$ so that it becomes very easy to compute the angular bias. In equation (2.1.26) t_c is the retrieval time constant, C_D is the drag coefficient of the satellite, S its cross section (the tether cross section is neglected because the bias angle builds up when the tether is short), ρ_A is the atmospheric density, R_e the earth radius and H the orbital altitude.

The software implementation of the torque and force package in our computer code is presently underway. The torque $\vec{N}_{Ten}$ due to the tether tension is already available. The torque $\vec{N}_{Damp}$ due to the satellite attitude dampers has been examined only in a simplified way. The implementation and design of roll and pitch passive dampers has been recently studied by the Italian prime contractor. We will contact AERITALIA in the near future to understand what the present status is in order to model the damping torques accordingly.

2.1.5 Current Status Of Rotational Dynamics Code -

Under NASA Contract NAS8-32199, a version of the DUMBEL program was created which includes the rotational dynamics of the subsatellite. This code has a model for a damping torque proportional to the rate of change of the angle between the wire and the vector from the center of mass of the subsatellite to the attachment point of the wire. The program is documented in Appendix III of the Final Report "Study of the Dynamics of a Tethered Satellite System (SKYHOOK)," Kalaghan et al., March 1978.

Under NASA Contract NAS8-33691, the code developed in DUMBEL, but without the damping model, was implemented in the SKYHOOK computer program. This work is described in the Interim Report, "Study of Tethered Satellite Active Attitude Control," G. Colombo, October 1982. The code was tested with a rudimentary thruster model that applied a constant torque about any of the three body axes. A special test case was also devised in which the subsatellite precesses under the torque of the wire at the same rate as the orbital angular velocity. In this case, the subsatellite maintains a fixed orientation between the symmetry axis and the rotating orbital reference frame. In order to show the orientation in the orbital frame, an equatorial orbit was run and the direction cosine matrix was rotated about the z-axis by the orbital angle in order to derive Euler angles in the rotating reference frame. The code was not developed to the point of being able to give Euler angles with respect to an arbitrary orbital reference frame.

2.1.6 Implementation Of The Transformation To The Rotating Orbital Reference Frame -

In order to perform simulations for arbitrary orbital elements and obtain meaningful displays of the subsatellite rotation it is necessary to be able to set up initial conditions in a rotating orbital reference frame and be able to display the output orientation angles in that coordinate system. In the method of direction cosines, the coordinates of a point $\vec{x}'$ with respect to the body axes are given as a function of the inertial coordinates $\vec{x}$ by the equation

$$\vec{x}' = A \vec{x} \qquad (2.1.27)$$

where

$$A = \begin{bmatrix} \alpha_1 & \beta_1 & \gamma_1 \\ \alpha_2 & \beta_2 & \gamma_2 \\ \alpha_3 & \beta_3 & \gamma_3 \end{bmatrix} \qquad (2.1.28)$$

The matrix A can be expressed as the product of three matrices representing rotations by the Euler angles. That is,

$$A = B(\psi)C(\theta)D(\phi) \qquad (2.1.29)$$

where

$$B(\psi) = \begin{bmatrix} \cos\psi & \sin\psi & 0 \\ -\sin\psi & \cos\psi & 0 \\ 0 & 0 & 1 \end{bmatrix}$$

$$C(\theta) = \begin{bmatrix} 1 & 0 & 0 \\ 0 & \cos\theta & \sin\theta \\ 0 & -\sin\theta & \cos\theta \end{bmatrix}$$

$$D(\phi) = \begin{bmatrix} \cos\phi & \sin\phi & 0 \\ -\sin\phi & \cos\phi & 0 \\ 0 & 0 & 1 \end{bmatrix}$$

In the case of an equatorial orbit with the Shuttle initially on the x-axis, the orbital reference frame initially coincides with the inertial reference frame so that equation (2.1.29) gives the initial conditions. In general the transformation from the inertial frame to the rotating orbital reference frame can be given as:

$$E = B(\gamma)C(i)D(\beta) \tag{2.1.30}$$

where β is the argument of the ascending mode, i is the orbital inclination, and γ is the argument of latitude (the angle from the node to the Shuttle in the plane of the orbit). Equation (2.1.30) has the same form as equation (2.1.29). The transformation E gives the coordinates of a point in the orbital reference frame as a function of the coordinates in the inertial frame. For arbitrary orbital elements the transformation from

$$F = GE \tag{2.1.31}$$

and

$$G = B(\psi\prime)C(\theta\prime)D(\phi\prime) \qquad\qquad (2.1.32)$$

The angles $\theta\prime$, $\phi\prime$, and $\psi\prime$ give the relationship between the orbital frame and the body axis frame. Equation (2.1.31) giving F as a function of six rotations can be used to set up the initial direction cosine matrix for arbitrary orbital elements and arbitrary orientation of the body axes with respect to the orbital reference frame.

The tension in the wire is computed using the distance from the Shuttle to the attachment point of the wire. In order to set up equilibrium initial conditions, the positions of the attachment point and the center of mass of the subsatellite must be known in inertial coordinates. If the coordinates of the attachment point in the body axis frame are given by the vector $\vec{r}\prime$, the coordinates in inertial space are given by

$$\vec{r} = F^T \vec{r}\prime \qquad\qquad (2.1.33)$$

where F^T is the transpose of the matrix F. In the DUMBEL program the vector $\vec{r}$ is subtracted from the position of the attachment point to compute the initial position of the center of mass of the subsatellite.

The rotational motion of the subsatellite is obtained by integrating vs time the nine elements of the matrix F and the three components of the angular velocity along the body axes. The angular quantities are not integrated directly. At any instant of time the nine direction cosines can be interpreted either as the results of three rotations as in the case of the matrix A, or as six rotations as in the case of matrix F. A convenient

form of output would be to give the three angles, $\theta\prime$, $\phi\prime$, and $\psi\prime$ which define the transformation G from the orbital frame to body axes. Since F = GE we can obtain the matrix G by post multiplying by E^T to give

$$EE^T = GEE^T = G \qquad (2.1.34)$$

We can then derive the angles $\theta\prime$, $\phi\prime$, and $\psi\prime$ from the matrix G. A method of obtaining these angles is derived in Section 2.1.2 of this report. The results of the derivation are

$$\tan\phi\prime = -\alpha_3/\beta_3$$
$$\tan\psi\prime = \gamma_1/\gamma_2 \qquad (2.1.35)$$
$$\tan\theta\prime = \sqrt{\gamma_1{}^2 + \gamma_2{}^2}/\gamma_3$$

where α and γ are direction cosines as defined for the matrix A. The explicit representation of the direction cosines in terms of Euler angles is given in equations (2.1.11) of the above cited Section.

2.1.7 Rotational Dynamics Co_) First Level Update -

As a first step in the present study, a few of the cases used to test the program have been rerun and the output checked against the original test runs. The original version of the program uses explicit expressions for the elements of the matrix in equation (2.1.28). The matrix F involves six rotations, which would be very cumbersome to do analytically. There-fore, a set of general purpose subroutines have been written to manipulate 3 x 3 matrices numerically. Subroutine ROTMAT(IAXIS,ANGLE,A) sets up a

matrix A to perform a rotation about axis number "IAXIS" through an angle "ANGLE." The explicit form of the matrices for each axis with ANGLE = θ are

$$
1 = \begin{bmatrix} 1 & 0 & 0 \\ 0 & \cos\theta & \sin\theta \\ 0 & -\sin\theta & \cos\theta \end{bmatrix}
$$

$$
2 = \begin{bmatrix} \cos\theta & 0 & -\sin\theta \\ 0 & 1 & 0 \\ \sin\theta & 0 & \cos\theta \end{bmatrix}
$$

$$
3 = \begin{bmatrix} \cos\theta & \sin\theta & 0 \\ -\sin\theta & \cos\theta & 0 \\ 0 & 0 & 1 \end{bmatrix}
$$

Subroutine MATMUL (A,B,C) performs the matrix multiplication C = A x B. Subroutine STATVEC (THETA, PUI, PSI, A) creates the direction cosine matrix $A = B(\psi)C(\theta)D(\phi)$. This has been tested against the original subroutine which uses analytic expressions for the nine direction cosines and gives the same results. Subroutine TRNSPOS (A, AT) performs the operation $AT = A^T$. Subroutine VECMUL(A, V, VP) performs the operation $\vec{VP} = A \times \vec{V}$ where $\vec{V}$ and $\vec{VP}$ are vectors and A is a 3x3 matrix. The original version of subroutine ROTSTAT in program DUMBEL has been replaced by a more general version ROTSTAT (AN,RI,AL,THETA,PHI,PSI,DTHETA,DPHI,DPSI,Y,A,DIRCOS), where AN is the argument of the node, RI is the orbital inclination, AL is the argument of latitude, THETA, PHI and PSI are the Euler angles with respect to the rotating orbital coordinate frame. DTHETA, DPHI, and DPSI are the

rates of change of the angles in inertial space but referred to the axes of the rotating orbital reference frame. The angular velocity in inertial space is the angular velocity in the rotating frame plus the orbital angular velocity. The way the Euler angles are defined, $\dot{\phi}\prime$ is parallel to the orbital angular velocity, so that the angular velocity in inertial space can be obtained by adding the orbital angular velocity Ω to the $\dot{\phi}\prime$ which is the rate of change of $\phi\prime$ with respect to the rotating orbital frame. The components of the angular velocity along the body axes can be obtained using the equations

$$\omega_1 = \dot{\phi}\sin\theta\prime\sin\psi\prime + \dot{\theta}\cos\psi\prime$$

$$\omega_2 = \dot{\phi}\sin\theta\prime\cos\psi\prime - \dot{\theta}\sin\psi\prime$$

$$\omega_3 = \dot{\phi}\cos\theta\prime + \dot{\psi}$$

where $\dot{\theta}$, $\dot{\phi}$, and $\dot{\psi}$ are the rates in inertial space.

Subroutine ROTSTAT creates the matrices

$$E = B(AL)C(RI)D(AN)$$

and

$$G = B(\psi\prime)C(\theta\prime)D(\phi\prime)$$

using subroutine STATVEC and then performs the operation $F = GxE$. The matrix F is returned as DIACOS, and placed in A, the rotational part of the state vector. (The positional part, Y, of the state vector is not used in this version). The position of the attachment point of the wire is com-

puted by the equation

$$\vec{R}_{s} = F^{T}\vec{R}_{B}$$

and returned via common.

In order to display the rotation of the subsatellite in the rotating orbital reference frame, we must have the instantaneous orbital parameters. These can be obtained from the position $\vec{P}$ and velocity $\vec{V}$. The unit vector normal to the orbit $\vec{n}$ is in the direction $\vec{P}x\vec{V}$. The orbital inclination is $\cos^{-1} n_{z}$. The argument of the node is $\tan^{-1} n_{y}/n_{x}$. If we call $\vec{x}$ a unit vector along the node and $\vec{y}$ a unit vector in the direction $\vec{n} \times \vec{x}$, we can get the sine and cosine of the argument of latitude from the components of $\vec{P}$ along $\vec{y}$ and $\vec{x}$. Subroutine ELEM (P,V,AN,RI,AL) computes the argument of the node AN, the inclination RI, and argument of latitude AL from the position $\vec{P}$ and velocity $\vec{V}$.

A routine called ANGROT has been written previously to rotate the direction cosine matrix about the z-axis and compute Euler angles from the rotated matrix. This routine has been used for equatorial orbits to give the orientation of the subsatellite in a rotating orbital reference frame. A new version ANGROT (AN,RI,AL,A,ANG) has been written where AN is the argument of the node, RI is the inclination, and AL is the argument of latitude, A is the instantaneous direction cosine matrix called F in the general case, and ANG is a three element array containing the Euler angles with respect to the orbital reference frame. Subroutine ANGROT performs the operation

$$G = FE^{T}$$

using subroutines STATVEC, TRNSPOR, and MATMUL. The vector ANG is then obtained from G. The calls to ELEM and ANGROT are coordinated by subroutine ROTCDORD (Z,A,ANG), where Z is the positional part of the state vector, A is the matrix of direction cosines and ANG is the Euler angles in the rotating orbital reference frame.

2.1.8 Rotational Dynamics Computer Simulations -

Various test cases have been run with the new software described in Section 2.1.6. In the first case the system is in an equatorial orbit with no initial rotation or angular velocity in inertial space. Angular damping is included in the model. In the original version of the program, the rotation of the wire at the orbital angular velocity causes the subsatellite to acquire the orbital angular velocity. Measured in the orbital reference frame, the subsatellite initially rotates away from equilibrium and then returns exponentially to equilibrium. The new software produces the same results and agrees numerically with the previous results.

The second test case is the same as the first but with an orbital inclination of 28°. This run appears to have integrated properly but the output angles were disrupted by a singularity in the angular representation. When the angle θ' is zero, one cannot distinguish between ϕ' and ψ'. In this case the program arbitrary sets $\phi' = 0$ and attributes all the rotation to ψ'. In an equatorial orbit, the z coordinates are always identically zero in the integration. However, in an inclined orbit, numerical roundoff allowed θ' to assume a slightly non-zero value, causing an erratic distribution of the angle between ϕ' and ψ' after the first four output points.

In order to avoid the singularity in the angular representation, a pair of runs was done with non-zero initial values of .1, .2, and .3 degrees for $\theta\prime$, $\phi\prime$, and $\psi\prime$ in the rotating orbital reference frame. Runs at 0° and 28° orbital inclination gave identical time histories of the angles measured in the orbital frame. Figures 2.1.2, 2.1.3, and 2.1.4 give plots of the Euler angles $\theta\prime$, $\phi\prime$, and $\psi\prime$ for the 0° inclination case, and Figures 2.1.5, 2.1.6, and 2.1.7 give the angles at 28° inclination. Small difference appear in the least significant digits.

The last test run is the special case where the subsatellite precesses at the same rate as the orbital angular velocity so that the symmetry axis maintains a fixed orientation with respect to the orbital reference frame. The initial conditions are with $\dot{\phi}$ equal to the orbital angular velocity, and a 28° orbital inclination. The angles $\theta\prime$ and $\phi\prime$ remained constant during the run just as in the equatorial case run with the original version of the program. Figures 2.1.8, 2.1.9, and 2.1.10 show plots of the angles vs. time.
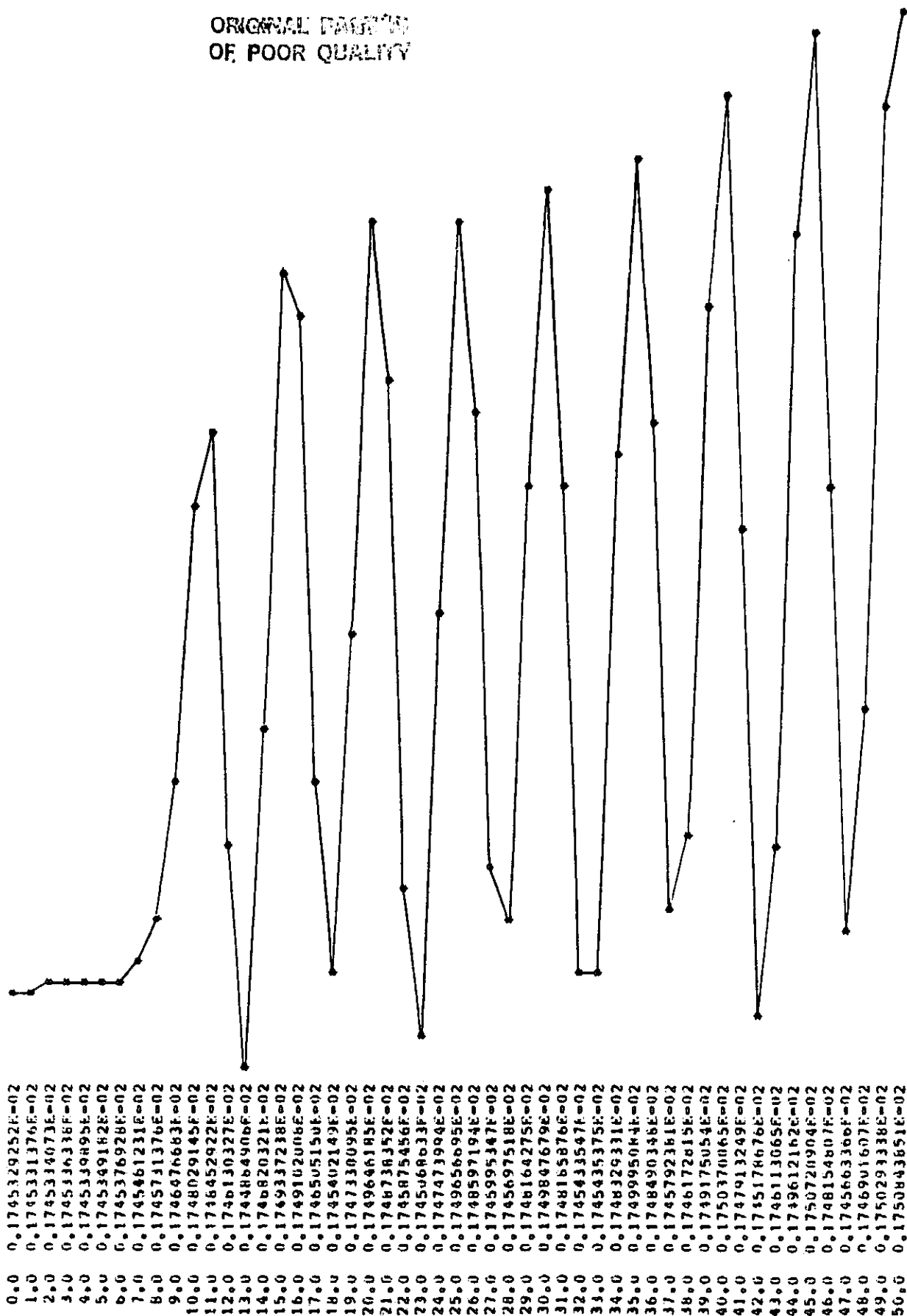
Figure 2.1.2 θ' (radians) vs. time (sec) in an equatorial orbit with initial conditions $\theta_0' = .1°$, $\phi_0' = .2°$, and $\psi_0' = .3°$.

ORIGINAL PAGE IS
OF POOR QUALITY

Figure 2.1.3 $\dot{\phi}'$ (radians) vs. time (sec) in an equatorial orbit with initial conditions $\theta_0' = .1°$, $\phi_0' = .2°$, and $\psi_0' = .3°$.

Figure 2.1.4 ψ' (radians) vs. time (sec) in an equatorial orbit with initial conditions $\theta_0' = .1°$, $\phi_0' = .2°$, and $\psi_0' = .3°$.

t	ψ'
0.0	0.5245987750E-02
1.0	0.4810569510E-02
2.0	0.4294294535E-02
3.0	0.4119414556E-02
4.0	0.4541413619E-02
5.0	0.5995495217E-02
6.0	0.8622719170E-02
7.0	0.1392809725E-01
8.0	0.2323922339E-01
9.0	0.3817784802E-01
10.0	0.5777755130E-01
11.0	0.6290564294E-01
12.0	0.3764379823E-01
13.0	-0.5364732136E-02
14.0	-0.4668494546E-01
15.0	-0.7003629983E-01
16.0	-0.6677480673E-01
17.0	-0.3684378408E-01
18.0	0.7628943447E-02
19.0	0.4824267586E-01
20.0	0.7149100510E-01
21.0	0.6503638459E-01
22.0	0.3269326876E-01
23.0	-0.1293223436E-01
24.0	-0.5327595308E-01
25.0	-0.7189634943E-01
26.0	-0.6154107570E-01
27.0	-0.2646654570E-01
28.0	0.1651194125E-01
29.0	0.5701414449E-01
30.0	0.7294637532E-01
31.0	0.5979157242E-01
32.0	0.2281687599E-01
33.0	-0.2297616646E-01
34.0	-0.6108507415E-01
35.0	-0.7387433486E-01
36.0	-0.5971812926E-01
37.0	-0.1946370643E-01
38.0	0.2875508313E-01
39.0	0.6608005462E-01
40.0	0.7676034847E-01
41.0	0.5690306401E-01
42.0	0.1374991534E-01
43.0	-0.3520966857E-01
44.0	-0.7114778231E-01
45.0	-0.7856250498E-01
46.0	-0.5511136695E-01
47.0	-0.1146648404E-01
48.0	0.3976643111E-01
49.0	0.7475068779E-01
50.0	0.7992468625E-01

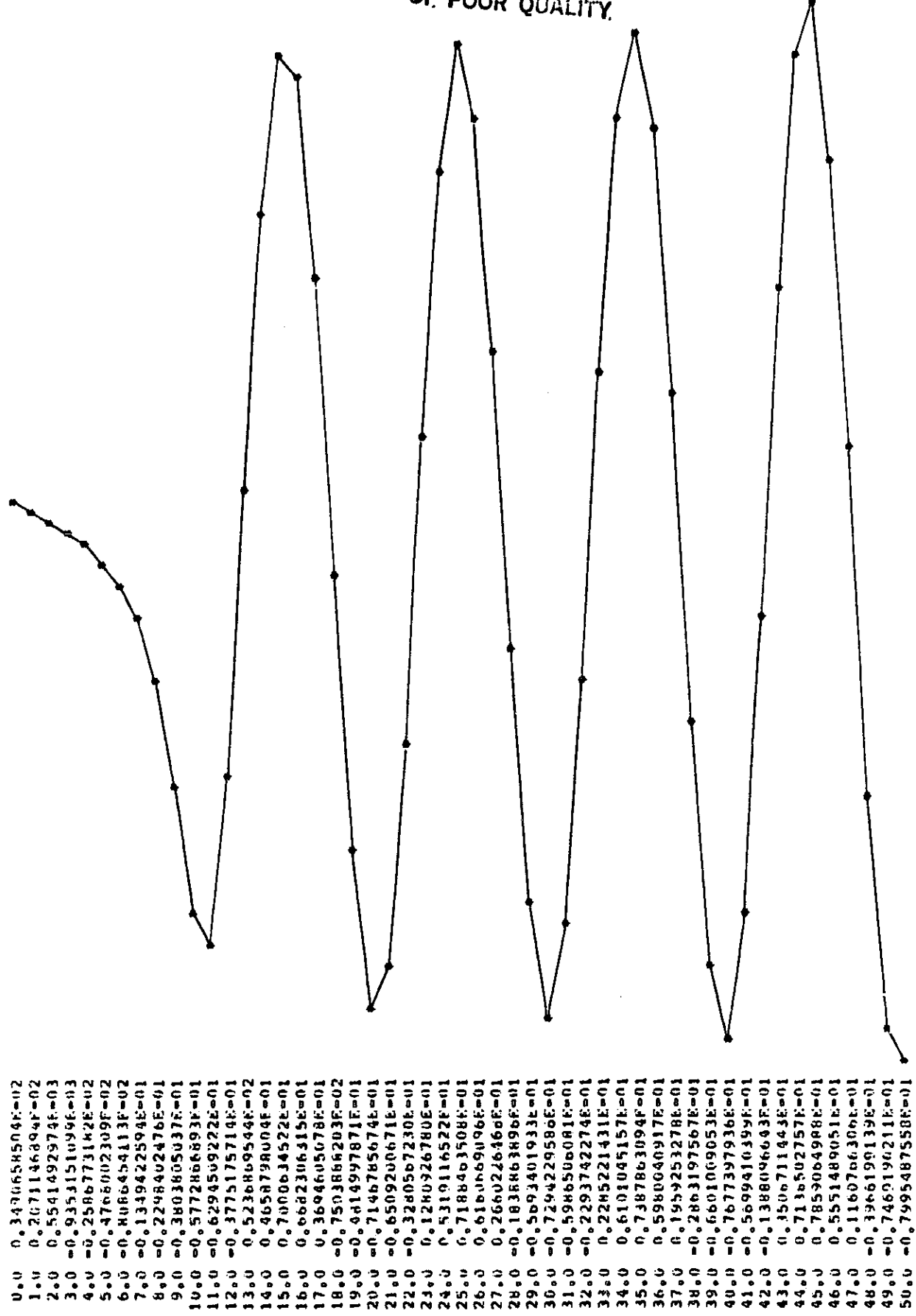| Time	θ'
0.0	0.1745329252E-02
1.0	0.1745331376E-02
2.0	0.1745334073E-02
3.0	0.1745336338E-02
4.0	0.1745339895E-02
5.0	0.1745349192E-02
6.0	0.1745376928E-02
7.0	0.1745461232E-02
8.0	0.1745731372E-02
9.0	0.1746476708E-02
10.0	0.1748029118E-02
11.0	0.1744452911E-02
12.0	0.1746130419E-02
13.0	0.1744484673E-02
14.0	0.1746820033E-02
15.0	0.1749336910E-02
16.0	0.1749101855E-02
17.0	0.1745505157E-02
18.0	0.1745402103E-02
19.0	0.1747329873E-02
20.0	0.1749645931E-02
21.0	0.1748738267E-02
22.0	0.1745875491E-02
23.0	0.1745068576E-02
24.0	0.1747473768E-02
25.0	0.1749654470E-02
26.0	0.1748597096E-02
27.0	0.1745095370E-02
28.0	0.1745497435E-02
29.0	0.1748164056E-02
30.0	0.1749847496E-02
31.0	0.1748185857E-02
32.0	0.1745433571E-02
33.0	0.1745435278E-02
34.0	0.1748329081E-02
35.0	0.1749994826E-02
36.0	0.1747490330E-02
37.0	0.1745792427E-02
38.0	0.1746172665E-02
39.0	0.1749174813E-02
40.0	0.1750369957E-02
41.0	0.1747913251E-02
42.0	0.1745178716E-02
43.0	0.1746112072E-02
44.0	0.1749611856E-02
45.0	0.1750720739E-02
46.0	0.1748154544E-02
47.0	0.1745618249E-02
48.0	0.1746901705E-02
49.0	0.1750293293E-02
50.0	0.1750842141E-02
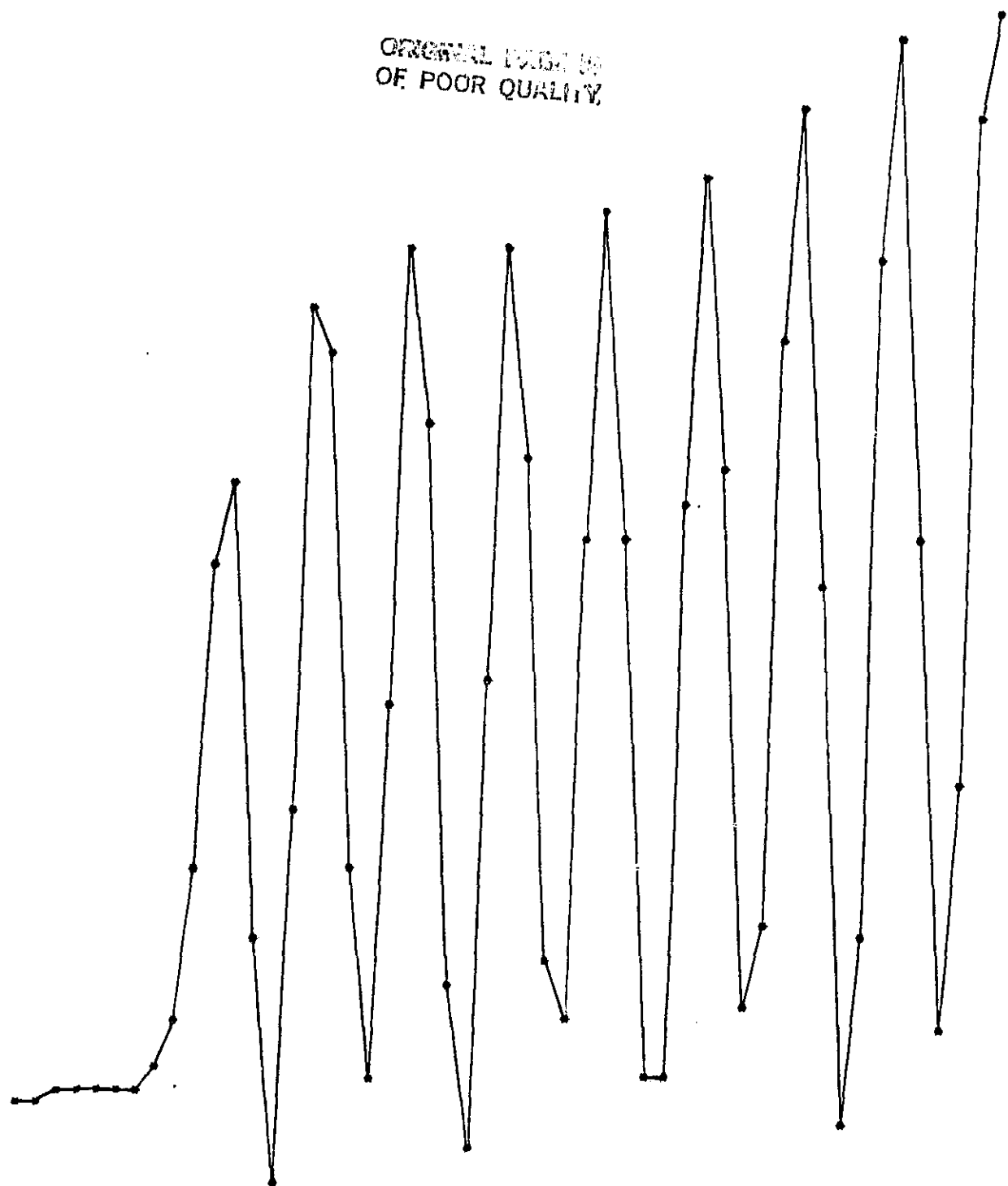
Figure 2.1.5 θ' (radians) vs. time (sec) in a 28° inclination orbit with initial conditions $\theta_0' = .1°$, $\phi_0' = .2°$, and $\psi_0' = .3°$.

t	φ'
0.0	0.3490658504E-02
1.0	0.2071146804E-02
2.0	-0.5541492872E-03
3.0	-0.9351151215E-01
4.0	-0.2586773143E-02
5.0	-0.4768007532E-02
6.0	-0.8086454807E-02
7.0	-0.1349424297E-01
8.0	-0.2298391865E-01
9.0	-0.3803798113E-01
10.0	-0.5772840088E-01
11.0	-0.6294449157E-01
12.0	-0.3775317150E-01
13.0	-0.5233865446E-02
14.0	0.4658460935E-01
15.0	0.7000387525E-01
16.0	0.6682195569E-01
17.0	0.3694651990E-01
18.0	0.7502091549E-02
19.0	-0.4814755103E-01
20.0	-0.7146593319E-01
21.0	-0.6509134731E-01
22.0	-0.3280646599E-01
23.0	0.1280733579E-01
24.0	0.5318893647E-01
25.0	0.7188303146E-01
26.0	0.6160601892E-01
27.0	0.2600328718E-01
28.0	-0.1836679183E-01
29.0	-0.5693199803E-01
30.0	-0.7294098504E-01
31.0	-0.5986500420E-01
32.0	-0.7293830374E-01
33.0	-0.2285025456E-01
34.0	0.6100831611E-01
35.0	0.7397644602E-01
36.0	0.5986059408E-01
37.0	0.1959454461E-01
38.0	-0.2862940593E-01
39.0	-0.6600816805E-01
40.0	-0.7677386365E-01
41.0	-0.5694926204E-01
42.0	-0.1388337669E-01
43.0	0.3508432469E-01
44.0	0.7138283587E-01
45.0	0.7858970374E-01
46.0	0.5551274980E-01
47.0	0.1160348865E-01
48.0	-0.3966397875E-01
49.0	-0.7469194604E-01
50.0	-0.7994323933E-01

Figure 2.1.6 φ' (radians) vs. time (sec) in a 28° inclination orbit with initial conditions $\theta_0' = .1°$, $\phi_0' = .2°$, and $\psi_0' = .3°$.

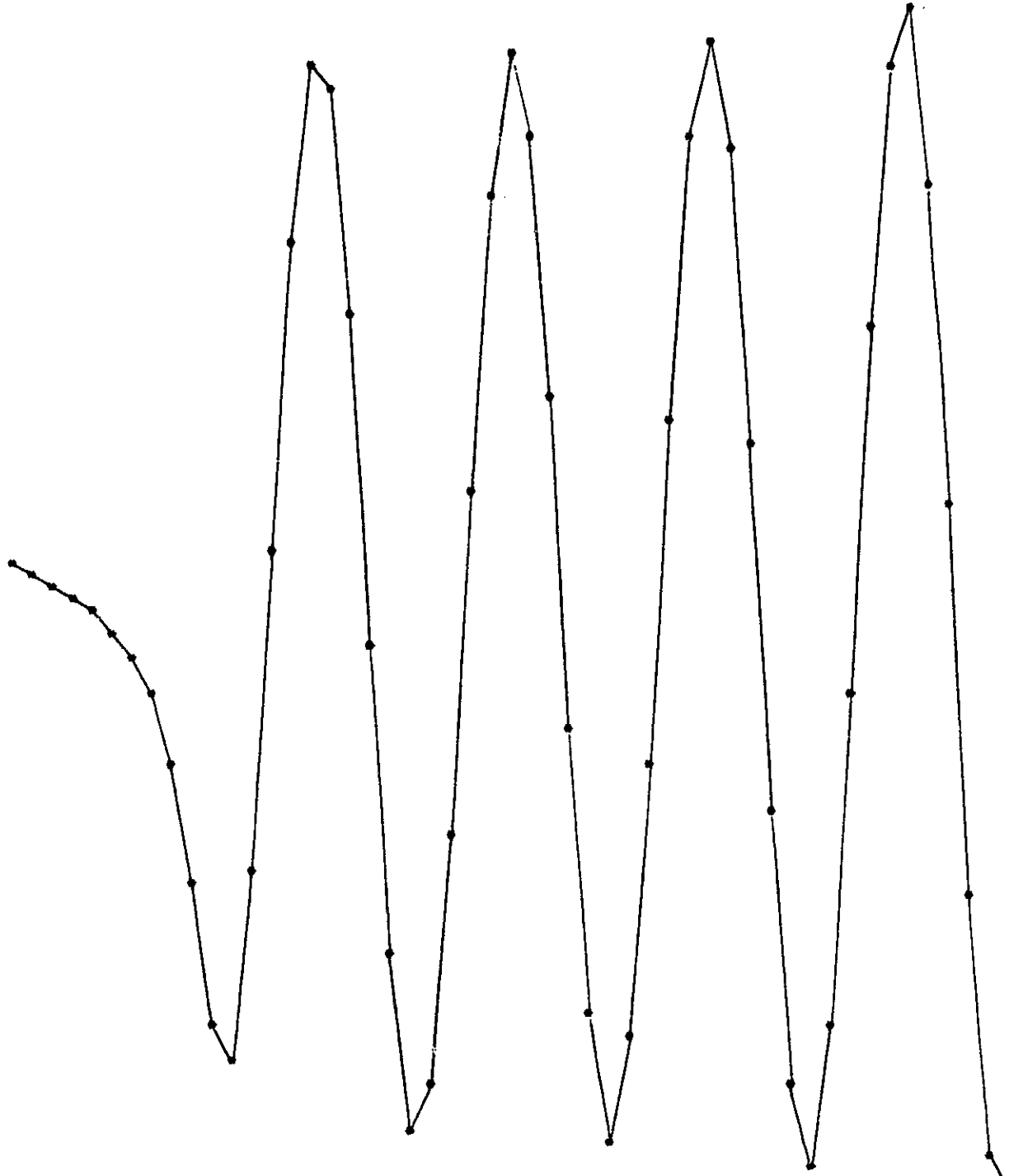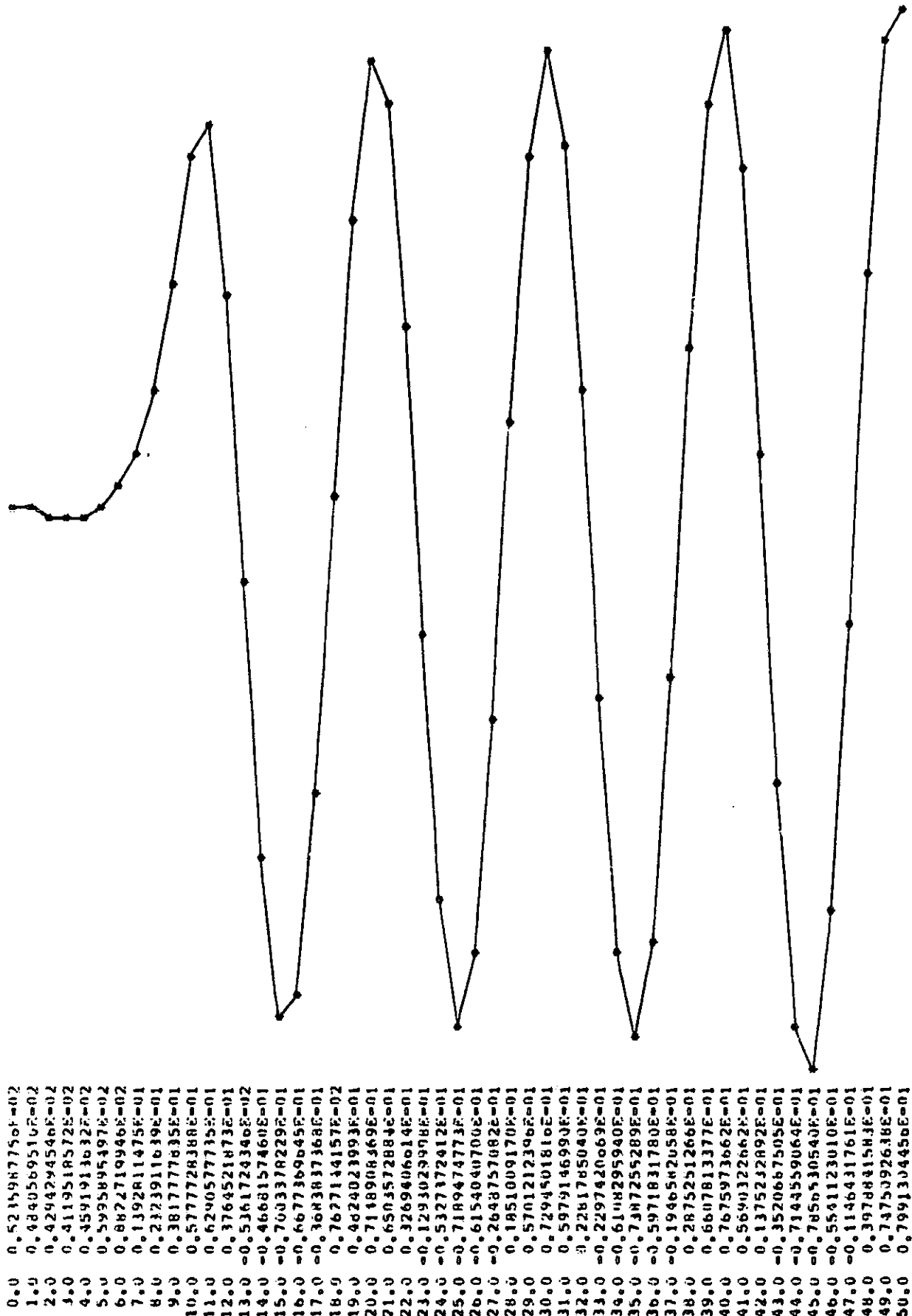| t	ψ'
0.0	0.5215987775E-02
1.0	0.4840569516E-02
2.0	0.4244294546E-02
3.0	0.4119518572E-02
4.0	0.4591915332E-02
5.0	0.5958954997E-02
6.0	0.8824719446E-02
7.0	0.1392811475E-01
8.0	0.2223911639E-01
9.0	0.3817777635E-01
10.0	0.5777728388E-01
11.0	0.6290577735E-01
12.0	0.3764521873E-01
13.0	0.5361724346E-02
14.0	-0.4668157460E-01
15.0	-0.7033378229E-01
16.0	-0.6677369645E-01
17.0	-0.3038373683E-01
18.0	0.7627144157E-02
19.0	0.4240239936E-01
20.0	0.7118908369E-01
21.0	0.6503572884E-01
22.0	0.3269406014E-01
23.0	-0.1293023998E-01
24.0	-0.5327172412E-01
25.0	-0.7189474773E-01
26.0	-0.6154040700E-01
27.0	-0.2648757082E-01
28.0	-0.1851009170E-01
29.0	0.5701212396E-01
30.0	0.7294501810E-01
31.0	0.5979146990E-01
32.0	0.2281785040E-01
33.0	-0.2297420069E-01
34.0	-0.6104295940E-01
35.0	-0.7347255289E-01
36.0	-0.5971831780E-01
37.0	-0.1946582058E-01
38.0	0.2875251266E-01
39.0	0.6607813377E-01
40.0	0.7675973662E-01
41.0	0.5690322662E-01
42.0	0.1375242892E-01
43.0	-0.3520667505E-01
44.0	-0.7144559064E-01
45.0	-0.7856530540E-01
46.0	-0.5541123010E-01
47.0	-0.1146431761E-01
48.0	0.3978884153E-01
49.0	0.7475092638E-01
50.0	0.7991304456E-01

Figure 2.1.7 ψ' (radians) vs. time (sec) in a $28°$ inclination orbit with initial conditions $\theta_0' = .1°$, $\phi_0' = .2°$, and $\psi_0' = .3°$.
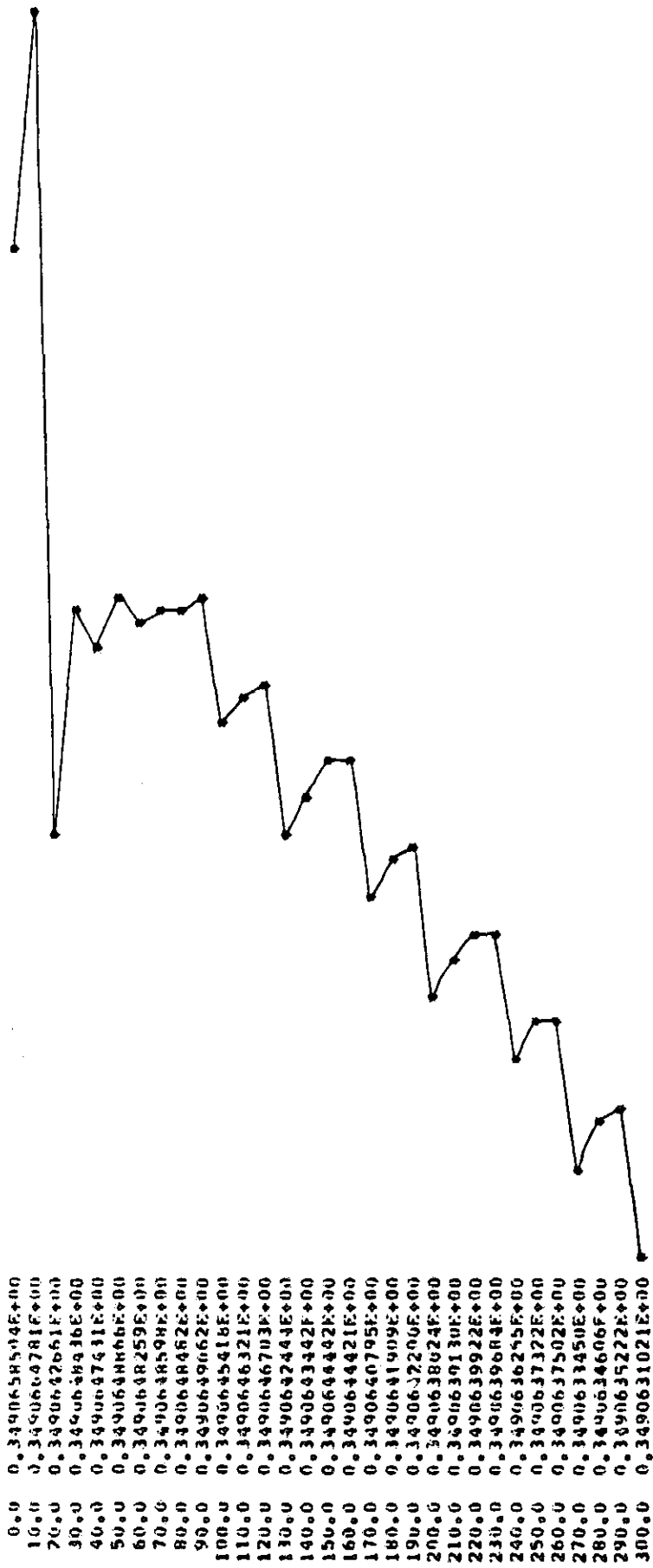
Figure 2.1.8 θ' (radians) vs. time in a 28° inclination orbit for the special test case where the precession rate is equal to the orbital angular velocity.

```
0.0       0.15707961377E+01
10.0      0.15707963172E+01
20.0      0.15707962211E+01
30.0      0.15707960126E+01
40.0      0.15707957773E+01
50.0      0.15707955561E+01
60.0      0.15707953114E+01
70.0      0.15707952291E+01
80.0      0.15707951597E+01
90.0      0.15707949798E+01
100.0     0.15707947155E+01
110.0     0.15707944445E+01
120.0     0.15707942001E+01
130.0     0.15707939931E+01
140.0     0.15707936111E+01
150.0     0.15707936634E+01
160.0     0.15707934533E+01
170.0     0.15707932278E+01
180.0     0.15707930986E+01
190.0     0.15707929510E+01
200.0     0.15707927031E+01
210.0     0.15707924666E+01
220.0     0.15707922100E+01
230.0     0.15707919500E+01
240.0     0.15707917701E+01
250.0     0.15707914831E+01
260.0     0.15707912931E+01
270.0     0.15707911200E+01
280.0     0.15707909540E+01
290.0     0.15707907470E+01
300.0     0.15707905180E+01
```
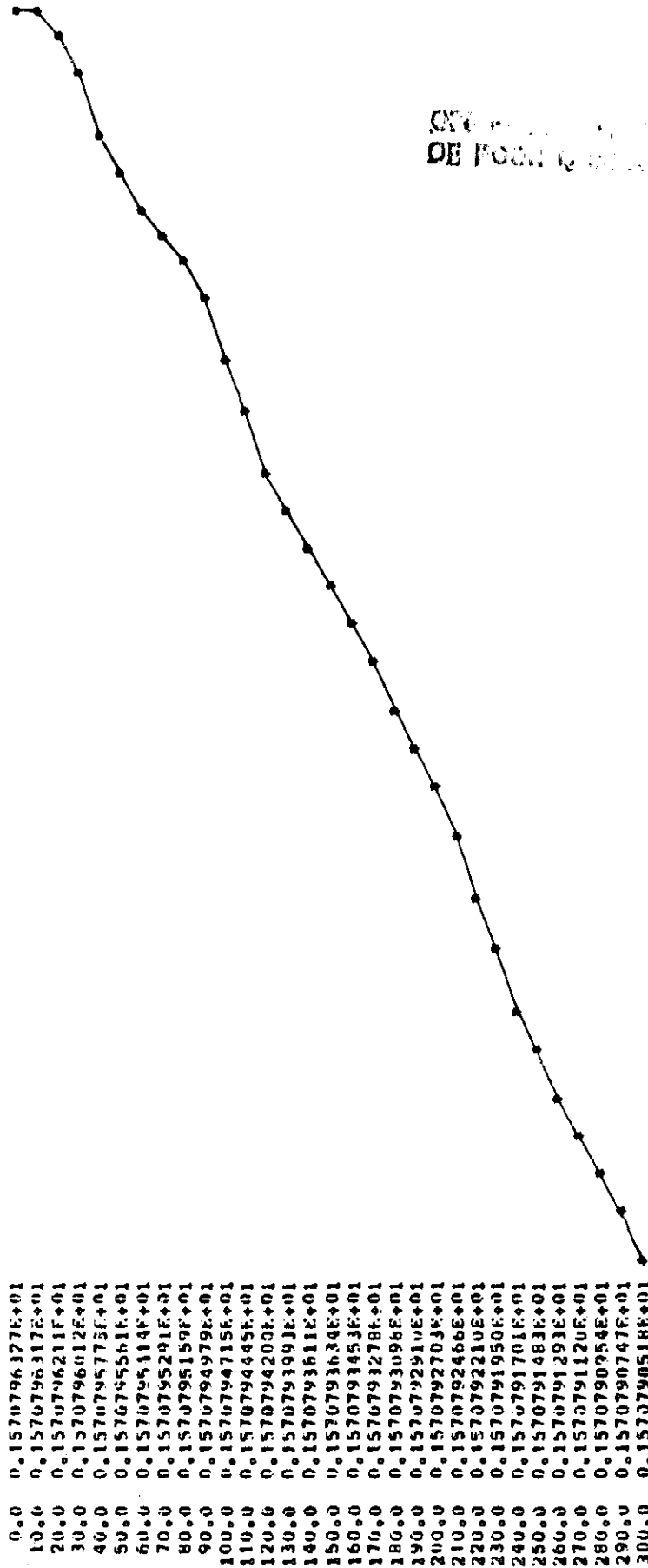
Figure 2.1.9 ϕ' (radians) vs. time in a 28° inclination orbit for the special test case where the precession rate is equal to the orbital angular velocity.
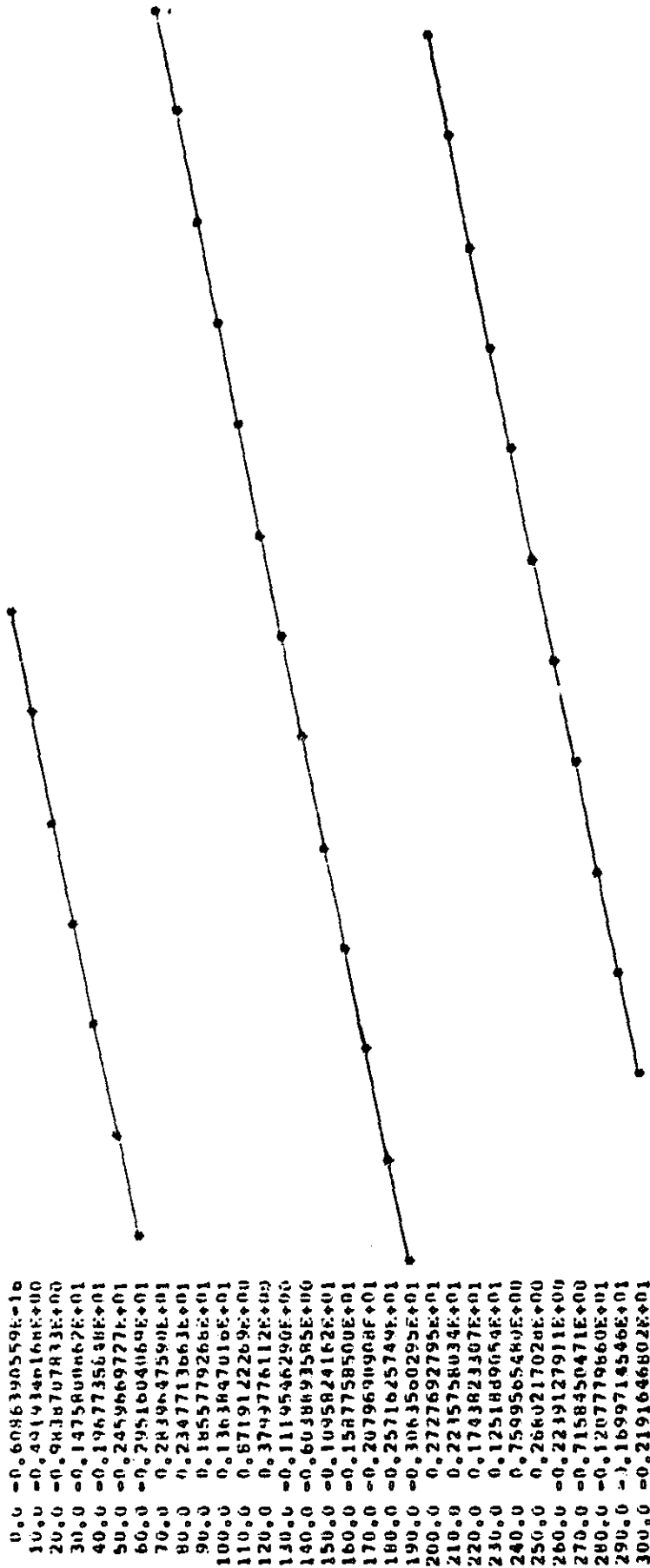
0.0	-0.6096390559E-16
10.0	-0.4914341616E+00
20.0	-0.9838707813E+00
30.0	-0.1475809462E+01
40.0	-0.1967735694E+01
50.0	-0.2459669727E+01
60.0	-0.2951604064E+01
70.0	-0.2839647590E+01
80.0	-0.2347713661E+01
90.0	-0.1855577926E+01
100.0	-0.1363847010E+01
110.0	-0.6719122269E+00
120.0	-0.3749776112E+00
130.0	-0.1114546290E+00
140.0	-0.6038693585E+00
150.0	-0.1095824162E+01
160.0	-0.1587758500E+01
170.0	-0.2079690908E+01
180.0	-0.2571625744E+01
190.0	-0.3063500295E+01
200.0	-0.2727692795E+01
210.0	0.2215758034E+01
220.0	0.1743823607E+01
230.0	0.1251809059E+01
240.0	0.7599565480E+00
250.0	0.2680221702E+00
260.0	-0.2239127911E+00
270.0	-0.7158450471E+00
280.0	-0.1207779660E+01
290.0	-0.1699718546E+01
300.0	-0.2191646802E+01

Figure 2.1.10 ψ' (radians) vs. time in a 28° inclination orbit for the special test case where the precession rate is equal to the orbital angular velocity.

2.2 Slack Tether Studies

2.2.1 Introductory Remarks -

Several advances have been made in the consideration of the slack
tether (tether break) problem during the reporting period.

Perhaps most significantly, the SLACK2 program described in the last
quarterly report has been extended to SLACK3, a fully three-dimensional
treatment:

- The motion of the masses is three dimensional.
- The deployment boom may point in any direction, out of the or-
  bital plane as well as in-plane.
- The tether may be deployed in any direction (though it is still
  restricted to a straight line deployment).
- The Shuttle is allowed to rotate about an arbitrary axis at a
  specified rotation rate and/or rotational acceleration.
- The vibration of the boom on release takes account of the various
  directions involved, e.g. the direction of initial tension due
  to the tether.

SLACK2 previously treated damping in the tether (when the masses
caused a section to come into tension and "bounce") in an ad hoc fashion.
A more correct treatment was developed and applied in SLACK3.

RECOIL, a high resolution program to model the initial loss of tension
process following a tether break, was written. The results (for a per-
fectly elastic tether) verify the initial conditions we have been using in
SLACK2 and SLACK3: the tether is recoiling at a constant velocity along
its length, with no deformation. These initial conditions had been used on

the basis of some low resolution SKYHOOK runs and plausibility arguments.

SAO, with Prof. Robert Hohlfeld of Boston University, has also begun consideration of slack tether dynamics, and the tether loss-of-tension problem, from an analytical viewpoint. These investigations are expected to provide valuable results not readily obtainable from computer modeling (e.g., the typical scale size of loop formation in the cut tether), to provide a check on computer results, and to guide the development of modeling algorithms for partially slack situations. Prof. Hohlfeld has contributed a section, 2.2.5, detailing the results so far.

2.2.2   Treatment Of Damping -

The algorithm for treating damping in SLACK2 was simple and ad hoc: When two of the masses in the model separated by the natural length of the (assumed massless) tether segment between them, they undergo a "bounce," reversing their momentum components along the segment joining them. Allowance was made for damping by reducing the velocity of the rebound by a constant percentage. This much is reasonable, simply from consideration of the linearity of the processes (see below). What is ad hoc about our treatment is the way in which we determine what the percentage velocity reduction is. In the absence of any better knowledge, we simply input a percent value, which applied to all segments regardless of length.

We have now put the damping considerations on a more physical level, so that we not only have the percentage velocity reductions for the various segments to proper scale, but compute them from an input constant characteristic of the tether material.

Although our results are certainly not new, we have not found them in a search of readily available sources in any form easily applicable to the situation at hand. Hence, we shall give a simple derivation from first principles. We wish to derive the dependance of the damping constant for a piece of tether material on the length of the piece, under some very general assumptions. Specifically, we assume that the material is viscous but not plastic. That is, there will be resistance to motion, but no permanent change in the equilibrium state. We assume a simple Hooke's law form for the elastic portion of the stress, and the viscous damping will add a term proportional to velocity.

Consider a simple physical system: a length of tether fastened to a wall at one end and a mass M at the other. Neglect the tether mass. Let x be the extension of the segment past natural length. Then the equation of motion is

$$M\ddot{x} = -Kx - B\dot{x} \qquad (1)$$

where K is the Hooke's law spring constant and B is some damping constant. Now suppose we cut the tether in its center and place a small mass m between the pieces; denote the extension of the segment between the wall and mass m by y. Then the equations of motion are twofold:

$$\begin{cases} M\ddot{x} = -k(x-y) & -b(\dot{x}-\dot{y}) \\ m\ddot{y} = -ky & -b\dot{y} \\ & +k(x-y) & +b(\dot{x}-\dot{y}) \end{cases} \qquad (2)$$

If we let $\xi = (x-y)$, a bit of manipulation arrives at the equation

$$M\ddot{x} = -\tfrac{1}{2}kx - \tfrac{1}{2}b\dot{x} - \tfrac{1}{2}m(\ddot{x}-\ddot{\xi}) \qquad (3)$$

Let $m \to 0$ and compare the result to equation (1). If the accelerations in the third term of (3) remain finite, which we shall simply assume since this is not meant to be a rigorous proof, agreement between these two results for the motion of mass M requires that $k = 2K$, $b = 2B$. Generalizing the argument, we have that

$$k \propto \frac{1}{\ell} \qquad b \propto \frac{1}{\ell} \qquad (4)$$

where ℓ is the (natural) length of the tether segment. For the spring constant k, the proportionality constant is simply EA, Young's modulus times the cross sectional area. For the damping constant b, we shall follow a remark in Bodley and Park (1983; p. 54) and denote the proportionality constant by C_v. It seems reasonable that the energy dissipation, hence the resistive force, will be proportional also to the cross sectional area of the tether; hence, we define $c_v = C_v/A$. The two material properties E and c_v are thus input to a program such as SLACK3, which can then compute the spring motion parameters.

We now need to determine how the velocity after a "bounce" in SLACK3 depends on the relative velocity of the pair of masses before the "bounce." Consider only the velocity component along the tether; the orthogonal component cannot be changed by tether tension forces. Suppose we have equal masses m at either end of the tether (this won't be strictly true since SLACK3 allows the segment length to vary, and the masses depend on segment length), and a segment of length ℓ. Let the separation of the masses be $x+\ell$, so that x is the stretch of the segment. The displacement of each mass will be half x, so the equation of motion (acceleration = force) becomes

$$\tfrac{1}{2}m\ddot{x} = -kx - b\dot{x} \qquad (5)$$

Make the usual trial substitution $x(t) = e^{\alpha t}$, and write $\beta = b/m$, $\omega^2 = 2k/m$. Then the exponential will be a solution if

$$\alpha^2 + 2\beta\alpha + \omega^2 = 0 \tag{6}$$

There are two linearly independant solutions corresponding to the roots $\alpha = -\beta \pm \sqrt{\beta^2 - \omega^2}$ of this characteristic equation. We consider here only a small damping approximation, i.e. $\beta \ll \omega$. The complications become more complex for larger damping, and the implications of extreme cases for the model are still being investigated; the results should be good enough for most purposes when $\beta < \omega$. The two roots then form a complex conjugate pair and the solutions are more familiarly written as exponentially damped sine and cosine terms. If the bounce begins at t=0, we have initial conditions $x(0) = 0$, $\dot{x}(0) = v_{in}$, say. The cosine term will drop out and the solution becomes

$$x(t) = \frac{v_{in}}{\omega} e^{-\beta t} \cos(\omega t) \tag{7}$$

where we have replaced $\sqrt{\beta^2 - \omega^2}$ by ω. The tether segment comes out of the bounce (i.e., loses tension again) when $x(t)$ is next zero, i.e. at $t = \pi/\omega$. Taking the derivative of (7) at this time we have

$$v_{out} = v_{in} e^{\pi\beta/\omega} \tag{8}$$

The computation of segment damping parameter, and this small damping approximation for the velocity loss on bounce, have been implemented in the version of SLACK3 described in Section 2.2.3.2 below.

<div align="center">References to Section 2.2.2</div>

Bodley, C. S., and Park, A. C., Analysis of Tethered Satellite System Orbital Dynamics for Selected Mission Profiles, Report TSS-83-ACP-065, Martin Marietta Denver Aerospace, June 1983.

2.2.3 Full Three Dimensional Treatment -

SLACK2 restricted the motion of the masses to the orbital plane. The same physical model has been generalized to a three dimensional program, SLACK3. This involved the following modifications:

- The equations of motion of the masses now allow for out-of-plane motion.

- The deployment boom may point in any direction, out of the orbital plane as well as in-plane.

- The tether may be deployed in any direction (though it is still restricted to a straight line deployment).

- The Shuttle is allowed to rotate about an arbitrary axis at a specified rotation rate and/or rotational acceleration.

- The vibration of the boom on release takes account of the various directions involved, e.g. the direction of initial tension due to the tether.

- Randomization of tether segment direction is in a cone about the nominal tether direction, rather than just in the orbital plane.

Some additional modifications have been made (or are being coded), such as the improved damping model discussed in Section 2.2.2, and streamlining of the input.

There are still some restrictions from a fully adequate three dimensional treatment. The two most significant seem to be

- The air drag (wind) is still in the orbital plane.

- The deployment boom is assumed to be attached to the Shuttle at the Shuttle center of mass.

2.2.3.1 Preliminary Mathematics -

The equations of motion of a free mass in the orbiting coordinate system (i.e., relative to the orbit center ≈ the center of mass) are

$$\begin{cases} x'' & = & 3x & + & 2y' \\ y'' & = & & - & 2x' & - & D \\ z'' & = & -z \end{cases} \tag{1}$$

where the time has been scaled by the orbital angular velocity Ω to $\tau = \Omega t$; ()' means $d()/d\tau$; D is a scaled drag parameter, assumed constant; and the coordinate system is as shown in Figure 2.2.1. The third equation (for z) has solution $z(\tau) = z(0)\sin\tau + z'(0)\cos\tau$, and addition of these solutions to the program is trivial.

Much the more complicated part, both conceptually and in the actual programming, has been dealing with the three dimensional geometry and various angles involved. Although mathematically elementary, there is much room for confusion and failure to coordinate conventions, so we will spell out in some detail what we are doing.

Figure 2.2.1 shows the orientation of our reference coordinate frame, the standard frame centered at the center of mass (Shuttle) and rotating so as to keep the x-axis vertical. Also shown are the orientations of the pitch, roll and yaw rotations discussed below.

Figure 2.2.2 points up a distinction (in a two dimensional case for clarity) that it is extremely important to be clear about: that between physically rotating a physical object or vector by prescribed angles, and then asking for the coordinates of the new object in the original (or reference) coordinate system; and rotating the coordinate system in pre-
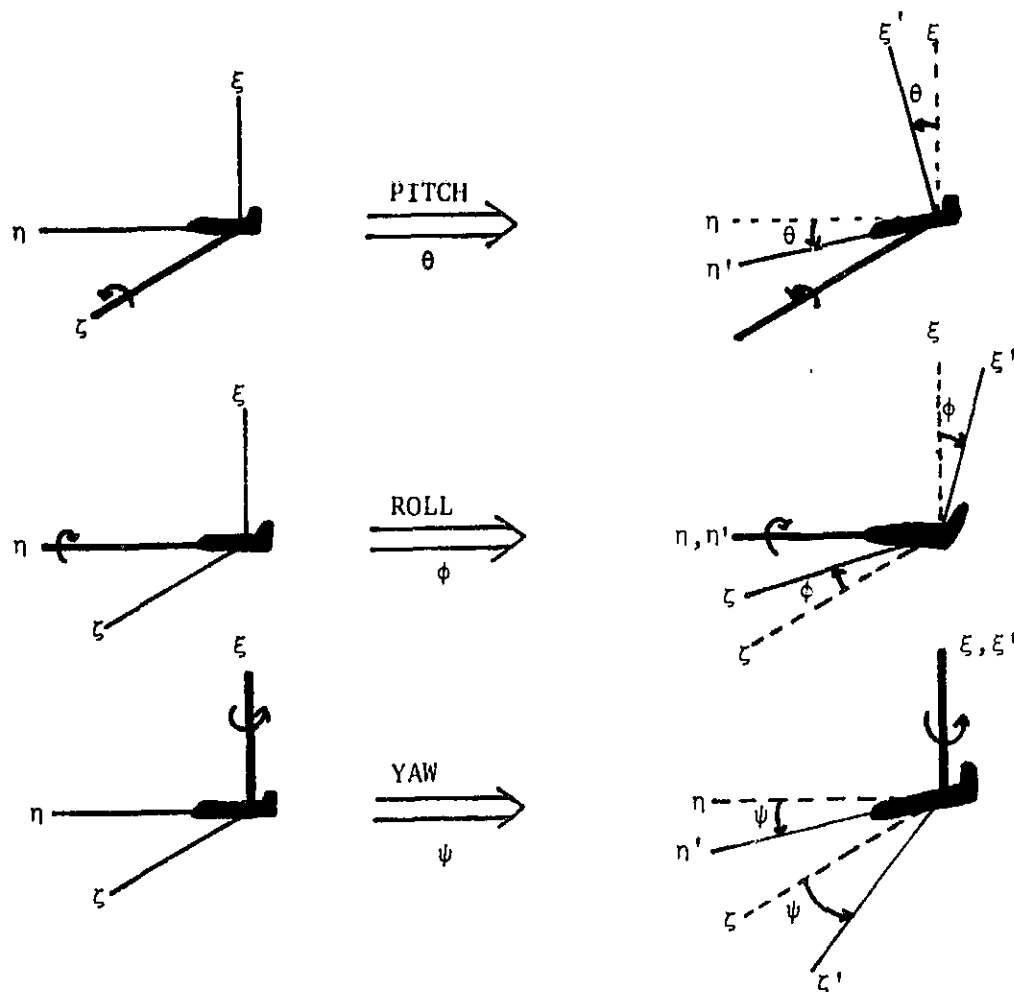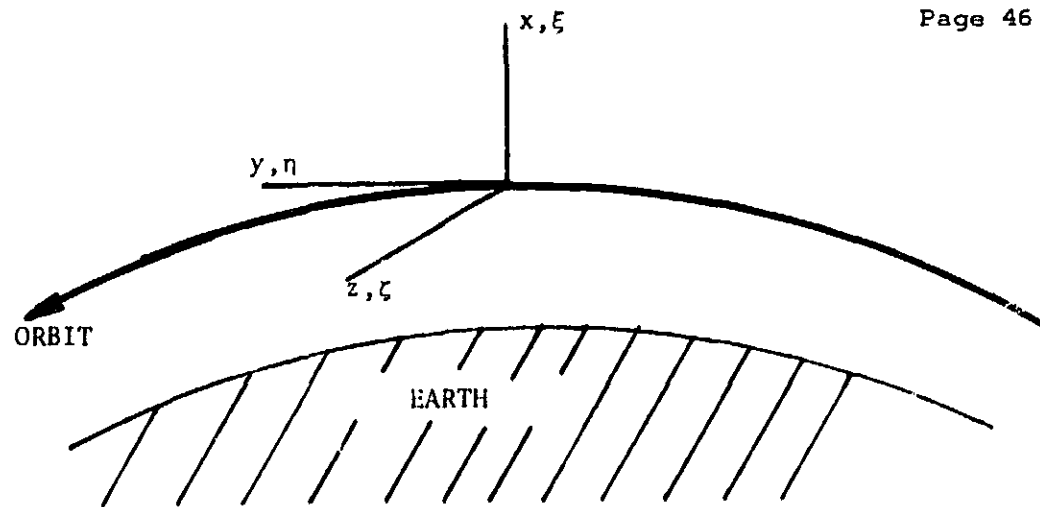
Figure 2.2.1. Orientation of the reference coordinate system and the pitch, roll and yaw rotations defined in the text.
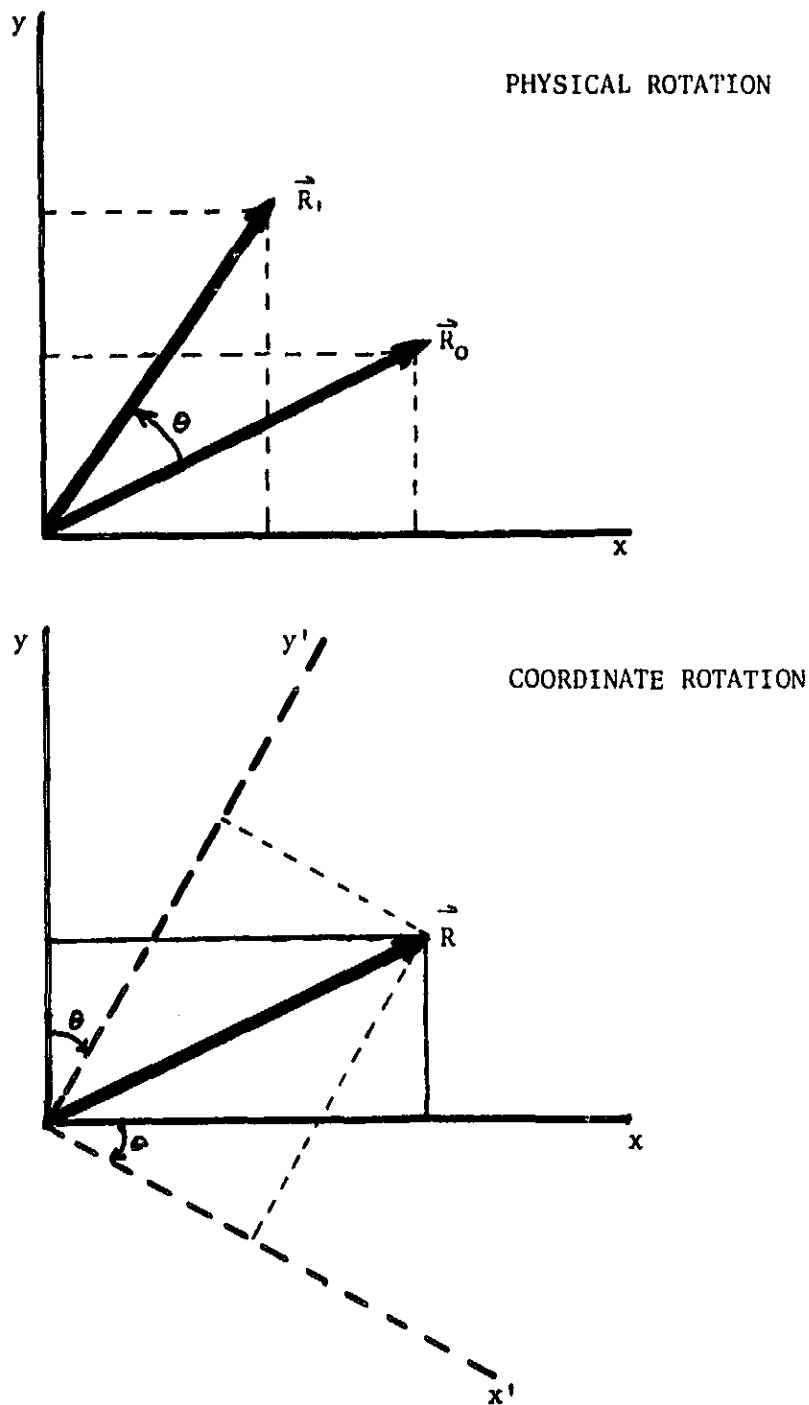
Figure 2.2.2. Physical vs. coordinate rotation. Physically rotating a vector or object about the coordinate rotation, and seeking the new object's coordinates in the original system, is the inverse of rotating the coordinate system and seeking an unmoved object's coordinates in the new system.

scribed fashion and then seeking the coordinates in the new system of an unmoving object. In both cases, the "input data" are the coordinates of the original object in the original system. We shall call these two situations "physical rotation" and "coordinate rotation" for brevity. Brief reflection, perhaps while pondering Figure 2.2.2, reveals that these are inverse situations: i.e., a physical rotation by a given angle produces the same numbers as a coordinate rotation by the opposite (negative) angle. We shall consider the physical rotations and their generating matrices to be the fundamental concepts.

The three fundamental units from which we shall construct all our rotations and angles are pitch, roll and yaw. These operations are always taken relative to a coordinate system fixed in the Shuttle (body coordinate system). They are somewhat easier to describe if we imagine the Shuttle to be oriented as in Figure 2.2.1, with nose pointing along-orbit and the landing gear pointed toward the Earth. Pitch by a positive angle then brings the nose down; roll causes a roll about the Shuttle's longitudinal axis clockwise as viewed by the pilot; and yaw by a positive angle swings the Shuttle's nose to the left. Unless otherwise specified, θ will refer to pitch, φ to roll, and ψ to yaw.

Each of these elementary maneuvers can be represented by a 3x3 matrix. These matrices are used to transform column vectors, e.g. for pitch

$$
\begin{bmatrix} x \\ y \\ z \end{bmatrix}_1 = \begin{bmatrix} \cos\theta & -\sin\theta & 0 \\ \sin\theta & \cos\theta & 0 \\ 0 & 0 & 1 \end{bmatrix} \begin{bmatrix} x \\ y \\ z \end{bmatrix}_0 \tag{2}
$$

or in more compact notation

$$
\vec{r}_1 = P_\theta \, \vec{r}_0 \tag{3}
$$

Here, the subscripts 0 and 1 refer to before and after the physical rotation, and the $\vec{r} = [x \; y \; z]^T$ are the coordinates in a fixed reference frame, coincident with the body frame before the pitch maneuver, of some physical object or vector which rotates with the Shuttle. Note that $\vec{r}$ is not a physical vector, but a column matrix of components. If the system in which these components are measured is not obvious, we may use notation such as

$$
\vec{r}_1|_{xyz}
$$

The roll and yaw matrices are similarly:

$$
R_\varphi = \begin{bmatrix} \cos\varphi & 0 & \sin\varphi \\ 0 & 1 & 0 \\ -\sin\varphi & 0 & \cos\varphi \end{bmatrix} \tag{4}
$$

$$
Y_\psi = \begin{bmatrix} 1 & 0 & 0 \\ 0 & \cos\psi & -\sin\psi \\ 0 & \sin\psi & \cos\psi \end{bmatrix} \tag{5}
$$

These rotations and matrices are defined so that the body coordinate system coincides with the reference coordinate system when the Shuttle is flying in a "normal" attitude, i.e. nose forward and head up. There may be some discrepancy in sign from the conventions used in, e.g., aircraft opera-

tions.

These matrices are examples of <u>orthogonal</u> matrices, i.e. those for which the transpose is the inverse. For these particular matrices, replacing the rotation angle (e.g. θ) by its negative results in the inverse matrix. From the comment made above about the inverse nature of physical rotation and coordinate rotation we see that the matrices for transferring the representation of a constant vector into a system rotated with the Shuttle will be just the transpose of those written down above; a general result for orthogonal rotation matrices.

It now becomes relatively simple to compute the rotation matrix corresponding to successive rotations, e.g. a sequence of pitch/roll/yaw maneuvers. In each case we suppose the rotation is described in the body coordinate system. First, perform a rotation described by matrix $\mathbf{A}$, then one described by matrix $\mathbf{B}$. These will transform a physical vector $\vec{r}_0$ to $\vec{r}_1$ to $\vec{r}_2$. Initially, the body system is coincident with the reference xyz system; after the first rotation, it will be coincident with a system, say x'y'z'; and finally, with x"y"z". Now, almost by definition, the coordinates of the final vector in the final system are numerically identical to those of the original vector in the original system. I.e.,

$$\vec{r}_2 \mid_{x"y"z"} = \vec{r}_0 \mid_{xyz}$$

and we may then write immediately $\vec{r}_2|_{xyz} = \mathbf{A} \{\vec{r}_2|_{x'y'z'}\} = \mathbf{A} \{\mathbf{B} \ \vec{r}_2|_{x"y"z"}\}$ $= \mathbf{AB} \ \vec{r}_0|_{xyz}$. This final expression is just in the form required for the total rotation matrix; i.e., the total rotation is described by the matrix $\mathbf{AB}$. In general, <u>a series of rotations, first A, then B, then C...</u> will <u>produce a rotation described by the matrix ABC...</u>. The order is important,

since matrices do not commute.

With this background, the required computations are almost obvious. Any direction, e.g. boom or tether, will be specified by two angles, first a pitch and then a roll which are pictured as rotating the vertical (x) axis into the desired direction. The full rotation matrix is easily computed as **PR**, and the unit vector in the appropriate direction is given by **PR** $[1 \ 0 \ 0]^T = [\cos\theta\cos\varphi \ , \ \sin\theta\cos\varphi \ , \ -\sin\varphi \ ]^T$. These unit vectors allow us to create suitable initial conditions.

Dealing with the boom vibration and Shuttle rotation is slightly more complicated. First, suppose we have computed the boom's position and velocity $\vec{B}_0$ and $\dot{\vec{B}}_0$ relative to an unrotated Shuttle. To describe the Shuttle rotation we have the angles θ and φ of the rotation axis, which allow us to compute a transformation matrix **PR**; and the rotation angle $\psi(t)$ as a function of time. Our prescription for performing the desired rotation can be stated: First, physically rotate the Shuttle with **PR** so that the body ξ-axis (vertical in the body frame) lies along the axis of rotation; second, rotate the Shuttle by ψ about the body vertical axis in a yaw maneuver, with matrix **Y**; third, rotate the Shuttle in the inverse manner $[\mathbf{PR}]^T$ so that the body vertical axis is coincident again with the reference frame vertical. From the theorem given above on combining rotations, this is equivalent to using a single total rotation matrix

$$\mathbf{A}(t) \ = \ [\mathbf{PR}] \ \mathbf{Y}_{\psi(t)} \ [\mathbf{PR}]^T \tag{6}$$

that is, the Shuttle position at time t is given by

$$\vec{B}_1 \ = \ \mathbf{A}(t) \ \vec{B}_0(t) \tag{7}$$

The velocity is found simply as

$$\dot{\tilde{B}}_1 = \dot{A}(t) \ \tilde{B}_0(t) \ + \ A(t) \ \dot{\tilde{B}}_0(t) \tag{8}$$

where

$$\dot{A}(t) = [PR] \ \frac{\partial Y_\psi}{\partial \psi} \ [PR]^T \ \dot{\psi}(t) \tag{9}$$

We still need to know the unrotated boom vibration, i.e. relative to the Shuttle. We already in SLACK2 compute the frequency and amplitude of the boom vibration, as detailed in a previous report. There, to get the amplitude we used the tether tension before the break based on vertical deployment. If the tether pulled away from vertical by air drag, and is in equilibrium, the tension is the same as if it had been vertically deployed with only the gravity gradient force; if the tether was in motion or held off vertical by thrusters, the force depends on factors and scenarios not input to SLACK3. Thus, we simply use the vertical deployment tension, with an optional "fudge factor" to adjust to specific cases. To treat the three dimensional case we use the two unit vectors along the boom and tether, $\hat{e}_B$ and $\hat{e}_T$, which we have computed as above based on the input angles. The displacement of the boom tip due to the deployed tether will be along a direction perpendicular to the boom, in the plane defined by the boom and tether direction. First note that the vector $(\hat{e}_B \times \hat{e}_T)$ is orthogonal to this plane. Then a suitable vector is

$$\vec{x}_P = (\hat{e}_B \times \hat{e}_T) \times \hat{e}_B = \hat{e}_B - (\hat{e}_B \cdot \hat{e}_B)\hat{e}_B \tag{10}$$

which we then normalize to form a unit vector

$$\hat{e}_P = \vec{x}_P \ / \ |\vec{x}_P| \tag{11}$$

(In the exceptional case that the tether and boom are collinear, $\vec{x}_P$ is zero and cannot be normalized, but there is no displacement and we simply use O in place of $\hat{e}_P$.) The displacing force, used to compute the boom deflection, will then be simply

$$F_P = \{Tension\} \ (\hat{e}_T \cdot \hat{e}_P) \ . \tag{12}$$

The initial, pre-break, displacement of the boom tip is then

$$\overline{\Delta B} = F_P \ \frac{b^3}{3(EI)} \ \hat{e}_P \ , \tag{13}$$

where b is the boom length and EI its stiffness. The motion of the boom tip, prior to overall rotation of the Shuttle, is then

$$\vec{B}_0(t) = \vec{B}_\bullet + (\overline{\Delta B}) \ \cos[2\pi ft] \tag{14}$$

and its velocity

$$\dot{\vec{B}}_0(t) = - 2\pi f \ (\overline{\Delta B}) \ \sin[2\pi ft] \tag{15}$$

where $\vec{B}_\bullet = b\hat{e}_B$ is the boom equilibrium position and $f = c_1 \sqrt{\dfrac{g \ EI}{W \ b^3}}$ is the frequency of the first mode of a clamped beam; we take values specified by NASA, $EI = 1.3 \times 10^8$ lb in^2, b = 849 in, weight W = 106.2 lb; the value of gravity is g = 385.06 in/sec^2, and c_1 is 0.56 cycle/sec. Rotating (14) and (15) with (7) and (8), we specify completely the motion of the boom tip.

One other application of these concepts is to a problem that at first sight appears trivial, the generation of vectors randomized about a given direction. We do this in randomizing the directions of the tether segments when we generate the initial conditions. We first compute (random) angles θ with respect to the reference direction and φ azimuthally about the reference direction (typically θ might be uniform with 5° mean and φ uniform on $[0,2\pi)$). Then we create a vector with these angles about, say, the x-axis in the reference coordinate frame:

$$\vec{s} = \left[\begin{array}{c} \cos\theta \\ \sin\theta\cos\varphi \\ \sin\theta\sin\varphi \end{array} \right] \tag{16}$$

Finally, we physically rotate this vector using any rotation which brings the x-axis into the desired reference direction. If the reference direction is $\hat{e}_T$, we need a unitary matrix satisfying:

$$U \left[\begin{array}{c} 1 \\ 0 \\ 0 \end{array} \right] = \hat{e}_T \qquad\qquad UU_T = I \tag{17}$$

If we partition $U = \begin{bmatrix} u_1 & | & u_2 & | & u_3 \end{bmatrix}$, then we see immediately that u_1 must be $\hat{e}_T$, and $\{u_1, u_2, u_3\}$ must form an orthonormal set. This may be easily done by choosing **any** arbitrary vector $\vec{t}$ not parallel to u_1 (we use unit vectors along the coordinate axes for simplicity; we will never have to try more than two). Then form $u_1 \times \vec{t}$ and normalize it to get u_2; and then take $u_3 = u_1 \times u_2$. We may now perform our rotation, which will bring the segment into an angle θ with respect to the tether direction; the effect on the azimuthal direction is not obvious, but it will leave the uniform distribution unchanged.

2.2.3.2 Slack3 Implementation -

The above considerations have been implemented in SLACK3. The improved damping of Section 2.2.2 is also included, as well as improvements in the randomization processes. We are in the process of coding streamlined input procedures, in which there are default values of many parameters and a menu system allows changing only those of interest. Only a few test cases have been run (which verify correct deployment of boom and tether, and boom rotation); the familiar side and rear view configuration diagrams are shown in Figure 2.2.3 for a sample run which includes boom rotation. SLACK3, with minimal further effort, is now suitable for running
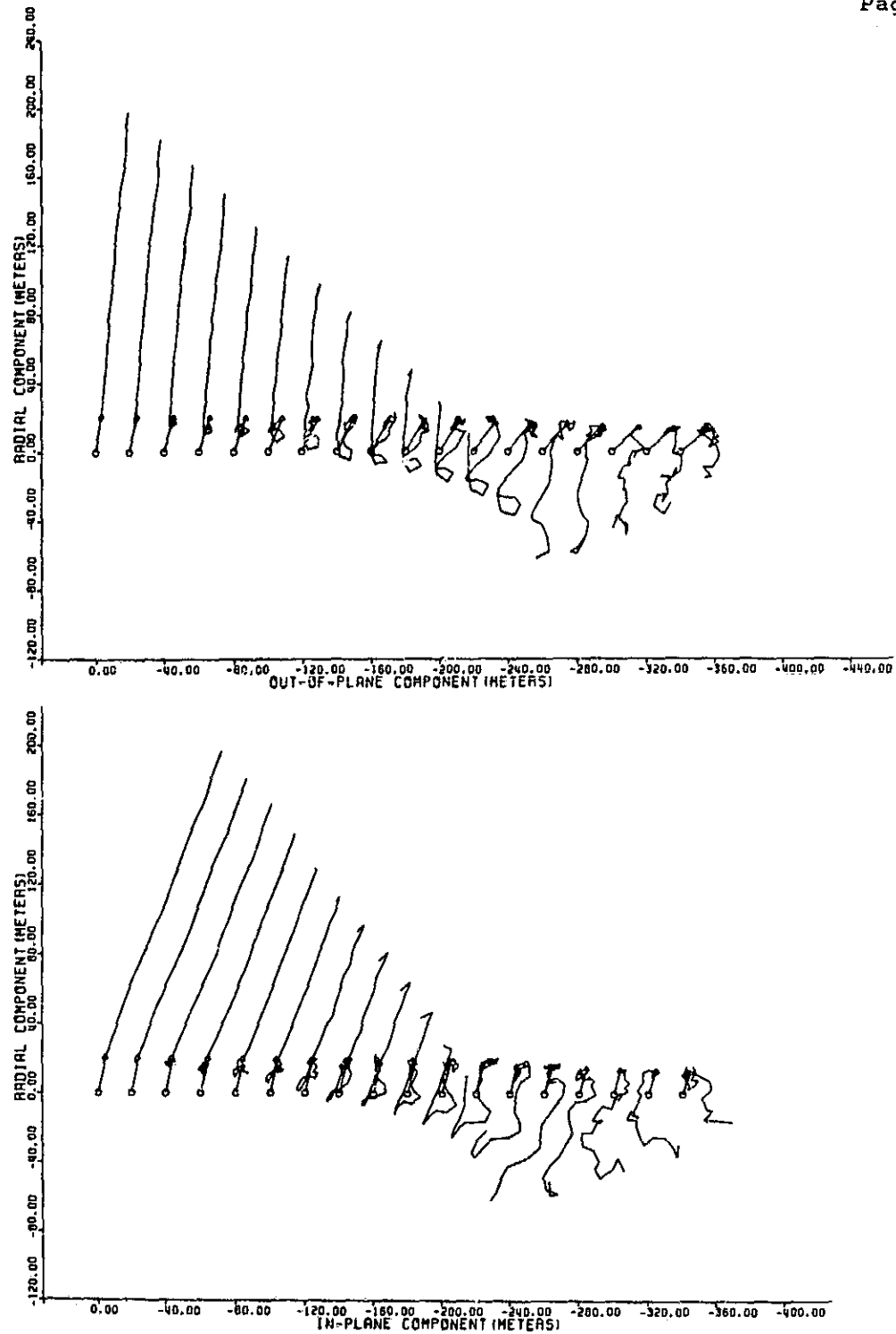
Figure 2.2.3. Sample results from the fully three dimensional SLACK3. A sequence of configurations of the tether are shown in the familiar format. Successive configurations are displayed from left to right. The "in-plane" figure is a side view, with the orbital direction to the left. In the "out-of-plane" figure, the system is viewed from behind.

some complex cases in the next reporting interval to determine the effect of deployment directions, rotation maneuvers, tether remnant length and other quantities of interest.
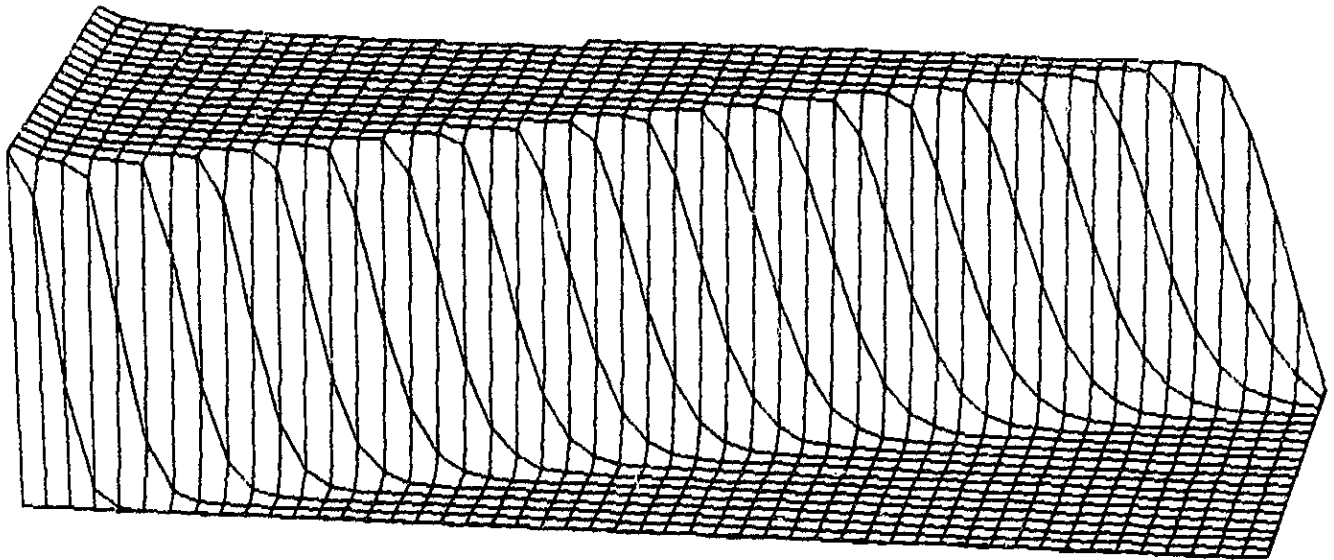
2.2.4 High Resolution Loss-Of-Tension Model -

The initial conditions used by SLACK2, that the tether was recoiling with constant velocity and no compression initially, were based on some old SKYHOOK simulations with only a few masses, and on some plausibility arguments. It was decided to check these assumptions by means of a lumped mass model similar to SKYHOOK, but simplified to the extreme to allow a large number of masses to be included.

The model, embodied in a program RECOIL, is capable of handling up to 100 masses with reasonable efficiency. The restrictions made are primarily:

- The only forces included are the internal tether forces. Specifically, no gravity gradient, drag, or Coriolis forces are included.
- All motion is one dimensional.
- All segments are the same length.
- Once a segment goes slack we ignore any tension that may develop if it again becomes stretched.

The equations of motions are solved with a simple fourth order Runge-Kutta integrator, starting from the moment the tether is severed. For simplicity, the problem is scaled so that the only free parameter is the damping constant.

VEL05 DRAG=0.0 50M

Figure 2.2.4. High resolution loss of tension: development in time. This is a view of a three dimensional surface whose height represents the (negative of the) recoil velocity. This is a function of the time and the distance along the tether, in the "horizontal" plane: the tether/boom attachment is at the right, the cut end at the left, and successive configurations recede into the distance. Fifty mass model with RECOIL; zero damping.

Sample results are shown in Figure 2.2.4, which shows a three dimensional plot of the velocity vs. time and distance along the tether. Note the propagation of a sharp wave front, behind which the velocity is approximately constant. The state of the tether at the moment it goes completely slack is shown in Figure 2.2.5. It is seen that these detailed calculations confirm the initial conditions we have been using.

Attempts to run RECOIL with non-zero damping lead to sharply oscillating results. There is probably a coding error in the program or a numerical instability. We shall investigate this in the next reporting period. The efficiency of the approach used suggests the possibility of adding extra forces (e.g. gravity gradient) as well as damping.

It is interesting to see how this lumped mass model relates to the tether considered as an elastic continuum. By letting the number of tether segments become infinite, and scaling the ball masses and segment spring constants appropriately, we can derive a partial differential equation, which is (as expected) a simple wave equation. Using a standard low order finite difference approximation we arrive at exactly the same equations as in the ball-and-spring model. Except that the cut end boundary condition is not treated appropriately. There are several ways to treat such free end (zero stress) boundary conditions which maintain the order of approximation; simply considering it as another ball with the same mass as the interior balls in the lumped mass model, however, is equivalent to treating the boundary condition with a lower order of approximation than the interior points. It is a truism of numerical analysis that the order of the total solution is strongly influenced by the weakest link. (This sort of consideration is hidden by the lumped mass approach of first discretizing
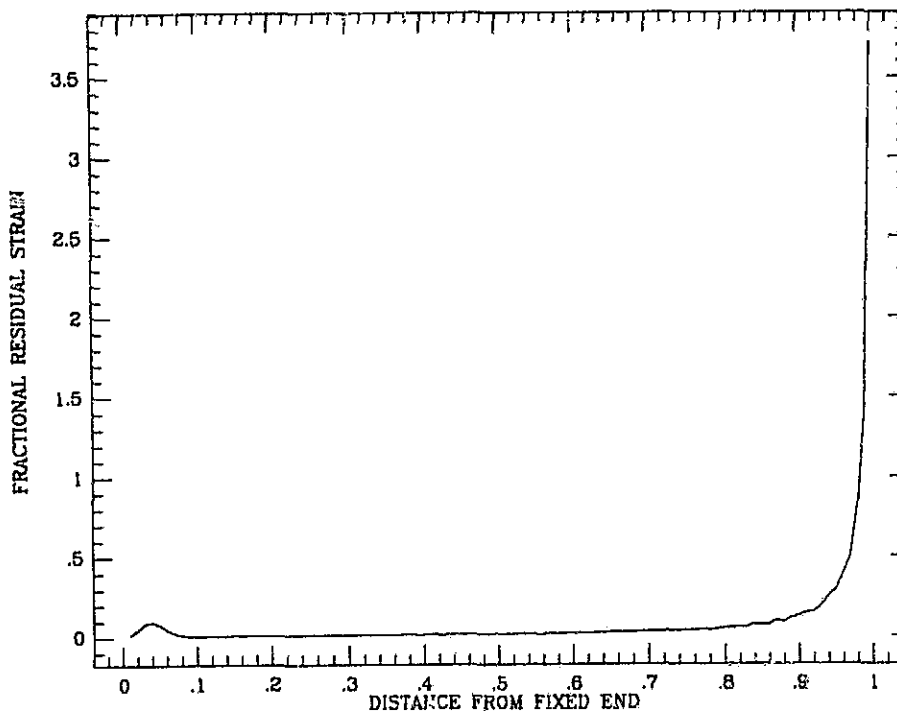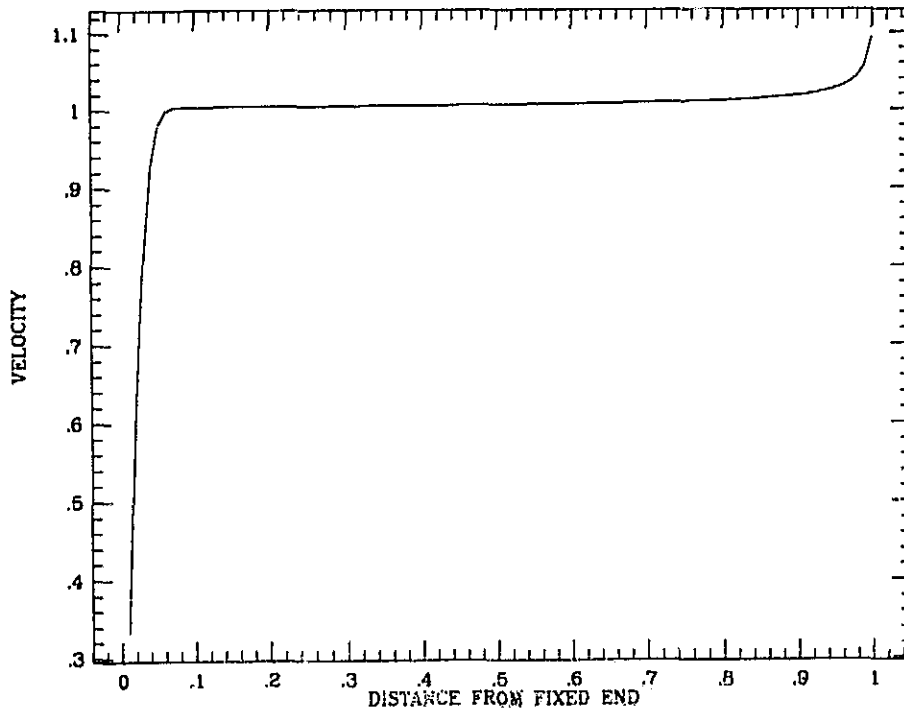
Figure 2.2.5. High resolution loss of tension: Final state. Here we plot the (negative of the) velocity, and the (negative of the) fractional residual strain immediately after the tether goes completely slack. By the fractional residual strain we mean the compression in the slack state divided by the original elongation. Note that strain values greater than 1 indicate that the tether segment is now extended in the opposite direction by more than its natural length; we do not model the resultant stress. One hundred mass model with RECOIL; zero damping.

the physical system conceptually before writing down any equations, which is why lumped mass models should always be examined carefully.) By properly treating the free end we might substantially improve the accuracy of the model (which can be easily checked in the zero damping case). The possibility of improving accuracy by, for instance, using a finite element approach, is also appealing.

It is also possible to derive the velocity and strain upon loss-of-tension by theoretical arguments. This solution is implicit in the material of Section 2.2.5, but not actually derived there. Thus, it is of value to write down the argument explicitly. We assume there is no damping or other energy loss. The loss of tension will then occur via the propagation of a **constant amplitude** tension wave with velocity $c = \sqrt{E/\rho}$. Since the wave is propogating along a characteristic (in the space-time plane) with no dissipation, it will remain constant in form and amplitude. Thus, the velocity of recoil after it passes will be the same at all points. To be concrete, suppose the tether is fixed at $x = 0$, is of natural length L, and has been stretched by a small fraction δ. Then, where the coordinate s describes the natural length of tether from the fixed end, and x its actual position, what we have described may be written:

$$x(s,0) = (1 + \delta)\, s \quad \text{(evenly stretched initially)} \tag{1}$$

$$\frac{\partial x(s,t)}{\partial t} = \begin{cases} 0 & t < \dfrac{L - s}{c} \\[2mm] -V & t > \dfrac{L - s}{c} \end{cases} \tag{2}$$

where V is the recoil velocity which we shall determine below. Then we immediately have:

$$x(s,t) = \begin{cases} (1+\delta)\,s & t < \dfrac{L - s}{c} \\[2mm] (1+\delta) - V\left[t - \dfrac{L - s}{c}\right] & t > \dfrac{L - s}{c} \end{cases} \tag{3}$$

Upon evaluation at $t = L/c$, when the wave reaches the point of attachment, this is simply

$$x(s, L/c) = \left[1 + \delta - \frac{V}{c} \right] \tag{4}$$

The final step is to compute the recoil velocity. Our assumption of no dissipation allows us to simply equate the elastic energy stored in the tether segment with the kinetic energy after recoil. The spring constant of the tether as a whole is $k = EA/L$, and the force upon extension to $L+u$ is just $F = -k\,u$. Integrating $F\,du$ from 0 to $u = \delta L$, we get the total elastic energy stored when the tether is stretched to length $(1+\delta)L$, $E_{elastic} = \frac{1}{2}k(\delta L)^2 = \frac{1}{2}EAL\delta^2$. Equating this with the total recoil kinetic energy, $E_{kinetic} = \frac{1}{2}(\text{mass})(\text{velocity})^2 = \frac{1}{2}(\rho AL)V^2$, gives

$$V = \sqrt{\frac{E}{\rho}}\; \delta = c\,\delta \tag{5}$$

and then evaluation of (4) gives simply $x(s,L/c) \equiv s$. I.e., <u>there is no residual strain.</u> Thus, the initial conditions we have been using in SLACK2/3 are <u>exact</u> under the assumption of zero dissipation.

2.2.5 Analytical Studies Of The Slack Tether Problem -

2.2.5.1 Introduction -

A program of analytic studies of tether dynamics pertinent to treatment of the slack tether problem has been undertaken. While it is not realistic to expect that a complete understanding of the slack tether problem may be obtained solely by analytic techniques, compelling reasons motivate analytic studies as an extremely useful adjunct to numerical modeling of the slack tether. Among these reasons are:

- Analytic calculations may give insights into the physical processes important for the dynamics of the slack tether. Some of these processes may be obscured by the complexity of the numerical simulations.

- Numerical modeling of the slack tether using the present ball-and- spring techniques is computationally intensive. Analytic studies will help to direct the numerical modeling, and perhaps to suggest new, efficient modeling techniques.

- Analytic calculations will aid in the validation of the results of the computer-generated numerical models.

- Information generated by the analytic work will frequently complement the results of numerical simulations.

The analytic calculations will be initially focussed on processes occuring just as the tether is going slack, i.e. going from a tensioned to an untensioned state. In this context, it is appropriate to treat the tether

as a one-dimensional system, as long as the "loops" one would expect to develop in the slack state do not grow to large amplitude in the transverse directions.

The desired results of the initial theoretical effort is a calculation of the characteristic size for loops or wrinkles in the tether after it has gone slack. The characteristic size is of immediate importance for the safety of Shuttle operations in a slack tether situation. We expect that loops of small scale size (say on the order of 1 meter) will be much less apt to entangle the Shuttle than larger-sized loops. We shall outline below the progress being made toward this and other objectives.

The first step in this program of calculations is to determine conditions pertaining to the development of patterns of tensioned and slack (untensioned) regions along the length of the tether. For simple cases, such as a tether break near the tethered satellite, it is obvious that the tether will go slack through the mechanism of propagating a longitudinal (negative amplitude) stress wave along its length. More complex situations may be envisioned as a superposition of (positive and negative) finite-amplitude longitudinal stress waves propagating along the tether. An immediate result (which will not be given in detail here) is that when the tether fails, it is possible in principle, to have a nearly arbitrary distribution of tensioned and slack regions along its length. In particular, it is possible to construct initial conditions for the subsequent dynamics after tether failure consisting of a tensioned region bounded by two slack regions.

Such a discussion of longitudinal stress waves propagating through the tether suggests we apply the method of characteristics to the dynamics of

the tether as it is going slack and for times shortly thereafter (Morse and Feshback 1953, Courant and Hilbert 1962). Recall that a characteristic of a wave equation (hyperbolic partial differential equation) is the locus of points in time for the propagation of an infinitesimal amplitude wavelet.

A cable or tether going slack can be modeled (for times before the formation of well-developed loops) as a column capable of supporting a great deal of force in tension, and of supporting a comparatively small (but nonzero) force in compression (Landau and Lifshitz 1959, §§17, 20). The formation of transverse bends in the tether which will subsequently develop into loops is a generalization of the well-studied problem of column buckling.

Since the compressive force the tether can support is very small, a number of effects will have to be considered which are usually neglected for models of the tether in tension. While the tether in tension can be modeled as a string with a Hooke's law constitutive (stress-strain) relation, that slack tether will require a nonlinear viscoelastic or viscoplastic constitutive relation describing its resistance to transverse bending. Also, mathematical treatments of the slack tether will require a careful treatment of the tether inertia.

Recall that the dominant "mode" of column buckling for a column supporting a large compressive force and with negligible inertia is an approximately half-sinusoidal displacement over the entire column. Qualitatively, in this instance of generalized buckling, the tether inertia will favor wrinkling or buckling on smaller scales and the resistance to bending will tend to favor larger length scales. Consequently, we can hope to identify a fastest-growing scale size for buckling which will characterize

loop formation in the slack tether.

2.2.5.2 Motion Of A Medium Under Its Own Elastic Forces -

We shall develop a general equation of motion for a medium under the
influence of its own elastic forces. A special application will be made to
longitudinal stress waves in a cable, such as the tether of the TSS, in the
next section. While the general formalism is not necessary for this first
simple application, it is valuable to introduce this notation for later
calculations pertaining to the slack tether.

Following Morse and Feshbach (1953), define the stress dyadic

$$\bar{\bar{S}} = \bar{F}_x \hat{\imath} + \bar{F}_y \hat{\jmath} + \bar{F}_z \hat{k} \tag{1}$$

where $\hat{\imath}$, $\hat{\jmath}$, and $\hat{k}$ are the usual unit vectors in rectangular coordinates.
The force across a surface element $d\bar{A}$ is then $\bar{\bar{S}} \cdot d\bar{A}$.

The stress dyadic is related to the strain dyadic defined in (3) by

$$\bar{\bar{S}} = \lambda |\bar{\bar{G}}| \bar{\bar{I}} + 2\mu\bar{\bar{G}} \tag{2}$$

where $\bar{\bar{I}}$ is the unit dyadic. Equation (2) is immediately apparent by trans-
formation to the principal axes. The quantity, μ, is the shear modulus of
the solid, $\frac{1}{3}$ $(3\lambda+2\mu)$ is the bulk modulus of an elastic isotropic medium,
and $\mu(3\lambda+2\mu)/(\lambda+\mu)$ is the Young's modulus. The strain dyadic may be writ-
ten in terms of the displacement, $\bar{s}$, of the solid from its equilibrium
position,

$$\bar{\bar{C}} = \frac{1}{2}(\bar{\nabla}\bar{s} + \bar{s}\bar{\nabla}) \tag{3}$$

The equation of motion for the solid then, under the influence of its own elastic forces is

$$\rho \ \frac{\partial^2 \bar{s}}{\partial t^2} = \bar{\nabla}\cdot[\lambda\bar{\bar{I}}\bar{\nabla}\cdot\bar{s} + \mu\bar{\nabla}\bar{s} + \mu\bar{s}\bar{\nabla}]$$

$$= (\lambda+\mu)\bar{\nabla}(\bar{\nabla}\cdot\bar{s}) + \mu\bar{\nabla}\cdot(\bar{\nabla}\bar{s})$$

$$= (\lambda+2\mu)\bar{\nabla}(\bar{\nabla}\cdot\bar{s}) - \mu\bar{\nabla}\times(\bar{\nabla}\times\bar{s}) \tag{4}$$

The form of the equation of motion suggests that at least part of the vector displacement, $\bar{s}$, may be expressed in terms of the gradient of a potential, ψ. Let

$$\bar{s} = \bar{\nabla}\psi$$

and so

$$\nabla^2\psi = \frac{1}{C_c{}^2} \ \frac{\partial^2\psi}{\partial t^2} \tag{5}$$

where

$$C_c{}^2 = \frac{\lambda+2\mu}{\rho}$$

which is the usual wave equation, a hyperbolic partial differential equation.

If the shear modulus is zero, the wave speed squared is just the bulk modulus divided by the density, as expected. The longitudinal character of these waves is immediately apparent, since if the solution of equation (4) is taken to be a scalar, the dyadic operator

$$\bar{\bar{D}} = \bar{\nabla}(\bar{\nabla}\psi)$$

is symmetric, and the rotation dyadic

$$\bar{\bar{R}} = -\frac{1}{2}(\bar{\nabla}\times\bar{s})\times\bar{\bar{I}} = 0$$

and so $\bar{\bar{D}} = \bar{\bar{G}}$, the strain dyadic. For such a solution, there is no twisting of the medium, only stretching and squeezing, and so the wave is purely longitudinal (compressional). Therefore, for purposes of this discussion, it is possible to treat longitudinal waves in a cable as a special case of longitudinal waves in general solid media without loss of generality.

2.2.5.3 Longitudinal Stress Waves For Simple Viscoelastic Constitutive Relations -

The general case of a time-varying tension in a cable or tether can be treated using the method of characteristics as the superposition of a number of finite-amplitude longitudinal stress waves (Morse and Feshbach, 1953; Courant and Hilbert, 1962). For the case of a completely linear elastic constitutive relation (Hooke's law), wave propagation is non-dispersive. However, for the case of loss of tension in the tether, viscoelasticity must be taken into account.

We shall examine wave propagation in the context of two models of visco-elastic body strain, the Maxwell model and the Kelvin model (Drucker 1967). More complex models may perhaps b⸱ ⸱equired ultimately to account for details of slack tether dynamics, but fur the present we shall use these models to illustrate changes in elastic wave propagation by small perturbations of viscosity.

In the Maxwell model, the strain is taken to be the sum of elastic and viscous components, i.e.,

$$\epsilon = \epsilon^e + \epsilon^v$$

and the elastic and viscous stresses are constant at all times,

$$\sigma^v = \sigma^e = \sigma$$

The elastic stress and strain are related by

$$\epsilon^e = \sigma/E_M$$

and for the viscous component,

$$\frac{d\epsilon^v}{dt} = \sigma/C_M$$

independent of all prior history. The equivalent mechanical system for the Maxwell model is a spring and dashpot connected in series.

We can write a differential equation for the total strain, ϵ,

$$\frac{d\epsilon}{dt} = \frac{d\epsilon^\bullet}{dt} + \frac{d\epsilon^v}{dt} = \frac{1}{E_M} \frac{d\sigma}{dt} + \frac{\sigma}{C_M}$$

(Note that treatment of the strain, ϵ, in this section is equivalent to the treatment of the displacement, $\bar{s}$, of the previous section.) Since there is no restoring force associated with the displacement of the "dashpot," i.e. the viscous strain, the perturbed wave equation for the Maxwell model is

$$\frac{\partial^2}{\partial x^2} \epsilon^\bullet = \frac{1}{C_c{}^2} \frac{\partial^2}{\partial t^2} (\epsilon^\bullet + \epsilon^v)$$

but $d\epsilon^v/dt = \sigma/C_M$, and so the equation can be rewritten as a wave equation for the stress in the cable,

$$\frac{\partial^2 \sigma}{\partial x^2} - \frac{1}{C_c{}^2} \frac{\partial^2}{\partial t^2} \sigma = \frac{E_M}{C_c{}^2 C_M} \frac{\partial \sigma}{\partial t}$$

We shall consider the viscous term as a small perturbation on the hyperbolic partial differential equation and attempt to find a solution of the form

$$\sigma = f(x \pm c_c t) \exp\left[-\alpha |x-x_o|\right]$$

a wave spatially damped from some initial point of propagation, x_o. Substitution of this form into the wave equation gives, to lowest order in viscous terms,

$$\alpha = \frac{E_M}{2C_c C_M}$$

which relates the model parameters to the damping parameter of the wave. Therefore, treating a damped wave in the context of the Maxwell poses no difficulties or inconsistencies.

A similar treatment may be undertaken for the Kelvin viscoelastic model. In the Kelvin model, the stress is at all times the sum of the stresses in an elastic and in a viscous element,

$$\sigma = \sigma^e + \sigma^v$$

and the strains are equal,

$$\epsilon^e = \epsilon^v = \epsilon$$

with

$$\sigma^e = E_k \epsilon \qquad \text{and} \qquad \sigma^v = C_k \; \frac{d\epsilon}{dt}$$

independent of the history of the system. The equivalent mechanical system of the Kelvin system is a spring and a dashpot in parallel. The wave equation for the Kelvin system may, after some minor manipulation, be cast in the form of a wave equation for the strain,

$$\left(\frac{\partial^2}{\partial x^2} - \frac{1}{C_c^2} \; \frac{\partial^2}{\partial t^2} \right) \epsilon = - \; \frac{C_K}{E_K} \; \frac{d}{dt} \left[\left(\frac{\partial^2}{\partial x^2} - \frac{1}{C_c^2} \; \frac{\partial^2}{\partial t^2} \right) \epsilon \right]$$

which manifestly describes the propagation of a damping wave with damping coefficient,

$$\alpha = \frac{E_K}{C_c C_K}$$

Generalization to more ..mplex viscoelastic relations is straightfor-
ward. It can be seen on the basis of these calculations that we can treat
the propagation of tensioned and slack regions in a viscoelastic tether in
a tractable fashion as a perturbative extension of the method of character-
istics.

2.2.5.4 Analytical Studies Status -

We have begun a series of calculations relevant to the slack tether
problem when tension has been lost. At present, this work has been con-
cerned with the situation in which the tether is going from a tensioned to
a slack state. Further research will address dynamical problems of the
slack tether.

This program of calculations has begun from the application of the
method of characteristics to the dynamics of longitudinal stress waves for
a tether with a purely elastic constitutive relation. This work has first
of all verified analytically the approximate validity of the constant ve-
locity initial condition used in simulations of the slack tether in the
program SLACK2. Further, it has been demonstrated that for a tether with
an elastic constitutive relation, arbitrary patterns of slack and tensioned
tether segments can be built up by superposition of longitudinal stress
waves. In particular, the important result has been obtained that is pos-
sible to have a bounded, tensioned tether segment bounded by two slack
segments, the boundaries moving with the velocities of characteristics for
the hyperbolic equation for longitudinal stress waves.

Work is underway developing the dynamics of a slackening tether exhibiting a viscoelastic constitutive relation, e.g. a Maxwell or Kelvin relation. As the tension of the tether diminishes, eventually viscous effects must dominate the dynamics of the tether. This work has shown, as a perturbation upon the hyperbolic equation for the elastic constitutive relation, that the stress waves do not exhibit a nonlinear steepening for physically reasonable constitutive relations.

The work outlined above is of importance for defining the initial conditions for a semi-analytic treatment of the slack tether problem. As outlined by Landau and Lifshitz (1959), a slack tether can be modeled as a rod with small (not necessarily positive) tension with inertial forces and resistance to transverse bending. A taut string is the opposite limit in which a positive tension dominates the dynamics. The advantages of this type of mathematical treatment are several:

1) A relatively consistent formalism may be developed applicable to both tensioned and slack tether segments.

2) The beginnings of loop formation may be treated in a manner similar to the problem of a column buckling under compression. This would allow identification of the scale size of loop formation in the slack tether.

3) No nonphysical mathematical singularities are introduced into the behavior of the tether at zero tension.

4) Provided deviations from a linearly extended tether remain small, tether dynamics will be accessible by relatively standard mathematical techniques.

References to Section 2.2.5

Courant, R., and Hilbert, D., Methods of Mathematical Physics, Interscience
    Publishers, John Wiley & Sons, New York (1962).

Drucker, D.C., Introduction to the Mechanics of Deformable Solids,
    McGraw-Hill Book Company, New York (1967).

Landau, L. and Lifshitz, D., Theory of Elasticity, vol. 7 of Course of
    Theoretical Physics, Addison-Wesley Publishing, Inc., Reading, MA
    (1959).

Morse, P.M. and Feshback, H., Methods of Theoretical Physics, McGraw-Hill
    Book Co., New York (1953).

2.2.6 Concluding Remarks -

During the reporting ;   od SAO has substantially enhanced the simula-
tion program SLACK2/3:   The treatment of viscoelastic damping has been
improved, and the program has been extended to full three dimensional capa-
bility.   In the next reporting period we expect to finalize the coding of
SLACK3 (simplified input procedure and a few other minor items) and use the
program to conduct a series of operational mission simulations relevant to
safety issues.   We shall also investigate the scale length for critical
damping in the tether material and the implications for the bounce calcula-
tions in the SLACK3 model.

An efficient, high resolution (yet strongly restricted) program for a
partially slack ball-and-spring model has been developed.   The program has
confirmed the initial conditions being used by SLACK2/3 (which assumes the
tether has become completely slack and hence cannot follow the initial
loss-of-tension).   These initial conditions have also been confirmed ana-
lytically in the undamped case.   In the next period we hope to extend the
program to include damping.   Other possible extensions include modeling

with the gravity gradient force, and 2 or 3 dimensional modeling with coriolis and drag forces; and proper treatment of the free end boundary condition from numerical analysis of the governing partial differential equation. Perturbation (stability) studies might also be feasible.

Analytical studies of the slack tether have been initiated, with the intent both of supporting the SLACK2/3 simulations and producing significant results not amenable to direct modeling. In the next period, we expect these studies to provide a good idea of the scale of the wrinkles or loops resulting from the initial buckling as a cut tether goes slack. This result will be relevant to safety studies and will also suggest how initial conditions for SLACK2/3 should properly depart from purely symmetric recoil, a consideration now handled by ad hoc randomization.

A continuing frustration, one which is becoming critical for some of the projected effort, is the lack of hard data on tether material properties beyond the simple axial stiffness (EA). We have asked Martin Marietta Corporation to send us what data they have on tether properties, and we also intend to request samples of tether from MMC, upon which we may perform some s. ple experiments.

2.3 Development Of A Computer Code To Model The Electric Potential Around
     A Severed Tether Immersed In A Plasma

2.3.1 Introductory Remarks -

In the Quarterly Report #1, we showed that the prolate spheroidal
model of the broken tether was very inaccurate at distances close to the
wire. We are now developing a numerical model which represents the wire as
a small cylinder. The program uses the Poisson's equation to calculate the
electric scalar potential on an axially symmetric three-dimensional grid.
The grid lines are closely spaced near the end of the wire but the spacing
increases geometrically as one moves away from the end. The lines parallel
to the wire are spaced 0.1 mm apart inside the wire and within one wire
radius. Then the spacing is increased geometrically as the distance from
the wire is increased. For example by choosing a geometric factor of 1.2
(each grid spacing is 20% larger than the preceeding one) and by adopting
for the first grid spacing a value of 0.1 mm, then 100 grid lines will span
a distance of 41.4 kilometers. The radial grid lines are, likewise,
closely spaced near the end of the wire, and their spacing increases as the
distance from the end increases.

While this approach could, in principle, be used to model the entire
tether, we decided to develop and use a more efficient model. Rather than
numerically modeling the entire length of the tether, the voltage at the
grid points within a region spanning a space of 10 to 100 meters from the
end of the wire is initialized by a prolate spheroidal model for the wire
immersed in an otherwise uniform electric field created by the motion of
the wire through a uniform transverse magnetic field $(\vec{V} \times \vec{B})$. The plasma
density is initialized at this potential and then the trajectories of a

number of "computer particles" each of which represents many real particles
is calculated. At each time interval the electric charge density on the
grid is calculated and a discrete implementation of Poisson's equation is
used to numerically estimate an updated electron potential. In this man-
ner, the motions of the electrons and ions near the end of the wire can be
modeled. While we have made considerable progress in developing this com-
puter program the code is not yet operational.

2.3.2 Generating The Coordinate System By Conformal Transformation -

Prolate Spheroidal Coordinates are the most useful coordinates for
calculating the electric field around a long wire. Moon and Spencer give a
most convenient transformation for generating an orthogonal set of hyper-
bolas and ellipses;

$$z = c \cosh(w) \tag{1}$$

where

$$z = x+iy \tag{2}$$

$$w = \eta+i\theta \tag{3}$$

Given a planar grid in the $w = \eta+i\theta$ coordinate system this transformation maps the straight lines η = constant and θ = constant onto ellipses and hyperbolas in the $z = x+iy$ coordinate system as shown in Figure 2.3.1. Rotation about the major axis of the ellipses generates the prolate spheroidal coordinate system. The purpose of this Section is to derive the relationships required to perform calculations in this interesting coordinate system.
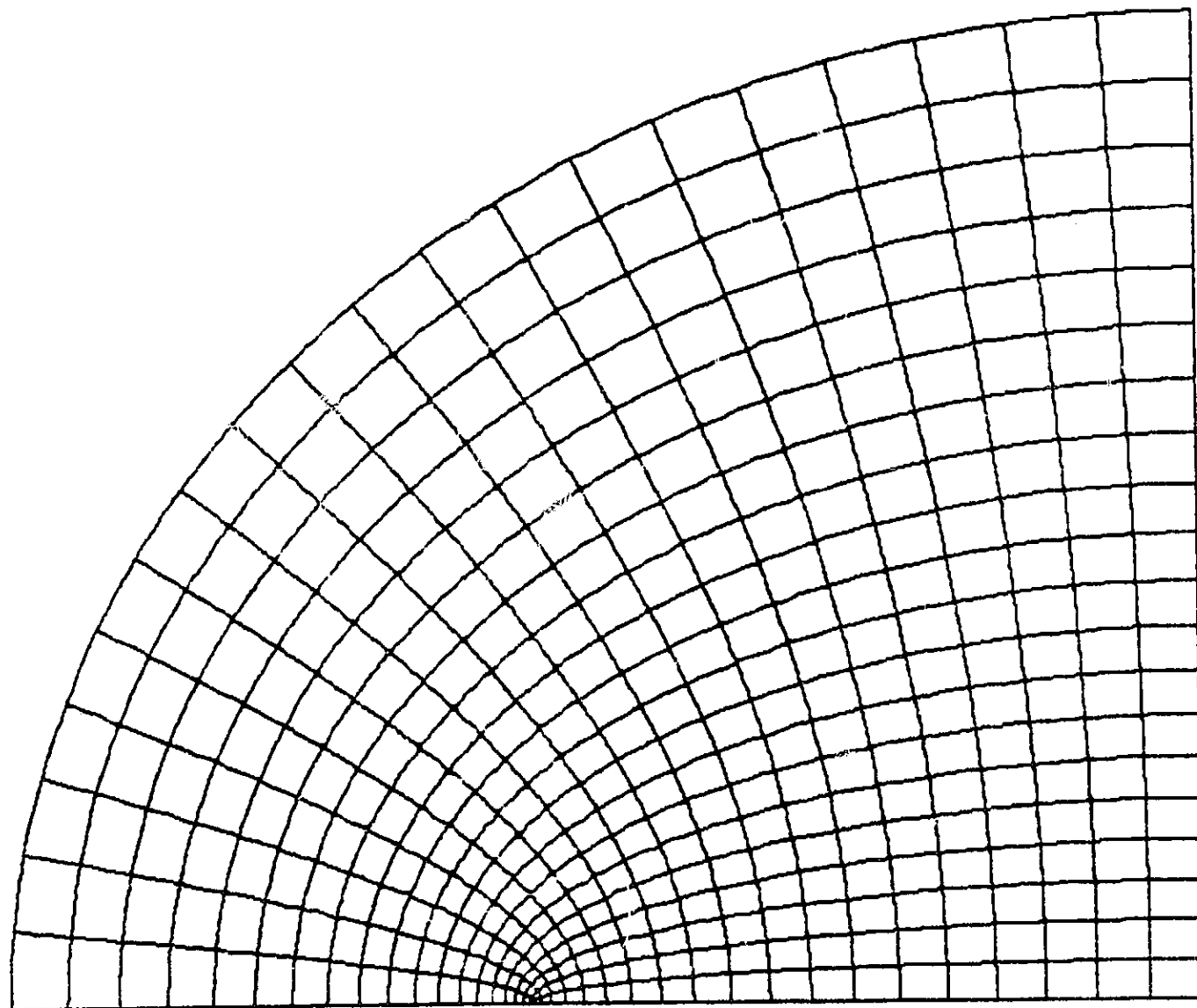
Figure 2.3.1   Prolate spheroidal coordinate system (a two-
dimensional view) obtained by conformal transformation.

2.3.3 Elliptical Coordinates -

Substituting (2) and (3) into (1) we find that

$$x+iy = c \cosh(\eta + i\theta)$$

$$= \frac{c}{2} (e^{\eta+i\theta} + e^{-\eta-i\theta})$$

$$= \frac{c}{2} e^{\eta}(\cos\theta + i\sin\theta) + e^{-\eta}(\cos\theta - i\sin\theta)$$

$$= \frac{c}{2} (e^{\eta} + e^{-\eta})\cos\theta + i(e^{\eta} - e^{-\eta})\sin\theta \tag{4}$$

from which we see that

$$x = c \cosh\eta \cos\theta$$

$$y = c \sinh\eta \sin\theta$$

Therefore,

$$\left(\frac{x}{c \cosh\eta}\right)^2 + \left(\frac{y}{c \sinh\eta}\right)^2 = \cos^2\theta + \sin^2\theta = 1 \tag{7}$$

Thus we have the equation for an ellipse where the major semi-axis is given by

$$a = c \cosh\eta \tag{8}$$

and the minor semi-axis is given by

$$b = c \sinh\eta \qquad (9)$$

From the definition of $\sinh\eta$ and $\cosh\eta$ it follows that

$$\cosh^2\eta - \sinh^2\eta = 1 \qquad (10)$$

and so

$$a^2 - b^2 = c^2 \qquad (11)$$

At this point it is useful to introduce two vectors which extend from the two foci at $x = \pm c$ to any point on the x-y plane; let their magnitudes be

$$r_1 = \sqrt{(x-c)^2 + y^2} \qquad (12)$$

and

$$r_2 = \sqrt{(x+c)^2 + y^2} \qquad (13)$$

Recalling that

$$x = c \cosh\eta \, \cos\theta \qquad (5)$$

$$y = c \sinh\eta \, \sin\theta \qquad (6)$$

it follows that

$$r_1 = \sqrt{(c \cosh\eta \cos\theta - c)^2 + c^2 \sinh^2\eta \sin^2\theta}$$

$$r_1 = c\sqrt{\cosh^2\eta \cos^2\theta - 2 \cosh\eta \cos\theta + 1 + \sinh^2\eta \sin^2\theta}$$

$$r_1 = c\sqrt{\cosh^2\eta \cos^2\theta - 2 \cosh\eta \cos\theta + 1 + \sinh^2\eta (1-\cos^2\theta)}$$

$$r_1 = c\sqrt{\cos^2\theta (\cosh^2\eta - \sinh^2\eta) - 2 \cosh\eta \cos\theta + \cosh^2\eta}$$

$$r_1 = c\sqrt{\cos^2\theta - 2 \cosh\eta \cos\theta + \cosh^2\eta}$$

$$r_1 = c\sqrt{(\cos\theta - \cosh\eta)^2}$$

$$r_1 = c|\cos\theta - \cosh\eta|$$

But $\cosh\eta \geq 1 \geq \cos\theta$, therefore

$$r_1 = c (\cosh\eta - \cos\theta) \tag{14}$$

Comparing the definition of r_1 and r_2 one sees that the same logic used to evaluate r_1 in terms of η and θ results in

$$r_2 = c(\cosh\eta + \cos\theta) \tag{15}$$

Therefore

$$r_1 + r_2 = 2c \cosh\eta \tag{16}$$

$$r_2 - r_1 = 2c \cos\theta \tag{17}$$

Two new parameters are now introduced which simplify the equations

$$\xi = \cosh\eta = \frac{r_1 + r_2}{2c} \tag{18}$$

and

$$\mu = \cos\theta = \frac{r_2 - r_1}{2c} \tag{19}$$

It was shown earlier that constant $\xi = \cosh\eta$ defines an ellipse. Now we shall see that constant $\mu = \cos\theta$ defines a hyperbola

$$\left[\frac{x}{c \cos\theta}\right]^2 - \left[\frac{y}{c \sin\theta}\right]^2 = \cosh^2\eta - \sinh^2\eta = 1 \tag{20}$$

The family of hyperbolas is orthogonal to the family of ellipses. This results from the conformal transformation which translates squares in the (η,θ) coordinate system into curvilinear squares in the x-y coordinate system. This is easily verified by testing and mapping function to determine if the Cauchy-Riemann conditions

$$\frac{\partial x}{\partial \eta} = \frac{\partial y}{\partial \theta}, \quad \frac{\partial x}{\partial \theta} = \frac{\partial y}{\partial \eta} \tag{21}$$

are met. Again recalling that

$$x = c \cosh\eta \cos\theta$$

$$y = c \sinh\eta \sin\theta$$

it follows that

$$\frac{\partial x}{\partial \eta} = c \sinh\eta \cos\theta \qquad \frac{\partial x}{\partial \theta} = -c \cosh\eta \sin\theta \qquad (22)$$

$$\frac{\partial y}{\partial \theta} = c \sinh\eta \cos\theta \qquad \frac{\partial y}{\partial \eta} = c \cosh\eta \sin\theta \qquad (23)$$

Thus we see that the Cauchy-Riemann conditions are met and the set of hyperbolas are orthogonal to the set of ellipses as illustrated in Figure 2.3.1. Rotating this coordinate system about the major axis of the ellipses generates the prolate spheroidal coordinate system in 3 dimensions ξ, μ, and ψ. It is conventional to rotate the ellipse with its major axis coincident with the z axis of the cartesian coordinate system. To accomplish this one must replace x by z and y by $R = \sqrt{x^2 + y^2}$ in the foregoing equations. The equations

$$x = c \cosh\eta \cos\theta \qquad (24)$$

$$y = c \sinh\eta \sin\theta \qquad (25)$$

are replaced by

$$z = c \cosh\eta \cos\theta \qquad (26)$$

$$R = c \sinh\eta \sin\theta \qquad (27)$$

$$x = R \cos\psi \tag{28}$$

$$y = R \sin\psi \tag{29}$$

Therefore the relationship between prolate spheroidal coordinates and cartesian coordinates is given by

$$x = c \sinh\eta \, \sin\theta \, \cos\psi \tag{30}$$

$$y = c \sinh\eta \, \sin\theta \, \sin\psi \tag{31}$$

$$z = c \cosh\eta \, \cos\theta \tag{32}$$

or

$$x = c\sqrt{\xi^2-1} \quad \sqrt{1-\mu^2} \; \cos\psi \tag{33}$$

$$y = c\sqrt{\xi^2-1} \quad \sqrt{1-\mu^2} \; \sin\psi \tag{34}$$

$$z = c \, \xi \, \mu \tag{35}$$

where

$$\xi = \cosh\eta = \frac{r_1 + r_2}{2c}$$

$$\mu = \cos\theta = \frac{r_2 - r_1}{2c}$$

$$r_1 = \sqrt{x^2 + y^2 + (z-c)^2}$$

$$r_2 = \sqrt{x^2 + y^2 + (z+c)^2}$$

2.3.4 The Gradient, Divergence, And Laplacian In Prolate Spheroidal Coordinates -

2.3.4.1 The Metric Coefficients -

To perform field calculations in prolate spheroidal coordinates it is necessary to calculate the gradient, divergence and curl in that coordinate system. The easiest approach to this problem is to derive the gradient, divergence and curl in generalized coordinates and then to evaluate the metric coefficients h_1, h_2, and h_3 using the transformation from prolate spheroidal to cartesian coordinates derived in Section 2.3.3.

To calculate vector relationships in generalized coordinates one must include the metric coefficients. In cartesian coordinates a differential length ds is given by

$$ds = \sqrt{(dx)^2 + (dy)^2 + (dz)^2} \tag{1}$$

In cylindrical coordinates ds is given by

$$ds = \sqrt{(dr)^2 + (rd\theta)^2 + (dz)^2}$$

not b_i

$$ds = \sqrt{(dr)^2 + (d\theta)^2 + (dz)^2}$$

In any orthogonal system,

$$(ds)^2 = (h_1 dq_1)^2 + (h_2 dq_2)^2 + (h_3 dq_3)^2 \tag{2}$$

where h_1, h_2 and h_3 are the metric coefficients.

Now to determine the metric coefficients we consider the following total differentials:

$$dx = \left(\frac{\partial x}{\partial q_1}\right) dq_1 + \left(\frac{\partial x}{\partial q_2}\right) dq_2 + \left(\frac{\partial x}{\partial q_3}\right) dq_3 \tag{3}$$

$$dy = \left(\frac{\partial y}{\partial q_1}\right) dq_1 + \left(\frac{\partial y}{\partial q_2}\right) dq_2 + \left(\frac{\partial y}{\partial q_3}\right) dq_3 \tag{4}$$

$$dz = \left(\frac{\partial z}{\partial q_1}\right) dq_1 + \left(\frac{\partial z}{\partial q_2}\right) dq_2 + \left(\frac{\partial z}{\partial q_3}\right) dq_3 \tag{5}$$

where q_1, q_2, and q_3 are the generalized coordinates.

Squaring these terms results in:

$$(dx)^2 = \left[\frac{\partial x}{\partial q_1} dq_1\right]^2 + \left[\frac{\partial x}{\partial q_2} dq_2\right]^2 + \left[\frac{\partial x}{\partial q_3} dq_3\right]^2 + \text{cross terms} \qquad (6)$$

$$(dy)^2 = \left[\frac{\partial y}{\partial q_1} dq_1\right]^2 + \left[\frac{\partial y}{\partial q_2} dq_2\right]^2 + \left[\frac{\partial y}{\partial q_3} dq_3\right]^2 + \text{cross terms} \qquad (7)$$

$$(dz)^2 = \left[\frac{\partial z}{\partial q_1} dq_1\right]^2 + \left[\frac{\partial z}{\partial q_2} dq_2\right]^2 + \left[\frac{\partial z}{\partial q_3} dq_3\right]^2 + \text{cross terms} \qquad (8)$$

In any orthogonal coordinate system the Pythagorean theorem demands that the cross terms must vanish. Thus, assuming that our generalized coordinate system is orthogonal, it follows that

$$(ds)^2 = \left[\left(\frac{\partial x}{\partial q_1}\right)^2 + \left(\frac{\partial y}{\partial q_1}\right)^2 + \left(\frac{\partial z}{\partial q_1}\right)^2\right](dq_1)^2$$

$$+ \left[\left(\frac{\partial x}{\partial q_2}\right)^2 + \left(\frac{\partial y}{\partial q_2}\right)^2 + \left(\frac{\partial z}{\partial q_2}\right)^2\right](dq_2)^2$$

$$+ \left[\left(\frac{\partial x}{\partial q_3}\right)^2 + \left(\frac{\partial y}{\partial q_3}\right)^2 + \left(\frac{\partial z}{\partial q_3}\right)^2\right](dq_3)^2 \qquad (9)$$

Comparing equation (9) to (2) we see that:

$$h_i^2 = \left(\frac{\partial x}{\partial q_i}\right)^2 + \left(\frac{\partial y}{\partial q_i}\right)^2 + \left(\frac{\partial z}{\partial q_i}\right)^2 \quad , \quad i = 1, 2, 3 \qquad (10)$$

Now to evaluate the metric coefficients for prolate spheroidal coordinates we make use of equation (10) and the coordinate defining equations obtained by the conformal transformation defined in Section 2.3.3.

$$x = c \sinh\eta \sin\theta \cos\psi \qquad o \le \eta < \infty \qquad (11)$$

$$y = c \sinh\eta \sin\theta \sin\psi \qquad o \le \theta \le \pi \qquad (12)$$

$$z = c \cosh\eta \cos\theta \qquad o \le \psi \le 2\pi \qquad (13)$$

where

$$q_1 = \eta, \quad q_2 = \theta, \quad q_3 = \psi.$$

The metric coefficients are calculated as follows:

$$h_1^2 = \left(\frac{\partial x}{\partial \eta}\right)^2 + \left(\frac{\partial y}{\partial \eta}\right)^2 + \left(\frac{\partial z}{\partial \eta}\right)^2$$

$$= (c \cosh\eta \sin\theta \cos\psi)^2 + (c \cosh\eta \sin\theta \sin\psi)^2 + (c \sinh\eta \cos\theta)^2 .$$

$$= c^2 \cosh^2\eta \sin^2\theta + c^2 \sinh^2\eta \cos^2\theta$$

$$= c^2 (1 + \sinh^2\eta) \sin^2\theta + c^2 \sinh^2\eta \cos^2\theta$$

$$h_1 = c \sqrt{(\sin^2\theta + \sinh^2\eta)} \qquad (14)$$

$$h_2^2 = \left(\frac{\partial x}{\partial \theta}\right)^2 + \left(\frac{\partial y}{\partial \theta}\right)^2 + \left(\frac{\partial z}{\partial \theta}\right)^2$$

$$= (c \sinh\eta \cos\theta \cos\psi)^2 + (c \sinh\eta \cos\theta \sin\psi)^2 + (c \cosh\eta \sin\theta)^2$$

$$= c^2 \sinh^2\eta \cos^2\theta + c^2 \cosh^2\eta \sin^2\theta$$

$$h_2 = h_1 \tag{15}$$

$$h_3^2 = \left(\frac{\partial x}{\partial \psi}\right)^2 + \left(\frac{\partial y}{\partial \psi}\right)^2 + \left(\frac{\partial z}{\partial \psi}\right)^2$$

$$= (c \sinh\eta \sin\theta \sin\psi)^2 + (c \sinh\eta \sin\theta \cos\psi)^2$$

$$h_3 = c \sinh\eta \sin\theta \tag{16}$$

2.3.4.2 The Gradient, Divergence and Laplacian in Generalized Coordinates

The gradient in generalized coordinates is given by:

$$\nabla\phi = \frac{\hat{u}_1}{h_1}\frac{\partial\phi}{\partial q_1} + \frac{\hat{u}_2}{h_2}\frac{\partial\phi}{\partial q_2} + \frac{\hat{u}_3}{h_3}\frac{\partial\phi}{\partial q_3} \quad , \tag{17}$$

where $\hat{u}_1$, $\hat{u}_2$, $\hat{u}_3$ are the unit vectors of the generalized coordinate system.

The divergence of a vector is defined as the limit of the total flux emerging normally from a closed surface divided by the enclosed volume as the volume approaches zero. Thus

$$\nabla\cdot\vec{A} = \lim_{\Delta V\to 0}\ \frac{1}{\Delta V}\int_{\Delta V}\vec{A}\cdot d\vec{S} \tag{18}$$

where

$$\vec{A} = A_1\hat{u}_1 + A_2\hat{u}_2 + A_3\hat{u}_3$$

Consider a differential curvilinear cube centered at $(q_1,\ q_2,\ q_3)$ as shown in Figure 2.3.2. The area of a differential square in the q_2, q_3 plane at the center of the cube is $h_2 h_3 \Delta q_2 \Delta q_3$. The area of the end of the cube located at $q_1 + \dfrac{\Delta q_1}{2}$ is therefore given by Taylor's theorem as

$$\left[q_1 + \frac{\Delta q_1}{2} \, , \, q_2 + \frac{\Delta q_2}{2} \, , \, q_3 + \frac{\Delta q_3}{3} \right]$$

$A_2 \hat{u}_2$

$$\left[q_1 + \frac{\Delta q_1}{2} \, , \, q_2 + \frac{\Delta q_2}{2} \, , \, q_3 + \frac{\Delta q_3}{2} \right]$$

$A_1 \hat{u}_1$

$$\left[q_1 + \frac{\Delta q_1}{2} \, , \, q_2 - \frac{\Delta q_2}{2} \, , \, q_3 \, \frac{\Delta q_3}{3} \right]$$

u_2

$$\left[q_1 + \frac{\Delta q_1}{2} \, , \, q_2 - \frac{\Delta q_2}{2} \, , \, q_3 + \frac{\Delta q_3}{2} \right]$$
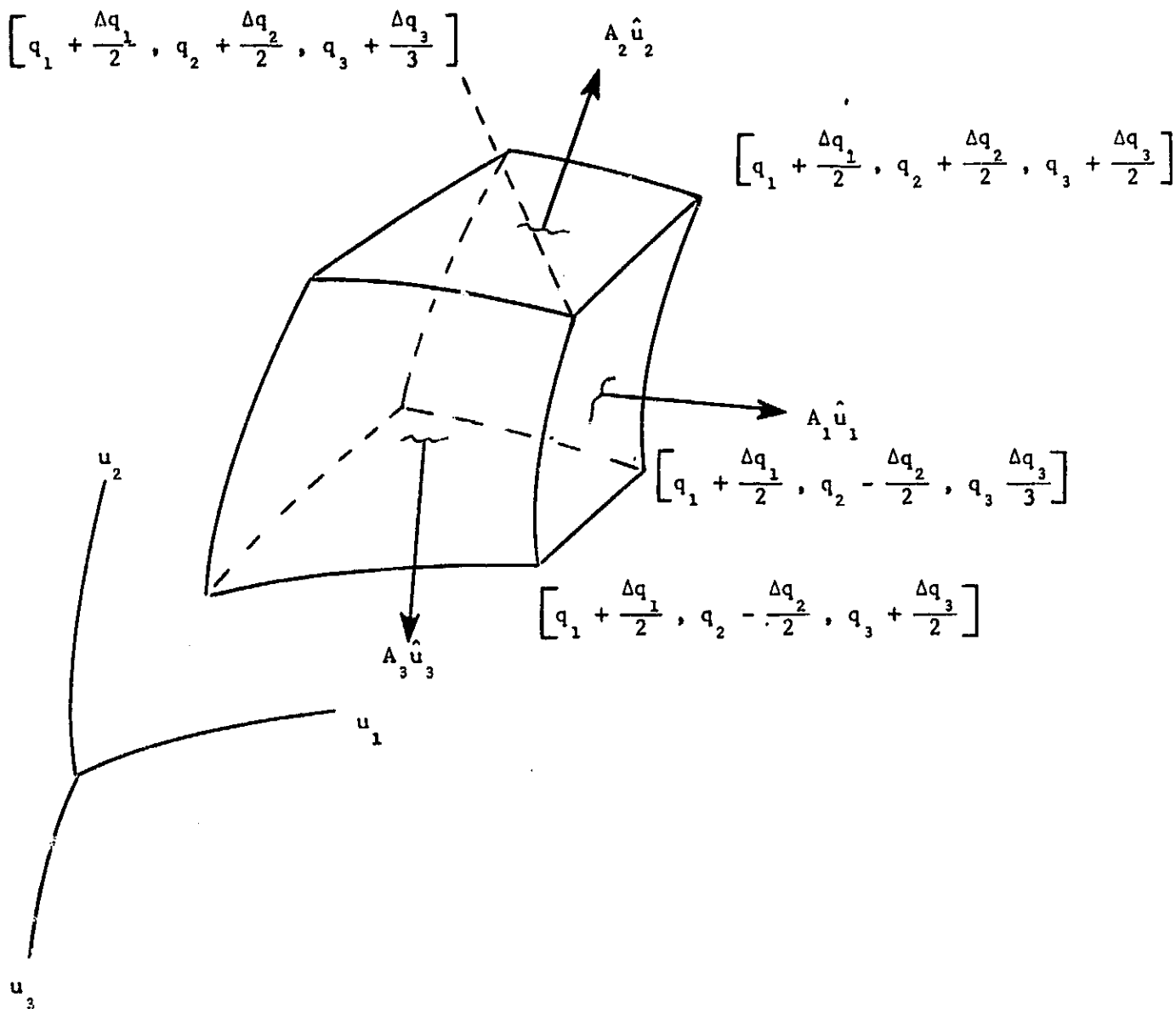
$A_3 \hat{u}_3$

u_1

u_3

Figure 2.3.3 Curvilinear Cube Illustrating
Divergence in Curvilinear Coordinates

$$\Delta a = \Delta q_2 \Delta q_3 \left[h_1 h_2 + \frac{\partial}{\partial q_1} (h_2 h_3) \frac{\Delta q_1}{2} \right]$$

It follows that the normal flux through this surface is given by

$$\Delta \Phi = \vec{A}_1 \cdot \Delta \vec{S}$$

$$= \Delta q_2 \Delta q_3 \left[h_1 h_2 A_1 + \frac{\partial}{\partial q_1} (h_2 h_3 A_1) \frac{\Delta q_1}{2} \right]$$

Adding to this the flux through the opposite side of the cube in the $-\vec{u}_1$ direction, we see that the total flux exiting normally in the $\vec{u}_1$ direction is given by

$$\Delta \Phi_1 = \left[h_2 h_3 + \frac{\partial}{\partial q_1} (h_2 h_3 A_1) \frac{\Delta q_1}{2} \right] \Delta q_2 \Delta q_3$$

$$- \left[h_2 h_3 + \frac{\partial}{\partial q_1} (h_2 h_3 A_1) \left(\frac{-\Delta q_1}{2} \right) \right] \Delta q_2 \Delta q_3 \tag{19}$$

But the volume of the curvilinear cube is

$$\Delta V = h_1 h_2 h_3 \Delta q_1 \Delta q_2 \Delta q_3$$

Therefore the $\vec{v}_1$ contribution to the divergence is given by

$$(\nabla \cdot \vec{A})_1 = \lim_{\Delta V \to 0} \frac{1}{\Delta V} \left[\frac{\partial}{\partial q_1} (h_2 h_3 A_1) \ \Delta q_1 \Delta q_2 \Delta q_3 \right] \tag{20}$$

Applying this procedure to the other two axes and summing the results, we see that the divergence of $\vec{A}$ in generalized coordinates is given by

$$\nabla \cdot \vec{A} = \frac{1}{h_1 h_2 h_3} \left[\frac{\partial}{\partial q_1} (h_2 h_3 A_1) + \frac{\partial}{\partial q_2} (h_1 h_3 A_2) + \frac{\partial}{\partial q_3} (h_1 h_2 A_3) \right] \tag{21}$$

Now that we have the equation for the divergence and the gradient in generalized coordinates, it is clear that the Laplacian is given by

$$\nabla^2 \phi = \frac{1}{h_1 h_2 h_3} \left[\frac{\partial}{\partial q_1} \left(\frac{h_2 h_3}{h_1} \frac{\partial \phi}{\partial q_1} \right) + \frac{\partial}{\partial q_2} \left(\frac{h_1 h_3}{h_2} \frac{\partial \phi}{\partial q_2} \right) + \frac{\partial}{\partial q_3} \left(\frac{h_1 h_2}{h_3} \frac{\partial \phi}{\partial q_3} \right) \right] \tag{22}$$

2.3.4.3 The Gradient And Laplacian In Prolate Spheroidal Coordinates -

Substituting (14), (15) and (16) into (17) gives the gradient operator in prolate spheroidal coordinates

$$\nabla\phi = \frac{\hat{\eta}}{c\sqrt{\sin^2\theta + \sinh^2\eta}} \frac{\partial\phi}{\partial\eta} + \frac{\hat{\theta}}{c\sqrt{\sin^2\theta + \sinh^2\eta}} \frac{\partial\phi}{\partial\theta} + \frac{\hat{\psi}}{c\,\sinh\eta\,\sin\theta} \frac{\partial\phi}{\partial\psi} \,. \qquad (23)$$

To calculate the coefficients of the Laplacian we utilize the following facts

$$h_1 h_2 h_3 = c^3 (\sin^2\theta + \sinh^2\eta)\,\sinh\eta\,\sin\theta \qquad (24)$$

$$\frac{h_2 h_3}{h_1} = h_3 = c\,\sinh\eta\,\sin\theta \qquad (25)$$

$$\frac{h_1 h_3}{h_2} = h_3 = c\,\sinh\eta\,\sin\theta \qquad (26)$$

$$\frac{h_1 h_2}{h_3} = \frac{c\,(\sin^2\theta + \sinh^2\eta)}{\sinh\eta\,\sin\theta} \qquad (27)$$

Introducing the prolate spheroidal metric coefficients into the Laplacian in generalized coordinates results in a cumbersome equation. It is clearer to deal with each term of (22) individually:

$$\frac{\partial}{\partial q_1}\left(\frac{h_2 h_3}{h_1}\frac{\partial\phi}{\partial q_1}\right) = \frac{\partial}{\partial\eta}\left(c\,\sinh\eta\,\sin\theta\,\frac{\partial\phi}{\partial\eta}\right)$$

$$= c\,\sin\theta\left(\sinh\eta\,\frac{\partial^2\phi}{\partial\eta^2} + \cosh\eta\,\frac{\partial\phi}{\partial\eta}\right) \qquad (28)$$

$$\frac{\partial}{\partial q_2}\left(\frac{h_1 h_3}{h_2}\frac{\partial\phi}{\partial q_2}\right) = \frac{\partial}{\partial\theta}\left(c\,\sinh\eta\,\sin\theta\,\frac{\partial\phi}{\partial\theta}\right)$$

$$= c\,\sinh\eta\left(\sin\theta\,\frac{\partial^2\phi}{\partial\theta^2} + \cos\theta\,\frac{\partial\phi}{\partial\theta}\right) \qquad (29)$$

$$\frac{\partial}{\partial q_3} \left(\frac{h_1 h_2}{h_3} \frac{\partial \phi}{\partial q_3} \right) = \frac{\partial}{\partial \psi} \left(c \frac{(\sin^2\theta + \sinh^2\eta)}{\sinh\eta \, \sin\theta} \frac{\partial \phi}{\partial \psi} \right)$$

$$= c \frac{(\sin^2\theta + \sinh^2\eta)}{\sinh\eta \, \sin\theta} \frac{\partial^2 \phi}{\partial \psi^2} \tag{30}$$

Substituting (24) through (30) into Laplace's equation (22) results in:

$$\nabla^2\phi = \frac{1}{c^2(\sin^2\theta + \sinh^2\eta) \, \sinh\eta \, \sin\theta} \left[\sin\theta \left(\sinh\eta \frac{\partial^2 \phi}{\partial \eta^2} + \cosh\eta \frac{\partial \phi}{\partial \eta} \right) \right.$$

$$\left. + \sinh\eta \left(\sin\theta \frac{\partial^2 \phi}{\partial \theta^2} + \cos\theta \frac{\partial \phi}{\partial \theta} \right) + \frac{(\sin^2\theta + \sinh^2\eta)}{\sinh\eta \, \sin\theta} \frac{\partial^2 \phi}{\partial \psi^2} \right]$$

which simplifies to:

$$\nabla^2\phi = \frac{1}{c^2 \sin^2\theta + \sinh^2\eta)} \left[\frac{\partial^2 \phi}{\partial \eta^2} + \coth\eta \frac{\partial \phi}{\partial \eta} + \frac{\partial^2 \phi}{\partial \theta^2} + \cot\theta \frac{\partial \phi}{\partial \theta} \right]$$

$$+ \frac{1}{c^2 \, \sinh^2\eta \, \sin^2\theta} \frac{\partial^2 \phi}{\partial \psi^2} \quad . \tag{31}$$

2.3.5 Solution Of Laplace'S Equation For The Electric Scalar Potential In Prolate Spheroidal Coordinates -

It was shown in Section 2.3.4 that Laplace's equation in prolate spheroidal coordinates is given by

$$\nabla^2\phi = \frac{1}{c^2(\sin^2\theta + \sinh^2\eta)}\left[\frac{\partial^2\phi}{\partial\eta^2} + \coth\eta\,\frac{\partial\phi}{\partial\eta} + \frac{\partial^2\phi}{\partial\theta^2} + \cot\theta\,\frac{\partial\phi}{\partial\theta}\right]$$

$$+ \frac{1}{c^2\,\sinh^2\eta\,\sin^2\theta}\frac{\partial^2\phi}{\partial\psi^2} \tag{1}$$

We solve this equation by the technique of separation of variables. Assume a solution of the form

$$\phi = H(\eta)\Theta(\theta)\Psi(\psi) \tag{2}$$

Substituting (2) into (1) and multiplying by $c^2\,\sinh^2\eta\,\sin^2\theta/H\Theta\Psi$ results in

$$\frac{\sinh^2\eta\,\sin^2\theta}{\sin^2\theta+\sinh^2\eta}\left\{\frac{1}{H}\frac{d^2H}{d\eta^2} + \coth\eta\,\frac{dH}{d\eta} + \frac{1}{\Theta}\frac{d^2\Theta}{d\theta^2} + \cot\theta\,\frac{d\Theta}{d\theta}\right\} + \frac{1}{\Psi}\frac{d^2\Psi}{d\psi^2} = 0 \tag{3}$$

The last term is a function only of ψ which does not appear in the rest of the equation. In order for the equation to hold for any value of ψ, $\frac{1}{\Psi}\frac{d^2\Psi}{d\psi^2}$ must be constant. By convention we choose this constant as $-m^2$, therefore

$$\frac{d^2\Psi}{d\psi^2} + m^2\Psi = 0 \tag{4}$$

From the geometry of the problem we know that (4) must have a single valued trigonometric solution; therefore, we deduce that

$$\Psi = A\,\sin m\psi + B\,\cos m\psi \tag{5}$$

and that m is a non negative integer.

$C-2$

Equation (3) may now be rewritten as

$$\frac{1}{H}\left(\frac{d^2H}{d\eta^2} + \coth\eta\ \frac{dH}{d\eta}\right) + \frac{1}{\Theta}\left(\frac{d^2\Theta}{d\theta^2} + \cot\theta\ \frac{d\Theta}{d\theta}\right) - \frac{m^2(\sin^2\theta + \sinh^2\eta)}{\sinh^2\eta\ \sin^2\theta} = 0 \qquad (6)$$

Now the rightmost term is easily shown to be

$$m^2\left[\frac{1}{\sinh^2\eta} + \frac{1}{\sin^2\theta}\right] \qquad (7)$$

Therefore equation (6) is easily rewritten as

$$\frac{1}{H}\left(\frac{d^2H}{d\eta^2} + \coth\eta\ \frac{dH}{d\eta}\right) - \frac{m^2}{\sinh^2\eta} + \frac{1}{\Theta}\left(\frac{d^2\Theta}{d\theta^2} + \cot\theta\ \frac{d\Theta}{d\theta}\right) - \frac{m^2}{\sin^2\theta} = 0 \qquad (8)$$

Since the first and second terms are dependent only on η and the third and fourth terms only on θ we may reasonably assume that they are independent of each other. Therefore each is equal to a constant which by convention is chosen to be $\ell(\ell+1)$

$$\frac{1}{H}\left(\frac{dH^2}{d\eta^2} + \coth\eta\ \frac{dH}{d\eta}\right) - \frac{m^2}{\sinh^2\eta} = \ell(\ell+1) \qquad (9)$$

$$\frac{1}{\Theta}\left(\frac{d^2\Theta}{d\theta^2} + \cot\theta\ \frac{d\Theta}{d\theta}\right) - \frac{m^2}{\sin^2\theta} = -\ell(\ell+1) \qquad (10)$$

These two equations may be rewritten as

$$\frac{d^2H}{d\eta^2} + \coth\eta\ \frac{dH}{d\eta} - \left[\ell(\ell+1) + \frac{m^2}{\sinh^2\eta}\right]H = 0 \qquad (11)$$

$$\frac{d^2\Theta}{d\theta^2} + \cot\theta\ \frac{d\Theta}{d\theta} + \left[\ell(\ell+1) - \frac{m^2}{\sin^2\theta}\right]\Theta = 0 \qquad (12)$$

Equations (11) and (12) may be simplified by the introduction of two new variables

$$\xi = \cosh\eta \tag{13}$$

and

$$\mu = \cos\theta \tag{14}$$

Considering first equation (11) we see that

$$\frac{d\xi}{d\eta} = \sinh\eta$$

$$\frac{d^2\xi}{d\eta^2} = \cosh\eta = \xi$$

$$\sinh^2\eta = \cosh^2\eta - 1 = \xi^2 - 1$$

$$\frac{dH}{d\eta} = \frac{dH}{d\xi}\frac{d\xi}{d\eta} = \sinh\eta\,\frac{dH}{d\xi} \tag{15}$$

$$\frac{d^2H}{d\eta^2} = \frac{d}{d\eta}(\sinh\eta)\,\frac{dH}{d\xi} + \sinh\eta\,\frac{d}{d\eta}\,\frac{dH}{d\xi}$$

$$= \cosh\eta\,\frac{dH}{d\xi} + \sinh\eta\,\frac{d\xi}{d\eta}\frac{d}{d\eta}\frac{dH}{d\eta}$$

$$= \xi\,\frac{dH}{d\xi} + \sinh^2\eta\,\frac{d^2H}{d\xi^2}$$

$$\frac{d^2H}{d\eta^2} = (\xi^2-1)\,\frac{d^2H}{d\xi^2} + \xi\,\frac{dH}{d\xi} \tag{16}$$

Substituting equations (15) and (16) into (11) results in

$$(\xi^2-1)\,\frac{d^2H}{d\xi^2} + 2\xi\,\frac{dH}{d\xi} - \left[\ell(\ell+1) + \frac{m^2}{\xi^2-1}\right]H = 0 \tag{17}$$

This is Legendre's equation with which we will deal later.

Applying the same method to equation (12) we see that

$$\frac{d\mu}{d\theta} = - \sin\theta$$

$$\frac{d^2\mu}{d\theta^2} = - \cos\theta = - \mu$$

$$\sin^2\theta = 1 - \cos^2\theta = 1 - \mu^2$$

$$\frac{d\Theta}{d\theta} = \frac{d\Theta}{d\mu}\frac{d\mu}{d\theta} = - \sin\theta \frac{d\Theta}{d\mu} \tag{18}$$

$$\frac{d^2\Theta}{d\theta^2} = - \cos\theta \frac{d\Theta}{d\mu} - \sin\theta \frac{d}{d\theta}\frac{d\Theta}{d\mu}$$

$$= - \cos\theta \frac{d\Theta}{d\mu} + \sin\theta \cdot \frac{d\mu}{d\theta}\frac{d}{d\mu}\frac{d\Theta}{d\mu}$$

$$= - \cos\theta \frac{d\Theta}{d\mu} + \sin^2\theta \frac{d^2\Theta}{d\mu^2}$$

$$= (1-\mu^2) \frac{d^2\Theta}{d\mu^2} - \mu \frac{d\Theta}{d\mu} \tag{19}$$

Substituting equations (18) and (19) into equation (12) results in

$$(1-\mu^2) \frac{d^2\Theta}{d\mu^2} - 2\mu \frac{d\Theta}{d\mu} + \left[\ell(\ell+1) - \frac{m^2}{1-\mu^2}\right]\Theta = 0 \tag{20}$$

Multiplying (20) by -1 results in

$$(\mu^2-1) \frac{d^2\Theta}{d\mu^2} + 2\mu \frac{d\Theta}{d\mu} - \left[\ell(\ell+1) + \frac{m^2}{\mu^2-1}\right]\Theta = 0 \tag{21}$$

Thus the separated equations for $H(\eta)$ and $\Theta(\theta)$ are of identical form and are both Legendre's equations for which the solutions are associated Legendre functions of the first kind $P_\ell^m(\xi)$ and the second kind $Q_\ell^m(\xi)$.

Thus the separated equations for $H(\eta)$ and $\Theta(\theta)$ are of identical form and are both Legendre's equations for which the solutions are associated Legendre functions of the first kind $P_\ell^m(\xi)$ and the second kind $Q_\ell^m(\xi)$. To solve equation (21) we set m=o and solve for the zero order Legendre function. The first few of which are listed here:

$$P_o(\xi) = 1 \qquad (22)$$

$$P_1(\xi) = \xi \qquad (23)$$

$$P_3(\xi) = \frac{1}{2}(3\xi^2 - 1) \qquad (24)$$

$$Q_o(\xi) = \frac{1}{2} \log \left[\frac{\xi+1}{\xi-1}\right] \qquad (25)$$

$$Q_1(\xi) = \xi Q_o(\xi) - 1 \qquad (26)$$

$$Q_2(\xi) = P_2(\xi)Q_o(\xi) - \frac{3}{2}\xi \qquad (27)$$

The Legendre functions of order m greater than zero are the Legendre associated functions which are derived from the zero order function by the following relationships

$$P_\ell^m(\xi) = (\xi^2-1)^{m/2} \frac{d^m P_\ell(\xi)}{d\xi^m} \tag{28}$$

and

$$Q_\ell^m(\xi) = (\xi^2-1)^{m/2} \frac{d^m Q_\ell(\xi)}{d\xi^m} \tag{29}$$

These functions are very useful for calculating the electric and magnetic fields in and around many objects which are most conveniently described in spheroidal coordinates.

2.3.6 Electric Scalar Potential Around A Solid Permeable Prolate Spheroid Immersed In A Uniform Field -

2.3.6.1 Introduction -

2.3.6.2 Matching Boundary Conditions At The Surface Of The Spheroid -

It is shown in Section 2.3.5 that when Laplace's equation is solved in prolate spheroidal coordinates by the method of separation of variables the resulting ordinary differential equations in the variables $\xi = \cosh\eta$ and $\mu = \cos\theta$ are Legendre equations. It is further shown there that the eigenfunctions of Legendre's equation are the Legendre functions of the first kind $P_\ell(\xi)$, the Legendre functions of the second kind $Q_\ell(\xi)$ and the associated Legendre functions of the first and second kind $P_\ell^m(\xi)$ and $Q_\ell^m(\xi)$. The potential around a prolate spheroid polarized parallel to its major axis is axially symmetric. Therefore only the Legendre functions of the first and second kinds are necessary to construct a solution.

2.3.6.2 Matching Boundary Conditions at the Surface of the Spheroid

Two potential functions, ϕ_1 inside the spheroid and ϕ_2 exterior to the spheroid, must be constructed. All of the Legendre functions of the second kind include the terms

$$Q_0(\xi) = \frac{1}{2} \log\left(\frac{\xi+1}{\xi-1}\right) \tag{1}$$

or

$$Q_0(\mu) = \frac{1}{2} \log\left(\frac{1+\mu}{1-\mu}\right) \tag{2}$$

Note that both functions in (1) and (2) approach ∞ as their arguments approach unity. Since the z-axis through the spheroid corresponds to $\mu=1$, the $Q_\ell(\mu)$ functions must be excluded from both ϕ_1 and ϕ_2. Similarly, the z-axis inside the spheroid corresponds to $\xi=1$, where

$$\xi = \frac{r_1+r_2}{2c} \tag{3}$$

and therefore $Q_\ell(\xi)$ must be excluded from ϕ_1.

Now that the pathological functions have been excluded we are ready to construct well behaved potential functions for ϕ_1 and ϕ_2. Using all of the allowed eigenfunctions of the axially symmetric Legendre equation we see that the general solution for ϕ_1 and ϕ_2 is

$$\phi_1 = \sum_{\ell=0}^{\infty} A_\ell P_\ell(\xi) P_\ell(\mu) \tag{4}$$

$$\phi_2 = \sum_{\ell=0}^{\infty} \left[B_\ell P_\ell(\xi) + C_\ell Q_\ell(\xi) \right] P_\ell(\mu) \tag{5}$$

where

$$\xi = \cosh\eta = \frac{r_1 + r_2}{2c} \tag{6}$$

$$\mu = \cos\theta = \frac{r_2 - r_1}{2c} \tag{7}$$

and r_1 and r_2 are the magnitudes of the vectors $\vec{r}_1$ and $\vec{r}_2$ from the two foci of the spheroid to any point in space, c is the semi focal length of the spheroid, and η and θ are the coordinates used to define the ellipsoidal coordinate system as shown in Section 2.3.2.

The unknown coefficients A_ℓ, B_ℓ and C_ℓ will be evaluated by imposing three boundary conditions:

1) At great distance from the spheroid the potential ϕ_2 must approach the potential of a uniform field. Since a potential function may have a constant added without changing the associated field $\vec{E}$ because

$$\vec{E} = - \nabla\phi \tag{8}$$

we are free to choose the origin of the spheroidal coordinate system as the point of zero potential. The potential function which gives rise to a uniform field E_0 in the z direction is

$$\phi' = -zE_0 \tag{9}$$

But from the transformation from prolate spheroidal to Cartesian coordinates
derived in Section 1, we see that equation (32) of Section 2.3.2 is

$$z = c\xi\mu \tag{10}$$

$$= cP_1(\xi)P_1(\mu) \tag{11}$$

At great distances from the origin, $Q_\ell(\xi)$ becomes negligibly small therefore
(5) simplifies to

$$\phi_2 = \sum_{\ell=0}^{\infty} B_\ell P_\ell(\xi)P_\ell(\mu) = -cP_1(\xi)P_1(\mu)E_o \tag{12}$$

It is therefore clear that

$$B_0 = 0$$

$$B_1 = -cE_o \tag{13}$$

$$B_\ell = 0 \quad \text{for all } \ell > 1$$

2) At the interface between regions 1 and 2 (the surface of the spheroid
where $\xi = \xi_0$) the potentials must be equal. From (4), (5) and (13) we see
that

$$\sum_{\ell=0}^{\infty} A_\ell P_\ell(\xi_0)P_\ell(\mu) = \sum_{\ell=0}^{\infty} C_\ell Q_\ell(\xi_0)P_\ell(\mu) - cE_o P_1(\mu)\xi_0 \tag{14}$$

Since the Legendre Polynomials $P_\ell(\mu)$ are orthogonal over the interval $-1 \leq \mu \leq 1$
we can multiply (14) by a Legendre polynomial $P_k(\mu)$ and integrate from -1 to $+1$
to separate the coefficients. This operation results in

$$A_0 P_0(\xi_0) - C_0 Q_0(\xi_0) = 0 \tag{15}$$

$$A_1 \xi_0 - C_1 Q_1(\xi_0) = -c E_0 \xi_0 \tag{16}$$

$$A_k P_k(\xi_0) - C_k Q_k(\xi_0) = 0 \quad \text{for all } k>1 \tag{17}$$

3) At the interface between the two regions 1 and 2 the normal derivatives of the potentials multiplied by the relative permeativities of their respective regions must be equal. This is required to insure continuity of the normal component of flux across the boundary. Thus both Dirichlet and Neumann boundary conditions are imposed. Thus

$$\varepsilon_r \frac{\partial \phi_1}{\partial \xi} = \frac{\partial \phi_2}{\partial \xi} \quad \text{when } \xi = \xi_0 \tag{18}$$

or from (4) and (5)

$$\varepsilon_r \sum_{\ell=0}^{\infty} A_\ell P_\ell'(\xi_0) P_\ell(\mu) = \sum_{\ell=0}^{\infty} \left[B_\ell P_\ell'(\xi_0) + C_\ell Q_\ell'(\xi_0) \right] P_\ell(\mu) \quad . \tag{19}$$

Again invoking the orthogonality of the Legendre polynomials over the interval $-1 \leq \mu \leq 1$ and using (13) we can separate the coefficients with the result:

$$\varepsilon_r A_0 P_0'(\xi_0) - C_0 Q_0'(\xi_0) = 0 \tag{20}$$

$$\varepsilon_r A_1 - B_1 P_1'(\xi_0) - C_1 Q_1'(\xi_0) = 0 \tag{21}$$

$$\varepsilon_r A_k P_k'(\xi_0) - C_k Q_k'(\xi_0) = 0 \tag{22}$$

Equations (20) and (21) can be simplified by recalling that

$$P_0(\xi) = 1 \qquad P_0'(\xi) = 0 \tag{23}$$

$$P_1(\xi) = \xi \qquad P_1'(\xi) = 1 \tag{24}$$

Since $P_0'(\xi)=0$, we conclude that

$$C_0 = 0 \quad . \tag{25}$$

From (15) we see that $A_0=0$.

At this point we shall deal with all of the coefficients for k>1 recalling (17) and (22)

$$A_k P_k(\xi_0) - C_k Q_k(\xi_0) = 0 \tag{17}$$

$$\epsilon_r A_k P_k'(\xi_0) - C_k Q_k'(\xi_0) = 0 \tag{22}$$

Multiplying (17) by $-Q_k'(\xi_0)$ and (22) by $Q_k(\xi_0)$ and adding the two equations, we find that

$$A_k \left[\epsilon_r P_k'(\xi_0) Q_k(\xi_0) - P_k(\xi_0) Q_k'(\xi_0) \right] = 0 \tag{26}$$

If we can prove that the term in the brackets is never equal to zero we have established that all A_k and C_k coefficients are zero for k>1. The Russian mathematician N.N. Lebedev[1] shows that the Wronskian $W(P_\ell(\xi), Q_\ell(\xi))$ which is defined as

$$W\left[P_\ell(\xi), Q_\ell(\xi) \right] = \begin{vmatrix} P_\ell(\xi) & Q_\ell(\xi) \\ \\ P_\ell'(\xi) & Q_\ell'(\xi) \end{vmatrix}$$

$$= P_\ell(\xi) Q_\ell'(\xi) - P_\ell'(\xi) Q_\ell(\xi) \tag{27}$$

is equal to $1/(1-\xi^2)$. Therefore, equation (26) can be rewritten as

$$A_k \left[(\epsilon_r - 1) P_k'(\xi_0) Q_k(\xi_0) + \frac{1}{\xi_0^2 - 1} \right] = 0 \tag{28}$$

Now $\xi_0>1$ and the Q_k functions are always positive for $\xi>1$. Furthermore, all of the roots of $P_k(\xi)$ lie in the interval $-1 \leq \xi \leq 1$. Thus $P_k'(\xi_0) >0$ for $\xi_0>1$. Since the term enclosed in the brackets is always greater than zero the only possible solution to (28) is

$$A_k = 0 \quad \text{for all } k>1 \tag{29}$$

from which we deduce from (17) that

$$C_k = 0 \quad \text{for all } k>1. \tag{30}$$

Thus we see that the only non-zero coefficients of (4) and (5) are A_1, B_1 and C_1. But it has already been shown by the first boundary condition that $B_1=-cE_0$ Therefore, equation (21) simplifies to

$$\varepsilon_r A_1 - C_1 Q_1'(\xi_0) = -cE_0 \tag{31}$$

But

$$\frac{d}{d\xi} Q_1(\xi) = Q_0(\xi) - \frac{\xi}{\xi^2-1} \tag{32}$$

Substituting (32) into (31) results in

$$\varepsilon_r A_1 - C_1 \left[Q_0 - \frac{\xi}{\xi^2-1}\right] = -cE_0 \qquad , \xi=\xi_0 \tag{33}$$

or

$$A_1 = \frac{C_1}{\varepsilon_r} \left[Q_0 - \frac{\xi}{\xi^2-1}\right] - \frac{cE_0}{\varepsilon_r} \qquad , \xi=\xi_0 \tag{34}$$

Substituting (34) into (16)

$$\frac{C_1}{\varepsilon_r} \left[\xi Q_0 - \frac{\xi^2}{\xi^2-1}\right] - C_1 Q_1 = -\frac{cE_0\xi}{\varepsilon_r} (\varepsilon_r-1) \qquad , \xi=\xi_0 \tag{35}$$

$$Q_1^{'}(\xi) = \xi Q_0(\xi) - 1$$

Therefore (35) simplifies to

$$C_1 \left[(\epsilon_r - 1) Q_1 + \frac{1}{\xi^2 - 1} \right] = \xi c E_0 (\epsilon_r - 1) \qquad , \ \xi = \xi_0 \qquad (36)$$

Dividing (36) by $(\epsilon_r - 1)$ results in

$$C_1 = \frac{c \xi E_0}{Q_1(\xi) + \frac{1}{(\epsilon_r - 1)(\xi^2 - 1)}} \qquad , \ \xi = \xi_0 \qquad (37)$$

Substituting (37) into (16) results in

$$A_1 = - c E_0 + \frac{c E_0 Q_1}{Q_1 + \frac{1}{(\epsilon_r - 1)(\xi^2 - 1)}} \qquad , \ \xi = \xi_0 \qquad (38)$$

which simplifies to

$$A_1 = \frac{- c E_0}{1 + (\epsilon_r - 1)(\xi^2 - 1) Q_1(\xi)} \qquad , \ \xi = \xi_0 \qquad (39)$$

Thus we have evaluated A_1 and C_1 in terms of c, E_0, ϵ_r and ξ_0, and we can write the solution for the potential in the two regions 1 and 2 as

$$\phi_1 = A_1 \xi \mu \qquad , \ 1 \leq \xi < \xi_0 \qquad (40)$$

$$\phi_2 = C_1^{'} Q_1^{'}(\xi) \mu - c E_0 \xi \mu \qquad , \ \xi_0 < \xi < \infty \qquad (41)$$

But by the transformation which generated the prolate spheroidal coordinates resulted in the relationship

$$z = c \xi \mu \qquad (1-35)$$

Therefore we see that the field within the spheroid which is given by

$$\vec{E} = - \nabla \phi_1$$

is uniform and is given by

$$\vec{E} = \frac{A_1}{c} \hat{z} \qquad (42)$$

We have solved the case of a dielectric spheroid immersed in an otherwise uniform electric field. To specialize to the case of a conducting wire we allow the dielectric constant to go to infinity. Under this condition $A_1=0$ and

$$C_1 = \frac{c\xi_0 E_0}{Q_1(\xi_0)} \tag{43}$$

We substitute (13) and (43) into (4) with the result

$$\phi_2 = cE_0 \left[\frac{\xi_0 Q_1(\xi)}{Q_1(\xi_0)} - \xi \right] \mu \tag{44}$$

Recalling (12), (13), (18) and (19) from Section 2.3.2

$$r_1 = \sqrt{x^2 + y^2 + (z-c)^2} \tag{12}$$

$$r_2 = \sqrt{x^2 + y^2 + (z+c)^2} \tag{13}$$

$$\xi = \frac{r_1 + r_2}{2c}$$

$$\mu = \frac{r_2 - r_1}{2c}$$

we see that for every point x, y, z in space we can calculate the electric potential ϕ. This equation is used to determine the boundary conditions for the numerical solution of the electric field around the wire in the presence of plasma. A plot of the electric field around a conducting spheroid is shown in Figure 2.3.3. The electric flux lines were calculated from an analog of the magnetic vector potential

$$\vec{D} = \nabla \times \vec{A}_0 \tag{45}$$

A smaller plot for a thin wire is shown in Figure 2.3.4. Equation (44) is also used to initialize all of the interior grid points before the iterative solution is begun. The details of this variable grid iterative solution will be described in the next report.
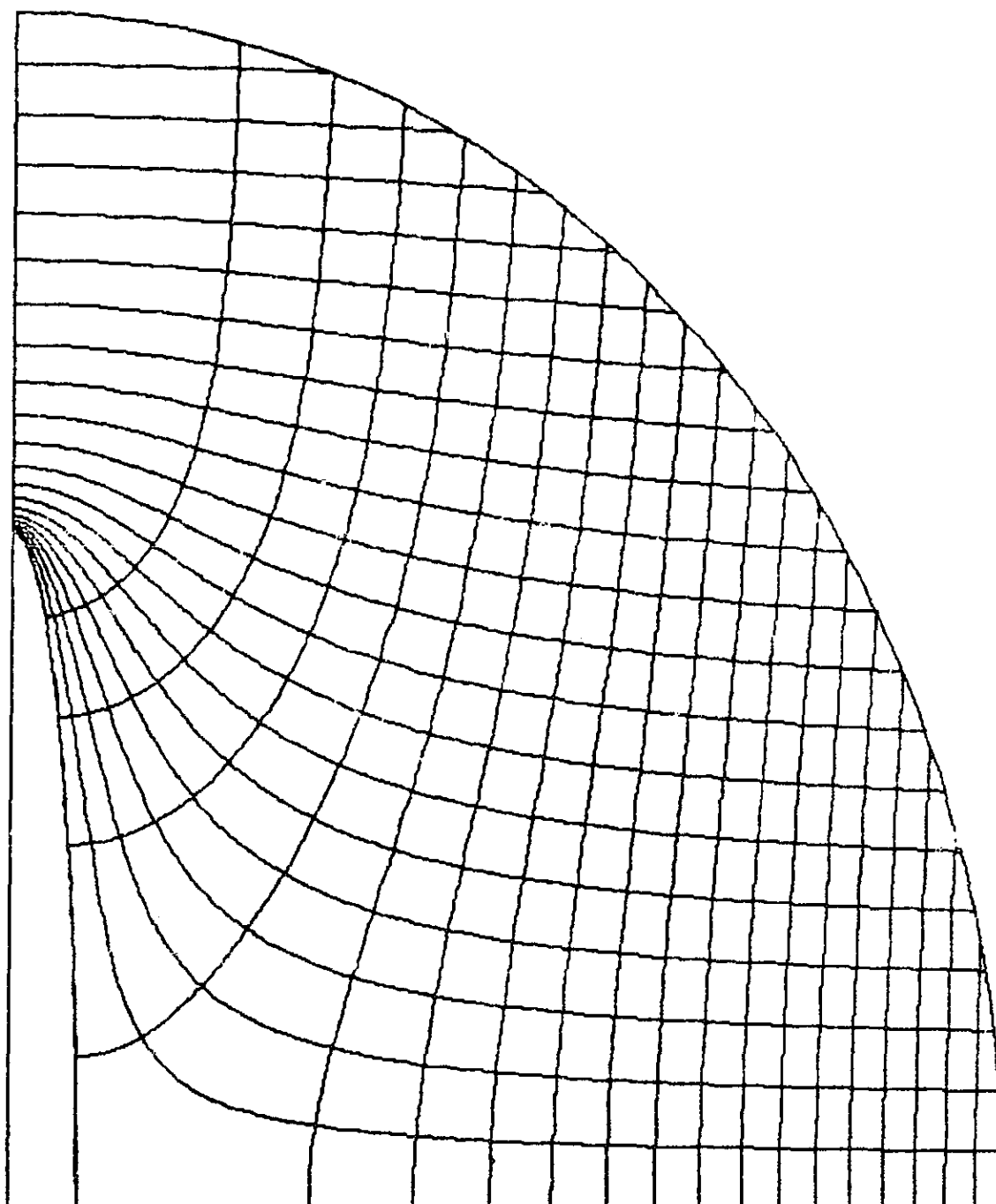
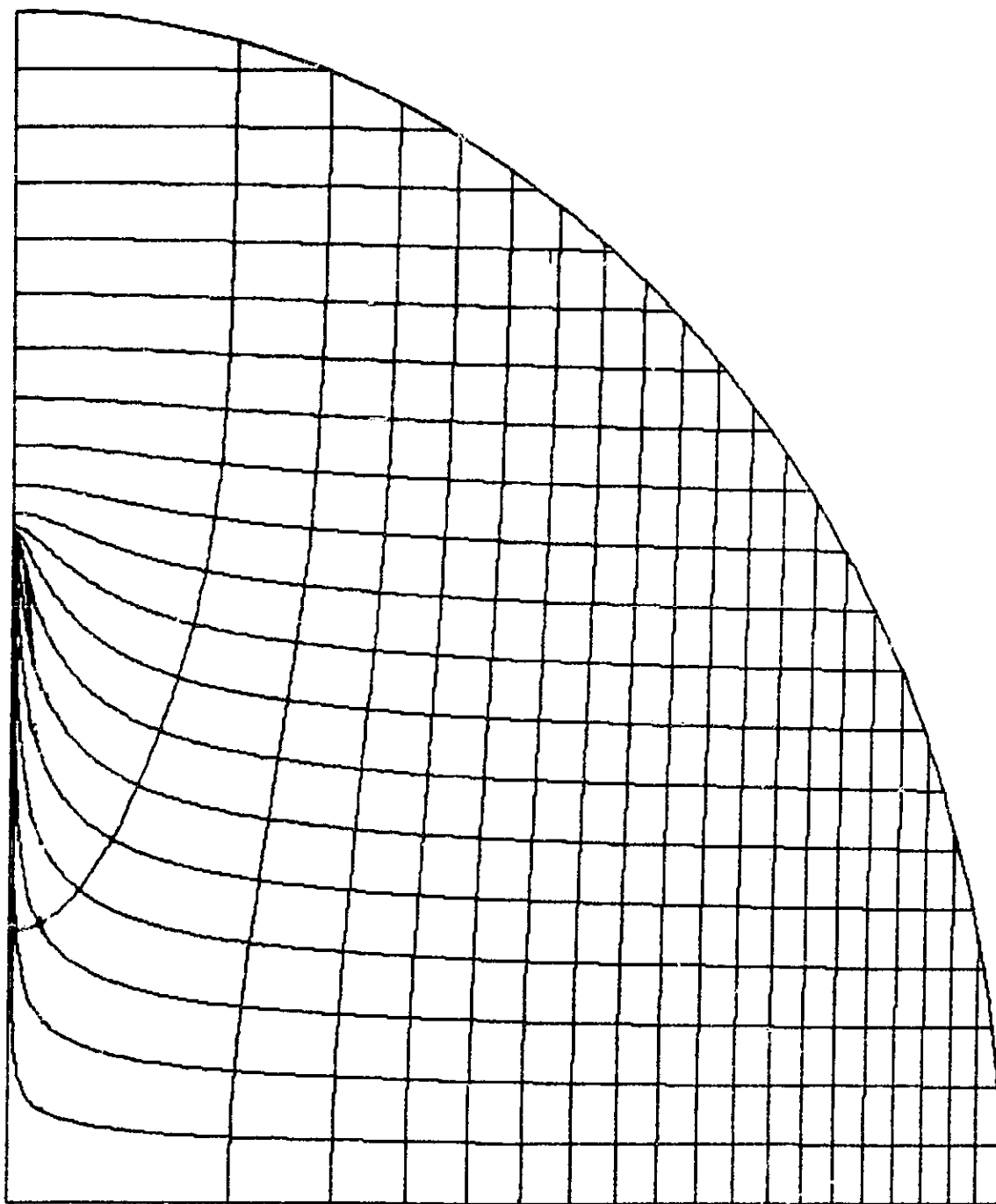Figure 2.3.3 Electric field around a conducting
spheroid.

Figure 2.3.4   Electric field around a conducting
thin tether.

REFERENCES

1. P. Moon and D.E. Spencer; Field Theory for Engineers, 1961; D. Van Nostrand Company, Inc., p. 348.

2. W. Harrold; Calculation of Equipotentials and Flux Lines in Axially Symmetrical Permanent Magnet Assemblies by Computer: IEEE Transactions on Magnetics Vol MAG-8 No. 1, March 1972.

3. P. Moon and D.E. Spencer; Field Theory for Engineers, 1961; D. Van Nostrand Company, Inc., Chapter 9.

4. John David Jackson; Classical Electrodynamics, 2nd Edition, 1975; John Wiley and Sons, Inc., p. 87.

5. N.N. Lebedev; Special Functions and Their Applications (translated by Richard Silverman); 1972; Dover Publications; p. 167.

6. Ibid., p. 183.

7. Ibid., p. 167.

8. I.S. Gradshteyn and I.M. Ryzhik; Table of Integrals, Series, and Products (translated by Scripta Technica, Inc.); 1965, Academic Press; p. 109.

9. A. Erdelyi, W. Magnus, F. Oberhettinger and F.G. Tricomi; Higher Transcendental Functions, Volume I; 1953; McGraw-Hill Book Company, Inc., p. 145.

10. Handbook of Mathematical Functions with Formulas, Graphs, and Mathematical Tables; Edited by M. Abramowitz and I.A. Stegun; 1965; National Bureau of Standards, p. 334.

11. N.N. Lebedev; Special Functions and Their Applications (translated by Richard Silverman); 1972; Dover Publications, p. 185.

12. P. Moon and D.E. Spencer; Field Theory for Engineers, 1961; D. Van Nostrand Company, Inc, p. 137.

13. G.H. Hardy; A Course of Pure Mathematics, 10th Edition; 1967; Cambridge University Press, p. 229.

14. N.N. Lebedev; Special Functions and Their Applications (translated by Richard Silverman); 1972; Dover Publications, p. 165.

15. P.M. Morse and H. Feshbach; Methods of Theoretical Physics; 1953; McGraw-Hill Book Company, Inc., p. 401.

16. Ibid., p. 547.

17. L.J. Chu and J.A. Stratton; Elliptic and Spheroidal Wave Functions; Journal of Mathematics and Physics Vol 20; 1941, pp. 259-309.

18. N.N. Lebedev; Special Functions and Their Applications (translated by Richard Silverman); 1972; Dover Publications, p. 182.

19. Ibid., p. 178.

20. Ibid., p. 4.

21. Ibid., p. 12.

22. A.I. Markushevich; Theory of Functions, Vol. I; 1965; Chelsea Publishing Company, p. 334.

23. Ibid., p. 404.

2.4 Potential Build-Up Due To Plasma Contactor Failure

In an easterly orbit, with the satellite deployed upward, the satellite collects electrons and the Shuttle collects ions. Because of the low thermal velocity of the ions, it is necessary to have a plasma contactor on board the Shuttle in order to maintain it at plasma potential. If the plasma contactor fails, the Shuttle will acquire a negative potential as a result of the inability of the Orbiter to neutralize the electrons coming down the wire from the satellite. If the satellite has a plasma contactor it will be a better collector and the Shuttle will acquire a large potential.

Two simulations have been run in order to estimate the potential acquired by the Shuttle if its plasma contactor fails. These simulations are relevant to the first electrodynamic mission with the Shuttle on an orbit of 28.5° inclination and 295 km altitude. The satellite is deployed upward on a 20 km long tether. These simulations refine and confirm the value of -2kvolt for the Shuttle potential as it was estimated in the Quarterly Report #1. In the first one the satellite has no plasma contactor and is modeled as a 1.5 meter disameter sphere. The Shuttle is modeled as a 12.4 meter diameter sphere. The wire is 20 km long and has a resistance of 4000 ohms. The Shuttle acquired a voltage of about -1195 volts and the satellite was at +1206 volts. The wire current was .253 amps. In the second simulation, the satellite has a plasma contactor and the other parameters are the same. The Shuttle acquired a potential of -2064 volts and the satellite was within a volt of plasma potential. The current in the wire was .337 amps.

3.0   PROBLEMS ENCOUNTERED DURING REPORTING PERIOD

   None.

4.0   ACTIVITY PLANNED FOR THE NEXT REPORTING PERIOD

   During the next reporting period we will carry out the software modification of the force and torque package in our rotational dynamics computer code. The implementation of the reeling control laws will then allow us to simulate actual maneuvers with a good fidelity. Our plotting program will also be modified because presently it is not formatted to receive and interpret the rotational dynamics variables.

   The three-dimensional slack tether computer code SLACK3 is now available and tested. During the next reporting period it will be used to simulate actual cases of tether break and to investigate suitable Shuttle avoidance maneuvers. In the mean time the analytic studies on the slack tether will continue. The major goal is the evaluation of the wrinkle's typical scale size at the onset of the compressional instability.

   The development of the computer code to evaluate the electric field around the severed tether is in progress. The next reporting period will be devoted to the implementation of the electric potential variations due to the plasma. Presently the program can evaluate the electric potential around a charged body in vacuo.